in red = reviewer #2 ; in blue = reviewer #1 ; in green = authors' initiative

Genesis of nanometric illite crystals elucidated by light-element (hydrogen, lithium, boron and oxygen) isotope tracing, and K-Ar and Rb-Sr dating

Norbert Clauer[1], Lynda B. Williams[2] and Anthony E. Fallick[3]

[1] Laboratoire d'Hydrologie et de Géochimie de Strasbourg (CNRS-UdS), 1 rue Blessig, 67084 Strasbourg, France
[2] School of Earth & Space Exploration, Arizona State University, Tempe, AZ 85287-1404, USA
[3] Scottish Universities Environmental Research Centre, East Kilbride, Glasgow G75 0QF, UK

Corresponding author: Dr. Norbert Clauer, Laboratoire d'Hydrologie et de Géochimie de Strasbourg (CNRS/UdS), 1 Rue Blessig, 67084 Strasbourg, France; office phone: 033 390 24 04 33; cell phone: 033 680 01 80 49; fax: 033 390 24 04 02; e-mail: nclauer@unistra.fr

Key words: hydrogen, lithium, boron and oxygen isotope geochemistry, K-Ar and Rb-Sr isotope dating, nanometric fundamental illite particles, illitization

Abstract

Illitization is a widely used tracer for evaluation of the thermal evolution in volcano-sedimentary sequences during burial, metamorphic and tectonic events. ~~Interestingly,~~ However, no agreement exists about how the process proceeds at the crystal scale, which ~~prompted~~ initiated

perspectives based on the challenging separation of nanometric "fundamental" illite-rich particles in the mid 1980s. Thirteen years later, in 1997, the first isotopic study on such nanometric crystals was published, followed by others that opened new potential to improve understanding of the illitization process.

The present review focuses on ~~both~~ the promising and still unsolved aspects of light-element isotopic (δD, δ^{7}Li, δ^{11}B, δ^{18}O) tracing, and K-Ar and Rb-Sr dating of nanometric illite-rich crystals extracted mainly from bentonites, but also from sandstones and shales in diagenetic to low-grade metamorphic conditions. If the study of nanocrystals from bentonite and sandstone beds now appears successful, problems remain in separating mechanically ~~the~~ authigenic illite-type crystals from detrital ~~components~~ minerals of shales, even at the nanometric size. An indirect way to distinguish the data of ~~such assemblages~~ these components is alkylammonium leaching, which has the specificity of stochiometrically replacing K in dioctahedral mica-type particles, and therefore to modify significantly ~~empty~~ their K-Ar system. The overall separation technique for nanometric illite crystals is ~~somewhat~~ specific with chemical treatments to remove the soluble phases, including organics, that are mixed with illite, "infinite" dispersion, high-speed fluid-flow centrifugation and removal of excess reagent by dialysis. Importantly, the initial K-Ar studies showed that no age information is lost during crystal nucleation and growth, with the whole illitization history apparently retained in the illite particles of different sizes. Based on combined K-Ar, Rb-Sr, δ^{18}O and δD studies, reaction rates and durations of illitization can be reconstructed, together with changing crystallization temperature and fluid chemistry depending on the water/rock ratio. On the basis of K-Ar dating, nucleation and growth can be continuous during a given period of time, or episodic. The Rb-Sr method complements ~~this with~~ the information about the origin of the interacting fluids by reconstructing ^{87}Sr/^{86}Sr ratios that depend on the water/rock ratios and interaction of the fluids with their pore environment. Combined with oxygen isotope data, such Sr isotope information points to differences in the origin of the solvents (by δ^{18}O) and the solutes (by ^{87}Sr/^{86}Sr). The δ^{18}O values of the illite crystals provide information about ~~crystal~~ nucleation or growth temperature, either increasing during burial or abnormally high ~~but~~ and constant during a thermal episode, or about changing fluid composition. Occurrence of organic matter could potentially bias the δ^{18}O of ~~crystallizing~~ nucleating and growing illite crystals, ~~if~~ when involved in initial organic maturation.

The largest B reservoir in sedimentary deposits is within the organic matter. When

released with oil and gas after maturation, most of this organic B yields isotopically light ^{11}B in the fluids relative to other natural waters, whereas ^{11}B fractionates preferentially into the bitumen. Put in context with oxygen and hydrogen isotope variations, the B data also confirm that the illite tetrahedral B-O bonds are as strong as or even stronger than the Si-O bonds, thus preserving the large isotopic variations that occur during thermal maturation of kerogen. The changing clay-organic interactions in sedimentary environments can, therefore, be traced by the B content and isotope composition during ~~progressive~~ maturation. The presently limited results on Li contents and isotope composition of nanometric illite crystals that potentially interact with organics outline trends similar to those of B.

Introduction

Since the middle of the 1960s, direct illite precipitation or smectite to illite conversion, both identified as illitization, are considered to be appropriate tracers for reconstructing the evolution of sedimentary basins, which is mainly driven by temperature increase and interaction with interstitial fluids during progressive burial (e.g. Hower et al., 1976; Velde, 1985; Jennings and Thompson, 1986; Pollastro, 1993; Šucha et al., 1993). The wide application of this tracer is partly due to the understanding of diagenetic to low-grade metamorphic mineral and organic-matter alteration in varied deposition environments. As temperature and chemistry of the interstitial fluids directly influence the chemistry of the crystallizing ~~or~~ and growing minerals, use of clay minerals, especially illite, for tracing progressive or instantaneous crystallographic-chemical changes is best suited by examining the trend between smectite and illite ordering of illite-smectite crystalline structures. In this process, the pertinent parameter is the quantitative recrystallization of smectite into illite via mixed-layered structures. Such changes have also been used in hydrocarbon exploration, as the progressive smectite to illite trend agrees fairly well with organic maturation indices and indigenous hydrocarbon grades, as a function of temperature increase.

However, many elemental and isotopic studies have focused, for a long time, on the fact that separation of authigenic illite-rich micrometric (first ~~from~~ for <2 ~~to >1~~ μm and later ~~form~~ ~~1 to~~ for <0.2 μm) particles from ~~systematic occurrence of~~ detrital minerals of any sedimentary host rock, ~~but~~ especially ~~of~~ shales, remains a tricky challenge (e.g. Weaver and Beck, 1971; Boles and

Franks, 1979; Clauer and Chaudhuri, 1995 and references therein; Pevear 1999). This difficulty was partly resolved by attempts to reduce as much as technically possible the size of the separated particles including disaggregation of illite-smectite mixed-layers (labeled I-S hereafter) instead of crushing, and by separating nanometric illite crystals from separated I-S. Such illite-rich nanoparticles with sizes as small as <0.02 μm were characterized by electron microscopy and high-resolution transmission microscopy, and were precisely identified by X-ray diffraction analysis aided by mathematical modeling (e.g. Reynolds, 1985; Drits et al., 1998; Eberl et al., 2002). Precise identification allowed evaluation of the crystal-size distribution ~~in~~ of the illite crystals from separated size fractions, indicating ~~elearlier~~ the crystallization processes and the crystal-growth trends (e.g. Nadeau et al., 1984; Eberl et al., 1998a). This progress encouraged a K-Ar dating attempt (Clauer et al., 1997), later a Rb-Sr application combined with hydrogen and oxygen isotope tracing (Clauer et al., 2003), and more recently boron and lithium isotope studies (Williams et al., 2013). Focus was mainly on bentonite beds to avoid as much as possible the problematic occurrence of detrital "contaminants" (Clauer et al., 1997; Środoń and Clauer, 2001; Clauer et al., 2003; Clauer et al., 2004; Środoń et al., 2006; Środoń et al., 2009).

The respective elements of interest ~~that are examined here~~ in the nanometric fundamental illite crystals are located in ~~their~~ tetrahedral sites for B, ~~their~~ octahedral sites for Li, ~~their~~ interlayer sites for K and its radiogenic daughter ^{40}Ar, as well as for ^{87}Rb and the corresponding radiogenic daughter ^{87}Sr, while oxygen forms the apices of the tetrahedrons and octahedrons, and hydroxyls the edges of the octahedral layers (Fig. 1). The varied locations of these elements in an illite crystal focus attention on the great potential of studies combining them. The following goals were set for the present review of light-element isotope geochemistry, and K-Ar and Rb-Sr geochronology of illite-type nanoparticles: (1) extract the key geochemical information that improves the understanding of illitization in diagenetic to low-grade metamorphic sedimentary rocks; (2) differentiate the potential processes that characterize illitization depending on the rock lithology and the degree of recrystallization; (3) identify potential changes in paleofluid compositions during crystal nucleation and growth; and (4) generate new information for the reconstruction of thermal histories of sedimentary basins. The review starts with a presentation of the illitization concept followed by specific aspects of the analytical and methodological approaches, and the alternative concepts for illitization. The core of the review will consist of discussing the conceptual nucleation and growth of nanometric crystals on the basis of the

available studies, with perspectives of improved isotope-based interpretations of the global illitization process.

The illitization process

Illite has been reported as forming in various environments, from continental soils to deeply buried sediments. Evidence of high temperature promoting the diagenetic formation of illite or the conversion of I-S (defined above) into illite is based mainly on studies of geologic conditions controlled by known geothermal gradients and/or temperature increase resulting from circulation of hydrothermal solutions at depth (e.g. Meunier and Velde, 2004). The formation of illite in different physical and chemical conditions is often attributed to processes such as precipitation favored by dissolution of K-bearing feldspar and micas. ~~Also concerned are~~ The reactions between solute K and clays depleted in or lacking K (e.g. kaolinite) are also included, as well as uptake of K ions and structural rearrangement of smectite or I-S crystal lattices into illite. However, these theoretical reactions are often difficult to adjust to natural conditions, because sources of K that are variably attributed to local dissolution of detrital K-feldspars and micas, or to K import from outside the rock volume by migrating fluids, are ~~still diversely~~ variably constrained (e.g. Pollastro, 1985; Freed and Peacor, 1992; Milliken, 1992; Furlan et al., 1996).

At this point, it is ~~probably~~ appropriate to recall that there is no aggrement about how illitization proceeds at the crystal scale. Theoretical models were conceived for varied mechanisms such as dissolution and precipitation in porous host rocks, and solid-state alteration in almost impermeable host rocks (e.g. Velde and Vasseur, 1992; Renac and Meunier, 1995; Altaner and Ylagan, 1997). Also, on the basis of experimental studies, the upper temperature limit of illite stability diverges from 250 ºC to 360 ºC (Yates and Rosenberg, 1996; Rosenberg, 2002). If illitization can be summarized as a nucleation and growth of fine crystals, it is neither ~~along~~ an Ostwald ripening process (Eberl and Środoń, 1988; Inoue et al, 1988), nor a "permanent recrystallization" (Velde and Renac, 1996), because dissolution of the first nucleated crystals has never been ~~demonstrated~~ documented. In fact, initial K-Ar studies have shown that no age information is lost during initial nucleation and growth, and that the entire ~~information of the~~ illitization process appears ~~therefore~~ to be retained in the illite particles (e.g. Clauer et al., 1997). This information includes nucleation of initial smectite-rich crystals, then simultaneous

nucleation of new illite-type crystals and growth of the initially nucleated crystals by a surface-controlled mechanism, and finally continuous mineral surface-controlled growth without nucleation (Środoń et al., 2002). Noteworthy also is the fact that illitization leads to lognormal crystal thickness distribution (CTD), at least in bentonites (Eberl et al., 1998). In shales, the shape of the CTD is generally asymptotic, which could result from a theoretical dominance of nucleation over growth, but also from the presence of ~~few~~ detrital illite (Dudek at al., 2002). Experimental results and thermodynamic databases have also shown variable effects of temperature on K-containing mineral equilibria (Aja, 1995). It is expected that crystallization of illite induces a lowering of K^+ concentration in the solute, and therefore a decrease of its ~~in the solute~~ K^+/H^+ ratio. Yates and Rosenberg (1996) reported such decreasing K^+/H^+ activity ratios in solution at equilibrium between low- and high-K illite phases mixed with kaolinite, during a temperature increase from 100 to 250 ºC~~, which implies a lowering of K in solution~~. Conversely, not much seems to be known about the impact of pressure on illitization, for instance in oil-bearing sandstone reservoirs. In this context, Dayal (1975) reported a layering of 10-Å illite at the expense of expandable smectite in an I-S when pressure was increased from 1 to 1000 kPa in seawater, at 22 °C.

"Fundamental" nanoparticles of illite (<0.02 μm = <20 nm) are theoretically among the first to nucleate from a supersaturated solution at diagenetic temperatures (Eberl et al., 1998). Also, because the crystal size distribution is normally asymptotic (reflecting constant nucleation) or lognormal (reflecting combined nucleation and growth) in nature, only a small proportion of the initially nucleated particles are expected to continue growing (Eberl et al., 2002). As the initial K-Ar studies of "fundamental" illite particles have suggested that no age information is lost, none of the finest crystals being therefore dissolved, separation of various size fractions or 'bins' of these nanometric particles (e.g. <0.02, 0.02-0.05, 0.05-0.1 μm) can potentially provide useful information about the conditions that promote nucleation of a specific clay mineral phase. The chemical and isotopic information in the successively larger size fractions ideally reveals changes in the chemistry of the interacting fluid over time, but that chemical and isotopic heterogeneity with increasing size fraction, of shales especially, can also be due to mixing of variable amounts of authigenic with detrital mineral phases. Also, ~~to be mentioned is,~~ if a fluid supersaturated in K relative to illite percolates a rock where illite crystals had already crystallized, a new generation of nucleating crystals may precipitate that are impossible to

physically separate from earlier crystallites. Nonetheless, nanometric particle-size separations have been useful in identifying the evolution of fluids during crystal growth (Clauer et al., 1997; Wilkinson and Haszeldine, 2002; Williams and Hervig, 2006; Muttik et al., 2011; Williams et al., 2013).

Illite-type fundamental nanoparticles represent the smallest and finest clay-type crystals that can presently be separated mechanically. Their size is at the nanometer scale with *ab* dimensions of 20 to 30 nanometers and *c* dimensions of 2 to 3 nanometers. The concept implies a process starting with dissolution of the smectite layers of I-S, progressively replaced by ~~crystallizing~~ nucleating and growing illite layers in the same mixed layering (Nadeau et al., 1984; Inoue et al. 1987; Eberl and Środoń, 1988). Depending on whether the mechanism of illitization was solid-state transformation or dissolution/precipitation (and also assuming that the particle separation was ideal), different geochemical and isotopic characteristics can be expected for fundamental particles of varied size, especially if nucleation and growth were progressing slowly, such as during burial diagenesis. Growth theoretically depends on temperature, chemical thermodynamic parameters, and accessibility of the interstitial fluid supplying ions to the particles. On the basis of K-Ar age data of nanometric size fractions from I-S separates, different ages associated with progressive crystal growth have been reported (Clauer et al., 1997). As ~~already~~ stated, if the first nucleated nanoparticles that did not grow can be separated from coarser ones, they should be the oldest. Alternatively, if crystal growth was not unique but periodic (episodic), the smallest fundamental particles could be younger than the associated coarser fundamental particles. Also, if crystal growth relates to a single fluid migration induced by a short-lasting hydrothermal activity, the fundamental particles of any size should be approximately of the same age. These theoretical aspects of illite crystal-growth were tentatively sketched relative to time on the basis of analytical evidence of I-S nanoparticles from bentonite beds of the East Slovak Basin (Fig. 2; Clauer, 2006).

In fact, clay material of most clastic sedimentary rocks not only ~~contains~~ consists of first-cycle coarse mica from crystalline parent rocks, but also varied clay-sized material resulting from either continental erosion or pedogenetic weathering, in addition to authigenic nucleating and growing illite-type particles. These aspects have been covered in ~~many~~ numerous publications (e.g. Perry and Hower, 1970; Burley and Flisch, 1989; Ehrenberg and Nadeau, 1989; Glassman et al., 1989a and b; Mossmann 1991; Freed and Peacor, 1992; Harris, 1992; Pevear, 1992; Girard

and Barnes, 1995; Clauer and Chaudhuri, 1996; Clauer et al., 1999). Notwithstanding some successful studies (e.g. Elliott et al., 1991), ~~a definite explanation regarding about~~ the mechanism of illitization at the crystal scale is still debated. Published studies clearly show dissolution and precipitation (e.g. Nadeau et al., 1984; Ahn and Peacor, 1987), while others ~~believe in~~ envision solid-state transformations (e.g. Drits et al., 1997). Case studies of both evidential bases can be evaluated over the last two decades in Inoue and Kitagawa (1994), Yates and Rosenberg (1996; 2011), Altaner and Ylagan (1997), Środoń (1999), Środoń et al. (2009) and Ferrage et al. (2011).

On the basis of published K-Ar, Rb-Sr and stable isotope data of nanometer- to micrometer-sized illite crystals of bentonite beds from sedimentary basins (Clauer et al., 1997; Środoń et al., 2002; Clauer et al., 2003; Honty et al., 2004; Środoń et al., 2006), Clauer (2006) published a preliminary conceptual model for the K-Ar and $\delta^{18}O$ characteristics of such nucleating and growing particles during progressive burial. The model envisages different reaction rates and durations, ~~also taking into consideration~~ as well as variable temperature increases and impacts of the fluid chemistry as influenced by the water/rock ratio. Nucleating particles that stop growing and remain small yield ~~the~~ older K-Ar ages in the particle-size distribution, whereas episodic crystal growth provides potentially younger K-Ar data for the smallest crystals than for the associated coarser micrometer-sized particles, because they nucleate while the earlier (therefore coarser) crystals are growing. Therefore, K-Ar dating of nanometric particles from any bentonite I-S size fraction does not always provide decreasing K-Ar ages when crystal size increases. Dating assemblages of young small particles comprising apparently older coarser sizes may therefore also provide unexpected and misleading results, not because of technical or conceptual problems, but for natural reasons. In any case, "fundamental" nano-particles are most appropriate for reconstructing the history of bentonite beds, because well defined illite crystals~~, being well defined,~~ are not affected by surface sorption and particle agglomeration, and their thickness distribution profiles conform to the crystal growth theory (Eberl et al., 2011). However, it cannot be ~~excluded~~ denied that different size fractions of a sample can integrate particles of the same or similar mineral types but of variable ages, resulting from episodic and variable K supply. As ~~already stated~~ discussed, such varied mineral types cannot be distinguished by the traditional analytical procedures such as classical X-ray diffraction (XRD) or wet chemical analysis, but they might be by XRD profile modeling (Reynolds, 1985; Eberl et al. 1996; Drits et al. 1998; Eberl et al., 1998b; Eberl et al. 2001; Eberl et al., 2011). And

last, but not least, it is appropriate, in dealing with K-Ar ages, to recall that these nanometric particles do not leak any radiogenic ^{40}Ar due to their particle size, as the smallest particles are sometimes older than the coarser ones (e.g. Clauer et al., 1997), which is crucial for the overall application of the K-Ar method being reviewed here.

In addition, K-Ar ages can also record information about the crystal-growth mechanism and associated reaction rate(s). For instance, the crystal-growth rate may ~~possibly~~ have remained constant during the entire process, with or without significant changes in temperature or chemical composition of the interacting fluids (Fig. 2; Clauer, 2006). Depending on ~~the~~ stable or variable temperature and fluid parameters, the mode of the K-Ar ages will locate either: (1) towards the middle of the theoretical illitization time span when the rate was about constant; (2) close to the beginning of the theoretical time span when the rate decreased or was interrupted; or (3) towards the end of the time span when the crystallization rate increased progressively. In summary, the K-Ar ages of bentonite illite-type nanoparticles are able to record a complicated illitization history that ~~could~~ might have occurred in sedimentary strata on the basis of constant or varied growth rates, and of one or more successive nucleation/growth episodes. If such scenarios occur in individual bentonite beds of a given stratigraphic age, the interpretation will be necessarily complicated, raising questions about the sample preparation and analysis, but also and more importantly about how to decrypt the complex evolution of the whole sedimentary basin, as is the case in the East Slovak Basin (Clauer et al., 2014b).

While electron microscope observations and XRD measurements of nanometer-sized particles are informative about the physical aspects of particle growth, the $\delta^{18}O$ values of the crystal separates can provide information about nucleation and growth conditions, especially about fluid-particle interactions (Fig. 4 of Clauer, 2006). A decrease of $\delta^{18}O$ from fine to coarse particles suggests either an increase in temperature, a change in the $\delta^{18}O$ of the interacting fluid, and/or a variable water/rock ratio during growth, whereas an increase in $\delta^{18}O$ implies the opposite. Only limited information is yet available on hydrogen isotopic results of nanometric particles, ~~partly~~ perhaps because of the difficulty in separating H from hydroxyl and interlayer water (e.g. Savin and Hsieh, 1998).

For completeness, it might be recalled that the label "fundamental" corresponds to extremely small size of crystals and aggregates that were obtained following a specific sample preparation and particle separation presented below. The term "fundamental" has no connotation

other than the fact that the particles are nanometric in size. However, to avoid any rhetorical debate about the meaning of "fundamental" whilst accepting the concept and definition of Nadeau et al. (1984), the term "nanometric" ~~is~~ has been adopted hereafter to identify these very fine and small crystals, although it is only partly appropriate because it refers to the thickness of the particles in nanometers, whereas their width can be of micrometric size.

An isotopic concept for a nucleation/growth model of nanometric illite

The location of the elements in an illite crystal~~lographic~~ structure ~~being~~ are of specific interest during the conversion of smectite to illite, ~~it is noteworthy to recall that incorporation of~~ as B ~~into~~ is hosted by ~~in~~ tetrahedral sites where it can ~~occur replacing~~ replace either Si or Al, ~~that~~ Li is integrated in octahedral ~~vacant~~ sites replacing Al, Mg or Fe, and ~~that~~ K is the dominant cation in the interlayers. Oxygen is at the corners of either the tetrahedral or octahedral sites, whereas structural hydrogen is mostly concentrated at the edges of the crystals where the tetrahedral and octahedral sites connect (Fig. 1).

Some basics about stable isotope geochemistry of light elements

Boron has two natural stable isotopes (^{11}B and ^{10}B) that represent respectively about 80 and 20% of the element. Its ~~contents~~ concentrations and isotopic signatures vary widely in surface environments, especially in natural waters, for which four orders of magnitude in concentration and δ^{11}B ranging from –16 to +59‰ were reported (Vengosh et al., 1994). ~~The~~ B isotopes ~~composition~~ ~~has~~ have been used for about two decades to trace the source of waters ~~masses~~ ~~sources~~ (Palmer and Sturchio, 1990), to ~~follow~~ trace the evolution of brines (Vengosh et al., 1991a and b; Moldovanyi et al., 1993), to determine the origin of evaporites (Vengosh et al., 1992; Swihart et al., 1996; Bottomly and Clark, 2003), and to examine hydrothermal flow systems (Leeman et al., 1992). Lithium has also two naturally stable isotopes (^{7}Li and ^{6}Li) with ~~natural~~ abundances of 92.5 and 7.5%, respectively. As Li is easily hydrated, it does not occur as a free element on Earth, ~~. Forming a~~ but represents a minor part of most igneous rocks. ~~Li also~~ ~~and~~ It occurs in many natural brines and fractionates isotopically ~~fractionates~~ in a wide variety of natural processes involving either mineral precipitation from and alteration by fluids, ~~and~~ or ~~during~~ ion exchanges (e.g. Chan and Edmond, 1988). Known to substitute for Mg and Fe in

octahedral sites of clay minerals, ^{6}Li is preferred over ^{7}Li (Teng et al., 2004; 2006; 2007; 2008). As for oxygen and hydrogen ~~isotope compositions~~ examined here, the B and Li isotope compositions are usually expressed as deviations (in ‰) from standard materials (Williams et al., 2012). ~~which are the boric acid NIST SRM 951 for B (Chetelat et al., 2005), and the LSVEC lithium carbonate NIST SRM 8545 for Li (Flesch et al., 1973). In practice, an internal reference standard calibrated against the NIST standard is used for checking the instrumental fractionation and drift. The $^{11}B/^{10}B$ ratios of the internal standard and the sample are determined on materials that went through the same chemical preparation procedure.~~

The $\delta^{11}B$ of seawater (+39.5 ‰) is enriched in ^{11}B relative to the oceanic and continental crust (Lemarchand et al., 2000; 2002). Although the reason for this is not yet well understood, it is assumed that it is due to a preferential adsorption of aqueous ^{10}B (predominantly from borate anion $^{10}B(OH)_4^-$) onto clay particles. Isotope exchange reactions between the two soluble species $^{11}B(OH)_3^0$ and $^{10}B(OH)_4^-$ control the B isotopic ~~fractionation~~ partitioning in solution (Schwarcz et al., 1969). These authors calculated a fractionation enriching ^{10}B in clays by about 30-40 ‰~~, and~~. They also noticed that it is in good agreement with a seawater $\delta^{11}B$ value calculated when assuming a steady state ocean with respect to both the B concentration and isotope composition. This steady state ~~could be~~ is approximately maintained by a ~~simple~~ combined input of B from continental weathered rocks and ~~a single~~ removal by sediment adsorption and mineral substitutions. Subsequently, Williams et al. (2001a and b) and Williams and Hervig (2002) made laboratory experiments on B fractionation during exchange processes between I-S and water, considering that diagenetic clay nucleation and growth induce incorporation of ^{10}B into illite-type structures (Spivack et al., 1987). They observed that the B-isotope exchange kinetic rates follow mineralogical recrystallization of smectite into illite. However, depletion of B contents in pore waters with increasing $\delta^{11}B$ is not the general rule, especially in the Gulf Coast Basin (Land and Macpherson, 1992; Moldovanyi and Walter, 1992), suggesting another source of ^{10}B in deep basinal environments. In an attempt to identify the source(s) of ^{10}B in deep sedimentary reservoirs, Williams et al. (2001a;b) studied the B isotope composition of organic matter from hydrocarbon reservoirs of the Gulf Coast and found that pore fluids associated with hydrocarbons are B-enriched. As ^{10}B is preferentially taken up by clay minerals, or retained in remnant kerogen, the pore fluid becomes progressively ^{11}B-enriched during fluid migration through clay-rich sediments. Bitumen has been recently shown to contain several hundreds of μg/g B

(Williams and Hervig, 2013), with isotopic compositions that are 10‰ heavier than associated kerogen, with $\delta^{11}B$ <0‰ for kerogen and clays and >0‰ for bitumen. Significant amounts of B are reported in kerogen from coals and oil source rocks, with $\delta^{11}B$ values all less than 0‰, similar to authigenic pore-filling clay minerals in sandstone reservoirs (Williams and Hervig, 2004; Tagahashi et al., 2011). Boron isotopes are also fractionated during hydrothermal mineral crystallization (Oi et al., 1989; Spivack et al., 1990; Leeman et al., 1992). In summary, there is no specific mineral isotopic fractionation for B isotopes, as there is for oxygen, but there is rather an ion-coordination dependence of the fractionation. In diagenetic environments, where the pH is buffered to <7, B is dominantly in trigonal coordination in the fluids as $B(OH)_3$, which preferentially accomodate ^{11}B, but it substitutes in tetrahedral sites of authigenic clay crystals, which prefer ^{10}B (Palmer and Swihart, 1996), inducing a major isotope fractionation as a function of temperature (Williams et al., 2001; 2007).

Li is commonly enriched in oilfield brines and saline formation waters of sedimentary basins (Collins, 1975; Connolly et al., 1990; Fontes and Matray, 1993; Moldovanyi et al., 1993; Stueber et al., 1993; Wilson and Long, 1993). Also, because of its long residence time, ocean water is homogeneous in Li concentration (about 180 μg Li/L) and isotopic composition (δ^7Li = 32‰; Chan and Edmond, 1988; You and Chan, 1996). Time-dependent $^6Li/^7Li$ variations in seawater have also been discussed recently (Misra and Froelich, 2012) based on Li-isotopes of foraminifera. These authors concluded that the δ^7Li of the seawater rose by 9‰ during the last 60 million years, resulting from changes in continental and seafloor weathering. However, evidence for the critical lack of diagenetic alteration in the analyzed foraminiferas that might produce similar trends was not given, and ~~the~~ a contribution of Li from organic sources was not considered. Marine sediments are generally rich in Li with concentrations ranging from about 100 μg/g in pelagic clays to 1 μg/g in carbonates and biogenic silica (Chan et al., 2002).

Oxygen and hydrogen, the latter as OH groups in the crystal structure of clay minerals, were a focus of extensive research on their fractionation between different types of clays and waters at temperatures from Earth's surface to 200 °C (e.g. Savin and Epstein, 1970a; Savin and Lee, 1988). The δD and $\delta^{18}O$ values of weathering clays plot on lines nearly parallel to the Meteoric Water Line with slopes close to 8, but with different intercepts. Such δD-$\delta^{18}O$ trends were also reported for varied hydroxides and oxy-hydroxides (Yapp, 1993). The relationships between δD and $\delta^{18}O$ in clay-water systems indicate that the clays are enriched in ^{18}O and

depleted in D in a temperature-dependent fashion. Savin and Epstein (1970a) and Lawrence and Taylor (1971, 1972) also demonstrated that ~~the~~ clay ~~material~~ crystals can retain ~~its~~ their isotopic signatures through further processes of erosion, transportation and deposition. Bird and Chivas (1988) showed that oxygen-isotope exchange in kaolinite being negligible, post-formational hydrogen-isotope exchange is possible at temperatures below ~80 °C. From δD and $\delta^{18}O$ of diagenetic kaolinite and 10Å clay minerals (illite, illite-smectite), Longstaffe and Ayalon (1990) reported that hydrogen-isotope re-equilibration between diagenetic kaolinite and formation water can be independent of oxygen-isotope exchange at temperatures as low as 40 °C.

Three kinds of water are usually reported in clay minerals: ~~that~~ adsorbed on the particle exterior surfaces, ~~that~~ held in interlayer positions, and OH groups held in structural sites of the mineral framework. Water held in the interlayer position of coarser clay particles is theoretically lacking in nanometric crystals as the smectite-type interlayers of the original I-S are basically dismantled by infinite dispersion. Therefore, the remaining adsorbed water isotopically exchanges with ambient water very fast; less than a few days. On the other hand, the rates of isotopic exchange between structural and ambient water are often slow and depend on the temperature and type of clay minerals. Unlike the rate of oxygen-isotope exchange, that of hydrogen-isotope exchange between structural hydrogen and hydrogen of ambient water can be relatively rapid at temperatures as low as 60 °C (O'Neil and Kharaka, 1976). As an ~~efficient~~ impressive application, Longstaffe and Ayalon (1987) reconstructed the evolutionary path for the $\delta^{18}O$ of pore fluids and associated clay minerals of the lower Cretaceous Viking Formation in the Western Canadian Basin. More studies with similar aims are available, ~~testifying for an interesting~~ with varied ~~variety of dominant~~ processes at different localities (e.g. Glasmann et al., 1989; Fallick et al., 1993; Robinson et al., 1993; Girard and Barnes, 1995; Kotzer and Kyser, 1995; Clauer et al., 1999; Zwingmann et al., 1999).

Some basics about K-Ar and Rb-Sr isotopic dating

The K-Ar method is a pioneer dating technique based on the natural decay of ^{40}K into ^{40}Ar (e.g. Dalrymple and Lanphere, 1969; Faure, 1986), which makes it especially well-suited for dating illite- and glauconite-type clay materials. It has been applied with varied success to dating such low-temperature and fine-grained separates since the attempt by Wasserburg et al. (1956), ~~however~~. This method is also ~~more~~ appropriate for dating nanometric illite-type crystals,

especially from bentonites~~, which are considered to be~~ that lack ~~detrital~~ very fine-grained detrital particles (e.g. Clauer et al., 1997), more than the related $^{40}Ar/^{39}Ar$ method, as it does not need a problematic irradiation with necessary aliquot encapsulation and restoration of the recoiled ^{39}Ar expelled during irradiation of crystals that are smaller than the recoil distance (Clauer et al., 2012; Clauer, 2013). It ~~certainly~~ needs complementary mineralogical, chemical and morphologic information on the separates. Closed-system behavior of the selected minerals is required, as for any isotopic dating method, ~~This requirement is, of course,~~ which is especially crucial for Ar ~~in~~ trapped in nanometric-sized particles, as it is not bonded to other atoms or ions in ~~a~~ the mineral structure like most of the analyzed cations of the classical isotopic dating methods. ~~Instead, Ar is~~ Rather it is only held ("squeezed") ~~physically~~ in interlayer sites without any chemical bonding with the surrounding elements due to its larger ionic radius than the radioactive ^{40}K; ~~thus making~~ it is particularly susceptible to be released by incipient alteration or weathering, ~~changes often~~ especially when ~~related to~~ temperature increases.

The Rb-Sr method, which is another pioneer method, is also well suited for the study of nanometric illite-type crystals. The behavior of K and Rb being identical in illite interlayers, it has been shown that in anchi-to-epimetamorphic conditions, the K-Ar and Rb-Sr methods often provide ~~the same~~ similar ages on the same illite fractions (e.g. Clauer and Chaudhuri, 1998), which is not found systematically in diagenetic environments (e.g. Clauer and Chaudhuri, 1995). Beside the dating aspect, the Rb-Sr method provides information in differentiating Rb, Sr, and other elements that are either substituted in the mineral structure, or adsorbed on the exterior surfaces and in interlayer sites (Clauer, 1982). This information can be ~~obtained~~ quantified by gentle leaching of various size fractions with dilute acid (e.g. 0.1M HCl or HAc), or other reagents (EDTA, acetates, etc; Clauer et al., 1993), and separate analysis of the leachates and residues ~~provides such information~~. Differentiating the Sr amounts and $^{87}Sr/^{86}Sr$ ratios from inside and outside the crystals has the advantage of identifying the content and $^{87}Sr/^{86}Sr$ ratio of Sr from interstitial fluids that interacted potentially with the nucleating and growing illite-type crystals, or from fluids that percolated through the pore system after mineral nucleation and growth (Clauer et al., 2003).

Specific analytical aspects

Illite-type nanometric crystals were first separated, studied, identified and defined by Nadeau et al. (1984). These authors explained their occurrence by dissolution of smectite layers from I-S, followed by crystallization and growth of new illite layers in the same mixed-layers. This model was ~~also~~ ~~adopted~~ promoted by Inoue et al. (1987), and Eberl and Środoń (1988). ~~Such~~ The illite-type layers of such mixed layers can be separated after infinite osmotic dispersion ~~(see~~ by a method briefly described below) to become so-called "fundamental" particles. Depending on the exact mechanism of illitization, solid-state transformation or dissolution/precipitation, and assuming that the particle separation was successful, one might expect different isotopic records for crystals of varied particle thickness, depending on the host rock, temperature and duration of the nucleation and growth processes, and chemistry of the interstitial water that contributed to the process.

Separation of fundamental particles

The whole-rock samples are gently crushed, sieved, mixed with deionized water, and disaggregated using either an ultrasonic bath or probe, or the freezing-thawing technique (e.g. Zwingmann et al., 1999). These two methods are recommended instead of crushing to avoid as much as possible communition of detrital grains into the clay-sized fractions, as the occurrence of detrital material is known to bias the results. The slurries are then treated with dilute sodium-acetate buffer, sodium dithionite and hydrogen peroxide to remove the soluble mineral phases and organic matter from illitic matrix (Jackson, 1975). The next step consists of separating the <2.0 μm size fraction of the samples by gravimetric sedimentation in deionized water following Stokes' law, and further separating the <0.2 μm fraction by centrifugation. The recovered <0.2 μm fraction is then ~~extensively~~ diluted to a concentration of 1g/40L, to ensure "infinite" osmotic swelling by breaking apart the smectite interlayers, and separated into smaller sub-fractions by continuous-flow high-speed ultra-centrifugation. The finest (<0.02 to <0.03 μm) and coarser (0.02-0.05, 0.05-0.1 μm) fractions are finally removed from corresponding diluted fluids by flocculating the suspended matter with NaCl (1M), and by removing the excess electrolyte by dialysis and repeated centrifugation (Środoń et al., 1992). The accuracy of the crystal separation can be monitored by TEM observations.

The fact that B and Li can also be held in the interlayer sites of I-S makes it essential to remove these interlayer species by cation exchange. The reason for this is the fact that the $\delta^{11}B$ of

the interlayer B can be significantly different from that of the illite tetrahedral sites (Williams et al., 2007; Fig. 3). The polyhydric alcohol mannitol is often used as a complexation agent (Hingston, 1964) to remove surface-adsorbed B, because it strongly binds to these light elements allowing easy cleaning. It is also recommended to check the purity of the reagents, especially in the case of B and Li isotopic studies, to avoid any potential chemical biases, as B and Li are common impurities in laboratory reagents. The individual size fractions are then ready to be analyzed for their mineralogical-crystallographic characteristics, and chemical and isotopic compositions.

Solid-state analysis

In recent decades, instrumentation has been developed for solid-state analysis of trace elements and of their isotopes at a microscale. In brief, instruments like the Secondary Ion Mass Spectrometer (SIMS) use a primary ion beam (most commonly consisting of O^-, O_2^+ or Cs^+) that is directed towards a flat polished sample at impact energies of a few to >20 keV under high vacuum (~10^{-9} Torr) conditions. Because the bond strength of minerals is on the order of a few electron volts (eV), these high-energy collisions break chemical bonds in minerals and a cascade of secondary atoms and molecules is ejected from sample surface, referred to as 'sputtering' (Wilson et al., 1989). A few percent of the secondary particles are ionized, and are accelerated away from sample. In most SIMS instruments, the ions pass through an electrostatic analyzer followed by a magnetic sector. After mass selection, the ions are detected ~~using~~ with either a Faraday cup or an electron multiplier for low intensity signals ~~to be quantified (~0.1 to <10^6 counts/s)~~. Complementary information about this analytical method can be found in Williams et al. (2012). Relative to traditional mass-spectrometry, SIMS has the ~~supplementary~~ advantage of eliminating the necessity for chemical extractions that may bias the isotopic ratio of interest. It can also provide high spatial resolution for examination of micro-scale chemical variations. For nanometric-sized crystals, such as fundamental clay particles, the SIMS advantage is the small volume (~10^{11} atoms) consumed for analysis with high precision allowing interpretation of chemical or temperature variations on the various nanometric size fractions (bins) potentially representing stages of crystal growth (Williams et al., 2012). The ~~lateral~~ resolution of these analyses has improved to the point where sub-micron resolution can be achieved and still provide useful precise isotope ratios (Valley and Kita, 2009); however, this resolution does not reach the

scale of nanometric clays. Solid-state SIMS analysis of Li and B (content and isotopic composition) has been applied to nanometric illite-rich clay crystals from volcanic and sedimentary rocks (Williams et al., 2012), with statistically significant results (e.g. errors <2‰ for a range of values >30‰).

Case studies of nanometric illite crystals from bentonites

Initial K-Ar results and hypotheses

Clauer et al. (1997) dated illite-rich fractions ~~smaller than~~ <0.02-0.03 µm from two bentonite beds near Trhovište and Čičarovce in the East Slovak Basin, reporting that the K-Ar age of the finest fractions was either younger (well Trh), or older than the slightly coarser fractions (well Cic; Fig. 4). This result was explained by two potential processes: either nucleation followed by growth, exemplified by coarser fractions younger than the finer, or episodic nucleation and growth with the finest crystals being the youngest. The $\delta^{18}O$ values of the same nanometric fractions appeared also to be different, relatively constant at 18‰ for the nanometric fractions of well Trh and decreasing from 12 to 10‰ for those of well Cic. These oxygen data will be discussed in a later section. In the Trhovište bentonite bed sampled at 3015 m depth, illitization lasted from ~15 Ma when the bentonite reached a temperature of 70-80 °C, to ~7 Ma when it reached a temperature of 150-160 °C. In the Čičarovce core located about 20 km away, illitization started at ~11.5 Ma in the sample buried at 2495 m depth, when it reached 70-80 °C, and it lasted until the present time at about 120 °C. ~~The point here is that~~ The data suggest that different processes can occur in the same type of rocks of the same basin that are located only about 20 km apart on a horizontal scale and 520 m apart on a vertical scale; this exemplifies how cross-basinal variations in diagenetic processes can exist and be evaluated.

The shales that sandwich the Trhovište and Čičarovce bentonite beds were also sampled for recovery of the illite nanoparticles of their I-S (Clauer et al. 1997; Honty et al. 2004). The obtained K-Ar data were systematically older than the stratigraphic age of the respective units, suggesting that the authigenic illite nucleated either on detrital particles that were already present in the rocks when illitization started, or next to such detrital crystals. This leads to the assumption that detrital particles were incorporated into the separated size fractions of the shale beds. Similar K-Ar ages older than the depositional age of nanometric illite crystals from shales were found in

other contexts, supporting the generally admitted occurrence of detrital "cotaminants" (Środoń and Clauer, 2001; Środoń et al., 2006). However, it cannot be denied that the authigenic crystals may have, alternatively, incorporated in their structure chemical elements, such as radiogenic ^{40}Ar, that were released by dissolution of previous detrital micaceous components~~, especially radiogenic ^{40}Ar,~~ in a postulated closed interstitial space. This hypothesis is reasonable as illitization occurred in very-low permeable, fine-grained sedimentary strata. Not being able to escape, this excess of "detrital" radiogenic ^{40}Ar could have been scavenged by the new illite precipitates, as reported for recent deep-sea red clays from Pacific Ocean sediments (Clauer, 2006). However, this explanation ~~does not hold~~ is not valid if comparing the results with those from bentonites, which are as impermeable as the nearby shales, containing probably even less interstitial fluids. The determining difference at this point is that the nanometric crystals of bentonites consist almost exclusively of authigenic illite, whereas those of shales apparently contain also nanometric detrital illite.

Concerning illitization in argillaceous sediments, it is ~~certainly~~ appropriate to mention a study by McCarty et al. (2008) who showed that nucleation of smectite-rich particles from Gulf Coast sediments occurred on the surface of detrital particles or grains and not in their interlayer sites. This observation could explain, at least partly, the unsuccessful attempts to date authigenic nanometric illite crystals from shales, and why separation of pure authigenic illite from associated detrital particles is especially difficult, if not impossible, in shale-type sediments. It also tends to imply that authigenesis of new illite-type particles in the general smectite-to-illite trend only depends on the alteration of associated detrital material if the reaction includes an overall dissolution of the detritus followed by a crystallization of a new generation of I-S.

In bentonites of the East Slovak Basin

Nanometric sized illite-type particles of I-S from other cored bentonite beds ~~in~~ of the East Slovak Basin were studied after the work by Clauer et al. (1997), to investigate the regional extent of illitization: K-Ar dating and the varied physical/chemical conditions during nucleation and growth interpreted from δ^{18}O and δD isotope characterization have been reported (Clauer et al., 2014b). The nanometer-sized particles next to salt-bearing formations showed more advanced illitization, but the duration of the process remained identical, whereas the oxygen and hydrogen isotope signatures of the parental brines were modified. A comparison of the stratigraphic ages of

the bentonite beds and the onset of illitization based on ~~the~~ K-Ar ages shows that illitization started during the regional mid-Miocene subsidence detected in most bentonite beds, from as early as ~17.5 to as late as ~11.5 Ma, depending on the varied timing at the different geographic locations. Based on age differences in the selected beds, the calculated sedimentation rate was found to vary from less than 300m/Ma to more than 500m/Ma, and the thermal gradient to range from as high as ca. 60 °C/km to less than 50 °C/km. The K-Ar ages also pointed to either short- or long lasting illitization in closely located beds: short (less than 2 Ma) when the onset of illitization started shortly after sedimentation and long (up to 6-8 Ma) when the onset started long after sedimentation. The K-Ar ages of the nanometric size fractions from eight different bentonite beds indicate episodic pulses that appear to have lasted from as short as 1 million years to as long as 6 million years (Fig. 5). The pattern also suggests episodic illitization at some locations.

~~The~~ Illite $\delta^{18}O$ varies little when crystal size changes, whereas δD ranges over almost 100‰, albeit more than half of the data lie within ±15‰ of -45‰ (Fig. 6). These wide δD changes are even more apparent in a diagram comparing them to the K-Ar ages (Fig. 7). As the crystallization temperature ~~recorded by different parameters~~ did not change significantly during crystal growth in most samples, the observed variations relate to changing interacting fluids, depending on sample location, immediate environment, timing and duration of illitization. These local variations in the timing and duration of illitization in bentonite beds contrast with generally accepted large-scale fluid connectivity, especially for sandstone aquifers. The stable isotope compositions of nucleating and growing illite-type crystals of bentonite beds that are of limited porosity and permeability, and therefore of reduced fluid-rock ratios, give ~~another~~ a local insight into the fluid-temperature regime of sedimentary basins ~~in identifying local~~ rather than large-scale processes. The key concept is in the effective fluid-rock ratio of the host rocks during nucleation and growth of the authigenic clay material. At this scale, illitization appears more to be of an episodic diagenetic process lasting variably along different crystallization pathways and to various extents, in closely located samples, but obviously depending on conditions that vary even within beds that were considered to be mineralogically and chemically homogeneous. ~~This homogeneity may be disturbed by tectono-thermally driven migrating fluids able to affect locally the mineralogical and chemical compositions of the beds by nucleation of a new generation of illite-type crystals.~~

B and Li contents and isotopic compositions were also measured in nucleating and

589 growing nanometric illite-rich crystals from I-S of the same bentonite beds in the same East
590 Slovak Basin (Clauer et al., 2009). Most of the B contents correlate positively with the $\delta^{11}B$ of
591 the nanometric crystals (Fig. 8). ~~Interestingly,~~ The B content and $\delta^{11}B$ of three analyzed
592 nanosized fractions of most bentonite beds from East Slovak Basin correlate positively and define
593 a common initial field with a theoretical high B content of about 475 µg/g and a $\delta^{11}B$ of about
594 +7‰. This "reservoir" could correspond to B-rich minerals, for instance of evaporitic origin
595 (Swilhart et al., 1986; Vengosh et al., 1992; Bottomly and Clark, 2003), and such were described
596 in the East Slovak Basin (Honty et al., 2004). These evaporites could have dissolved during the
597 progressive burial-induced diagenetic alteration and slightly increasing temperature, and
598 ~~releasing~~ released some of the scavenged B. The second B-rich component, with much lower
599 contents of about 30 µg/g and a $\delta^{11}B$ of -5‰ or of about 100 µg/g with a $\delta^{11}B$ of -17‰, could
600 relate to organic matter that occurs in almost all sedimentary beds. When sediment layers are
601 interbedded with bentonite beds, their fluids carrying organic matter-derived components
602 ~~penetrate~~ migrate into the bentonite layers during progressive burial (Williams et al., 2013). This
603 transfer of organic-derived B into bentonite beds was also reported by Środoń (2010). If this
604 transfer is continuous during burial-induced illitization, the coarser growing illite nanocrystals
605 should be enriched in B relative to the initial nucleating illite. However, this is not always true, as
606 shown in the studied illite nanofractions of bentonite beds from East Slovak Basin (Fig. 8). When
607 growing, the nanometric fractions (numbered 1 to 3 from finest to coarsest) that are identified
608 with distinct symbols for each sample do not systematically trend towards a "reservoir"
609 containing high B amounts with high $\delta^{11}B$ (to the upper right of the figure). The B contents can
610 also remain about constant, which is the case for the nanofractions of three samples (fractions 1
611 to 3 of the open squares, the full squares and the open circles). In the case of the three fractions of
612 another sample (identified by grey squares), the trend is again towards high B contents, but with
613 low $\delta^{11}B$.

614 The influence of temperature on $\delta^{11}B$ values of the <0.02 µm fractions is also visible from
615 correlations between $\delta^{11}B$ of the illite crystals and present-day temperature ~~in~~ of the ~~drill holes~~
616 wells for five out of seven <0.02 µm fractions ~~for which the bore-hole temperatures are available~~
617 (Fig. 9). Five data points fit a correlation line with a $\delta^{11}B$ close to 0‰ for the lower temperature
618 of about 120 °C and $\delta^{11}B$ of -12‰ for the higher temperature of 165 °C. The two other fractions
619 plot along a second correlation line indicating lower $\delta^{11}B$ values of -13.5 ‰ at 95 °C and -15.5‰

at 135 °C. This distribution suggests the input of more isotopically light ^{10}B derived from kerogen as temperature increases.

At the highest temperatures (>130 °C), most of the illite-rich nanometric clay fractions yield positive δ^7Li values (up to ~12‰), while the Li contents are systematically low, below 20 µg/g. At lower temperatures (<115 °C), the size fractions yield systematically negative δ^7Li values and most have higher Li concentrations (up to 140 µg/g; Fig. 10). This suggests that increasing temperature fractionates ^7Li from organic matter into the fluids. Comparing the Li contents and δ^7Li of the studied nanometric clay fractions indicates the major correlations. The less thermally mature sediments contain clays that are characterized by a Li content of 10 µg/g with a δ^7Li of -16‰, a Li content of 40 µg/g with a δ^7Li of about -13‰, or a Li content of about 140 µg/g with a δ^7Li of -22‰. This decreasing δ^7Li with increasing Li content suggests that higher Li organic-rich sediments preferentially derive ^6Li from organics, while ~~the~~ ^7Li goes preferentially into fluids during thermal maturation.

In bentonites of the Baltic Basin

The distribution of Li and B (and N) was ~~studied~~ examined in I-S from Ordovician-Silurian K-bentonites of the Baltic Basin (Williams et al., 2013). These elements are linked to thermal maturation of organic matter with fluid signatures that are distinct from those resulting from usual burial of sediments or from those migrating ~~partly~~ through basement rocks. Boron and Li-isotope variations (>10‰) of three illite nanofractions (<0.02, 0.02–0.05 and 0.05–0.2 µm) relate mainly to changes in the fluid composition during illite growth and in the temperature gradient across the basin (SW to NE) ~~that was~~ induced by tectonic activity during the Caledonide orogen (Środoń et al., 2009).

The K-bentonite beds mark stratigraphic timelines (Late Ordovician-Early Silurian), and were correlated across the basin (Huff et al., 2002), while illitization ages of these K-bentonite beds reflect either the timing of a tectonic-related temperature gradient or that of deep burial. The K-Ar data define a central zone of mostly older ages (392-382 Ma) extending from Denmark to Estonia, bordered to the northwest and southeast by bentonite beds with younger ages (362-302 Ma) resulting from slower burial (Fig. 11A). Based on their oxygen isotope compositions, ~~the illite-rich clay~~ illite from the slowly buried bentonites precipitated from different (isotopically lighter) fluids than ~~those~~ that of ~~in~~ the central basin.

In the central Baltic Basin, bentonites were deposited on a carbonate platform near Estonia, grading to deep shales near Denmark and Poland. Compositional variations in illite of the K-bentonite beds reflect fluids from different sources. High B (>250 μg/g) and Li (>100 μg/g) contents were observed in bentonite illite of ~~the~~ northeastern Estonia ~~region~~. These trends follow a thermal gradient for illitization with high tectonically-induced temperatures recorded ~~for illites formed~~ near Poland (200 ˚C) to low temperatures (90 ˚C) documented in northeastern Estonia. The B- and Li- isotope ratios also show significant trends in ~~the~~ illite ~~crystals~~ across this thermal gradient: $\delta^{11}B$ decreases from southwest (+18‰) to northeast (-4‰), while $\delta^{7}Li$ increases from -10‰ near Poland to +32‰ (seawater value) near Estonia (Fig. 11B).

The Cambrian Alum shale, which is a regional hydrocarbon source rock, is an adequate potential source for interpretation of isotopically light B and Li in the migrating hydrocarbon-related fluids associated with illitization of the bentonite beds in the Baltic Basin. More than 50% of the B and Li from the Alum shale are associated with organic matter. Organics released from kerogen during thermal maturation created a fluid that mixed the isotopically light B and Li ~~released by~~ derived from hydrocarbon generation (with high B and Li concentrations), with the B and Li ~~derived~~ from basement (plutonic) sources near Estonia. With increasing thermal maturity, illite $\delta^{11}B$ and $\delta^{7}Li$ of the Alum shale varied by ~15‰ (Fig. 12). The $\delta^{11}B$ of illite was istotopically light at gas-generation thermal grades, while the $\delta^{7}Li$ was isotopically heavier, however still lighter than seawater $\delta^{7}Li$. This suggests a difference in the bonding of ^{10}B and ^{6}Li in the kerogen and therefore differences in the release temperatures of these atoms during thermal maturation. ~~Nonetheless,~~ The trends (magnitude of isotopic change) observed in the Alum shale source rock ~~are~~ being similar to those measured in the overlying bentonite beds, ~~and~~ it can be concluded that organic sources of B, Li (and N) dominated in fluids that migrated through the bentonites beds from the southwestern Baltic Basin, while basement-derived fluids dominated in those of the northeastern Baltic Basin. The B and Li contents and isotope compositions record paleofluid changes during illite crystallization, and on the basis of careful consideration of local chemical inputs, they can be used to identify regional pathways of chemically distinct oil and gas related fluids.

In bentonites of the Appalachian orogen

Nanometric illite particles from <0.02 to 0.2 μm of K-bentonites from northwestern

682 Georgia (USA) were studied for their oxygen and hydrogen stable isotope geochemistry, and K-
683 Ar isotopic dating in order to better constrain the tectono-thermal history of the Appalachian
684 orogen throughout the northern American Mid-Continent (Clauer et al., 2013). The crystal
685 populations are ordered I-S with very homogeneous crystal thickness distributions across the
686 particle sizes of each sample, but with variable crystallite thickness ranges depending on the
687 location of the samples. The volume-weighted and area-weighted mean thicknesses of the
688 crystallites were calculated according to the Bertaud-Warren-Averbach theory (Eberl et al.,
689 1997), as well as the parameters α (= mean of the natural logarithms of the thicknesses) and β^2 (=
690 variance of the natural logarithms of the thicknesses). On the basis of these parameters,
691 illitization occurred in all size fractions, except for one sample, by simultaneous nucleation and
692 crystal growth (Fig. 13). In that specific sample, simultaneous nucleation and growth was
693 followed by growth without nucleation.
694 The K-Ar ages of the nanometric fractions organize into two isochrons at 319.9 ± 2.0 Ma
695 with an initial $^{40}Ar/^{36}Ar$ ratio of 271 ± 66, and at 284.9 ± 1.2 Ma with an initial $^{40}Ar/^{36}Ar$ ratio of
696 310 ± 44 (Fig. 14). One data point above the older isochron and three between the two isochrons
697 suggest some detrital contamination for the former and a possible supplementary generation of
698 nanoparticles for the three others. Those with the older crystallization age consist of illite and
699 illite-rich I-S, whereas those with the younger age contain only I-S, mainly with expandable
700 interlayers. The two K-Ar isochron ages fit the age ranges published previously for similar K-
701 bentonites with ~~regional~~ age patterns between 240 and 270 Ma in the southwestern region,
702 between 270 and 300 Ma in the central and the southern Appalachians, and between 315 and 370
703 Ma to the north.
704 The two generations of illite crystals yield very consistent $\delta^{18}O$ values at +17 ± 1‰ for
705 the older and at +21 ± 1‰ for the younger (Fig. 15A), while the δD values do not show any
706 trend. The correlation between $\delta^{18}O$ and age is confirmed by a comparison with the K-Ar ages
707 (Fig. 15B). If crystallization temperatures of the nanometric illite were between 100 and 200 °C,
708 on the basis of complementary microthermometric determinations, the hydrothermal fluids had
709 $\delta^{18}O$ values of 4 to 8 ± 1‰ at the lower temperature of 100 °C, and of 11 to 15 ± 1‰ in the same
710 locations at the higher temperature of 200 °C. Apparently, the $\delta^{18}O$ of the fluids remained
711 unchanged during local illitization, but varied depending on the timing and geographic location
712 of the samples.

In Walsen Dike metabentonite

The Cretaceous Pierre Shale near Walsenburg (Colorado, USA) is an organic-rich shale containing bentonite beds that was cross-cut normal to bedding by a basaltic dike known as the Walsen Dike (Johnson, 1964). The thermal gradient across the contact metamorphic zone provides an ideal natural example of smectite illitization in the bentonite bed. This contact-metamorphosed bentonite has been used to ~~successively~~ model illitization in response to the thermal pulse (Lynch, 1985; Pytte and Reynolds, 1989), reaction kinetics of NH_4 fixation in the illite interlayer (Williams and Ferrell, 1991), timing of B substitution in the tetrahedral sites (Williams et al., 2007) and of Li in octahedral sites of the authigenic illite (Williams et al., 2006). Illitization of smectite in this contact metamorphic aureole was shown to have occurred from 500 ˚C at the contact with the basaltic dike (lamprophyre) to 200 ˚C in the buried country rock.

Bostick and Pawlewicz (1984) determined the thermal maturity using vitrinite reflectance of the Pierre Shale organic matter. The temperature zone that generated mature hydrocarbons (equivalent to the "oil window") occurred between 8 and 25 m away from the shale/dike contact. Both B and Li showed a maximum substitution in~~to~~ authigenic illite ~~in~~ of this oil window ~~of the shale~~ with highest concentrations of 75 µg/g tetrahedral B (Williams et al., 2007) and 40 µg/g octahedral Li (Williams et al., 2012). B-isotope values in the bulk Walsen Dike metabentonite range from +8 to -17‰ when approaching the dike (~500 ˚C). However, the tetrahedral-B values (after removal of interlayer-B) ~~range~~ scatter less, from -2 to -17‰, with $\delta^{11}B$ increasing up to +8‰ ~~at~~ about 10 m away from dike contact (Fig. 16). This $\delta^{11}B$ value of +8‰ in the tetrahedral site is maintained in the country rock away from dike. On the basis of the temperature gradient, the water $\delta^{11}B$ composition decreased from ~16‰ to 4‰ as temperature and organic maturity increased in the oil window. Again, addition of ^{10}B to the pore fluids at high temperatures was interpreted as resulting from release of B from the surrounding thermally matured organic matter.

The δ^7Li values of the same <2.0 µm I-S fraction increase from country rock toward the dike contact from -15 to -5‰ (Fig. 16). The isotopic composition in the shale is light away from dike, potentially influenced by the organic-rich source of light B and Li ~~in the shale~~ (Williams et al., 2012; 2013). It is also possible that the more positive δ^7Li near the dike has been biased by some ^7Li introduced by migrating metasomatic fluids. Assuming that the first illite crystals precipitated at ~80 ˚C in the country rocks, which is common in deeply buried sediments, the

744 δ^7Li composition of the water was initially ~22‰ (Williams et al., 2012). If the water
745 composition remained constant during temperature increasing to 200 ˚C, the coarse illite would
746 be expected to have a δ^7Li of +9‰. No reasonable temperature can be calculated, given the local
747 geological constraints that could produce the observed δ^7Li of –10.5‰ for the illite crystals
748 precipitated from a fluid with a +22‰ δ^7Li value ~~of value~~. An external source of ^{6}Li that lowered
749 the δ^7Li value of the pore water is therefore required. The decreasing δ^7Li value away from dike
750 is consistent with ^{6}Li diffusion away from heat source. If all of the illite grew at the maximum
751 regional temperature of 200 ˚C, the water would have had an initial δ^7Li composition of +15‰,
752 decreasing to 3‰ as illite grew. This scenario could be explained by diffusion of Li away from
753 the igneous heat source, with the light isotope diffusing faster than the heavy isotope.
754 Within the 13-m contact metamorphic aureole of the dike, the B and Li isotope trends are
755 parallel, ~~which is a~~ convincing proving that the minerals generated during one fluid event. Also to
756 be mentioned is the change in δ^7Li from +3 to -11‰ in progressively coarser crystals of the
757 bentonite from the contact zone (Williams et al., 2012). Such change could reflect the declining
758 temperature as the dike cooled, ~~the~~ with a water composition considered ~~to remaining~~ constant.
759
760 **Studies of nanometric illite crystals of shales and sandstones**
761
762 *In shales of the East Slovak Basin*
763 The initial test of K-Ar dating nanoparticles from shales was made as a comparison with
764 nanocrystals from nearby bentonite beds in the East Slovak Basin reported in a previous section
765 (Clauer et al., 1997). The age differences were significant among the shale and bentonite
766 nanometric separates of identical stratigraphic age: the K-Ar age of the <0.02 μm fractions of the
767 Cic 1/20 bentonite was at 7.4 ± 2.4 Ma, while that of the nearby Cic 1/16 shale yielded 39.0 ± 1.9
768 Ma. The K-Ar age of the shale fractions increased to about 68 Ma for the 0.02-0.05 and 0.05-0.1
769 μm fractions, while those of the corresponding bentonite remained at 3.8 ± 2.0 Ma. The coarser
770 0.1-0.3 μm fraction of the shale even increased more to about 109 Ma relative to a constant 5.1 ±
771 1.2 Ma age for the equivalent size fraction of the bentonite. Significantly older than the 13-Ma
772 deposition timing (Lower Sarmatian), the K-Ar ages of the shale-bearing nanoparticles require
773 the generally admitted occurrence of detrital crystals or mineral fragments. In summary, the K-Ar
774 age of the nanoparticles extracted from shales continuously increased from 39.0 ± 1.9 to 108.8 ±

775 3.0 Ma, while those of the nearby bentonite unit remained at about 5.0 ± 2.0 Ma. Considering the
776 age of the detrital nanoparticles at ~110 Ma and that of the authigenic nanoparticles at ~5 Ma, a
777 rough calculation suggests that the finest nanoparticles from the shale unit already consisted of
778 one third of detrital components, and that this amount increased to two thirds of the total
779 nanocrystals in the coarser 0.02-0.1 μm size.

780 This initial result was somehow disappointing, therefore not raising much concern to look
781 more into abnormally high K-Ar ages ~~only a few other studies were devoted since to decrypt~~
782 ~~explain how the abnormally high K-Ar ages~~ of diagenetic nanocrystals from shales ~~are~~
783 ~~abnormally high~~. ~~This is mainly due to~~ The belief that even nanometric size fractions of shales
784 consistently represent mixtures of detrital and authigenic crystals that are not separable by the
785 available techniques did obviously not encourage further studies on the topic. However, if ~~the~~
786 ~~belief of~~ a ~~challenging~~ physical separation of both, the authigenic and detrital clay crystals ~~is yet~~
787 ~~correct~~ seems impossible, ~~that of an impossible~~ an independent analysis of the authigenic and
788 detrital crystals is not. In fact, a way for a separate analysis of both in ~~mineral fractions of~~ any
789 size fraction, is possible by subjecting illite mixtures to alkylammonium leaching (Chaudhuri et
790 al., 1999; Clauer, 2011). The leaching is based on the specificity of alkalammonium cations of
791 stochiometrically replacing K in dioctahedral micas, not in trioctahedral micas. If the detrital illite
792 of the leached mixture is di-octahedral, the K-Ar age of the residue after leaching will be
793 indicative of the crystallization age of the tri-octahedral authigenic illite. Conversely, if the
794 authigenic illite is di-octahedral, the K-Ar age of the residue after leaching will be close to that of
795 the detrital supply. For completeness another way to overcome ~~the~~ an impossible mechanical
796 separation of authigenic and detrital nanometric illite crystals was explored by mathematical
797 simulations combining the K-Ar system of the aggrading authigenic and degrading detrital
798 minerals (Lerman et al., 2007; Clauer and Lerman, 2009).

799 In studying flysch material from Podhale-Orava Basin in the Western Carpathians, Środoń
800 et al. (2006) reported that nanometric mineral assemblages only homogenize completely their K-
801 Ar system when subjected to low-grade metamorphic conditions, from 125 to 180 °C, which
802 confirmed earlier conclusions of Środoń and Clauer (2001) in a similar study on nanoparticles
803 across the Teisseyre-Tornquist tectonic zone of Pomerania (Poland). However, no information is
804 yet available about how authigenesis of nucleating crystals and altering detrital crystals combine
805 chemically. Środoń et al. (2002) provided a theoretical simulation of the illitization process using

a nucleation and growth mechanism, but they did not take into account the potential concomitant alteration of the ~~initial~~ detrital components. Interestingly, a fast burial followed by a slow burial provides older K-Ar ages for the nanocrystals than the reverse, a slow burial followed by a fast burial (Fig. 17), which is not necessarily the expected result if considering temperature increase as the only driving parameter.

In Paleogene shales of the French Massif Central

Nanometric fractions of the well-known "Illite du Puy" were also analyzed (Clauer, unpublished; data presented in Table 1). Interestingly, this illite described first in an 80-m thick Late Eocene (Ludian; 40-34 Ma) argillite-type unit that rests on the plutonic basement of the French Massif Central (Gabis, 1963) also consists of mixtures of authigenic and detrital nanometric crystals. ~~T. Bardot (1998) provided mineralogic and chemical analyses of this illite.~~ Five shale samples were collected near Brives-Charensac in the center of the Puy-en-Velay basin to document further the authigenic-detrital relationship of nanometric illite-rich shale separates.

The samples were subjected to the specific preparation of nanoparticle separation including chemical treatments, infinite dispersion and high-speed flow-through centrifugation. The size fractions consist of the 1Md illite polytype in sample 2, with some kaolinite in the coarser fractions of sample 5, and some authigenic K-feldspar in sample 1. Coarse size fractions (>10 μm) of four samples were also separated and purified, identified by XRD and K-Ar dated to establish the ages and amounts of the ~~expected detrital~~ components. The >10 μm fractions of samples 4 and 5 were selected because they consisted almost exclusively of recognizable detrital quartz, micas, K-feldspars and plagioclases with a small amount of secondary quartz. Conversely, the coarser >10 μm fractions of samples 1 and 2 were selected because XRD analysis did not detect detrital components, nor were the usual odd shapes observed by microscope (e.g. Hunziker et al., 1986).

Several fractions (<0.03, 0.03-0.05, 0.05-0.1, 0.1-0.3, 0.3-2 μm and >10 μm) of the selected samples were K-Ar dated. The individual K-Ar ages range from 42.8 $\pm$ 1.4 Ma for the <0.03 μm fraction of sample 3 to as old as 269.0 $\pm$ 6.0 Ma for the >10 μm fraction of sample 5 (Table 1). The K-Ar ages are positively correlated with size increase of the fractions, supporting the increasing content of detrital material when size increases. The four finest <0.03 μm fractions plot on a line that cuts the coordinates at the origin in the Harper (1970) diagram precisely

relating the K_2O with the radiogenic ^{40}Ar contents (Fig. 18). These data points being apparently representative of crystals for which the radiogenic ^{40}Ar relates strictly to the ^{40}K content without any excess in radiogenic ^{40}Ar from detritals, the extracted ages can be considered to be geologically meaningful as shown repeatedly in the literature (e.g. references in Clauer and Chaudhuri, 1995). The stratigraphic age of the host rocks is therefore close to about 46 Ma, which is slightly older than the attributed Upper Eocene deposition timing (40-34 Ma). At this point, either the dating technique or the attributed stratigraphic age should be reconsidered.

In addition to the ^{40}K and radiogenic ^{40}Ar equilibrium line cutting the coordinates at zero, noteworthy is the almost vertical array including the four size fractions of sample 3 and the coarse >10 µm fraction of samples 4 and 5 (Fig. 18). This vertical array suggests that the authigenic illite is mechanically mixed with illitic material of detrital origin without any visible interaction between both, the detrital illite having an identical K_2O content of about 6 wt% and an older K-Ar age of 260 $\pm$ 10 Ma. This older age corresponds to an already identified Upper Permian tectono-thermal episode that affected the Hercynian plutonic basement on which the Cenozoic sedimentary sequence was deposited, suggesting that the detrital illite of the Upper Eocene sedimentary sequence ~~originated in~~ represents broken micas from nearby Hercynian plutons. A second sub-vertical line fits through three data points of sample 2, suggesting the same mechanical mixture without crystal interaction in similar size fractions. Also ~~to be mentioned~~, the K-Ar system of the detrital components of the vertical lines appears not to have been affected by the 46-Ma diagenesis inducing authigenesis of nanometric illite.

~~Noteworthy~~ Of interest is also ~~is~~ the fact that this second vertical array fitting the data points of the finer fractions of sample 2 deviates into an oblique line towards higher K contents including either the coarser size fractions of sample 2 or most fractions of sample 1 (Fig. 18). A similar oblique line joins the finest fraction of sample 5 with the highest K content to the coarsest fraction of sample 5 that consists only of detrital particles. In fact, the diagram outlines three major linear directions: (1) an oblique line fitting through the data points of the nanometric pure authigenic illite crystals, and which provides the age of these authigenic crystals; (2) a vertical line corresponding to addition of detrital particles characterized by an excess of radiogenic ^{40}Ar for no change of the K content; and (3) oblique trajectories that combine addition of variable amounts of K and radiogenic ^{40}Ar, which is well illustrated by the data points of sample 5. Based on the finest nanometric fraction of sample 5, which basically does not contain detrital particles,

the K increase is induced by nucleation and growth of authigenic crystals. This hypothesis is supported by the other data points of sample 5 that trend towards the detrital end-member pole having the same K content as the other detrital crystals of similar size. Depending on individual sample evolution, the mechanical mixing of detrital and authigenic nanometric crystals could also be affected by some alteration of the detritals that would release K accumulating in an almost "closed" shale-type pore context. And last, but not least, it cannot be excluded that the age difference between the stratigraphic determination and the K-Ar age of the finest nanometric illite crystals at 46 Ma, instead of the expected 34-40 Ma, is biased by a very small addition of detrital material. An alternative discrete addition of radiogenic ^{40}Ar in excess due to in situ alteration of detrital minerals can be discarded as the data points of the authigenic and detrital crystal mixtures plot on the expected trends drawn through the authigenic and detrital end-members.

Complementary information is provided by the $^{40}Ar/^{36}Ar$ vs. $^{40}K/^{36}Ar$ isochron diagram that displays an array through the two finest size fractions of samples 3 and 5 (Fig. 19A). This array has an initial $^{40}Ar/^{36}Ar$ value of about 300, which matches the atmospheric $^{40}Ar/^{36}Ar$ ratio (Lee et al., 2006; Mark et al., 2011), therefore qualifying this line as an isochron with a meaningful age at 45.0 $\pm$ 2.2 Ma. This isochron, whose age does not match the stratigraphy for reasons just discussed, precisely includes the data points of the four finest nanometric fractions. The other ~~noteworthy~~ feature to consider is the unique trend for the data points of all fractions between 0.03 and 10 µm that intersects the $^{40}Ar/^{36}Ar$ ordinate at a significantly negative value (Fig. 19B). As the initial $^{40}Ar/^{36}Ar$ ratio of any mineral can never be negative, this trend ~~only~~ confirms the mixture of detrital and authigenic particles as demonstrated by Clauer and Chaudhuri (1995). The <0.03 µm fractions consist of 1Md illite without detectable contaminating particles of any type, and yield close individual K-Ar ages from 42.8 $\pm$ 1.4 to 48.2 $\pm$ 1.5 Ma (Table 1). When these fractions become larger, they appear to be progressively ~~"polluted"~~ mixed with ~~by~~ a detrital ~~admixture~~ component, despite the fact that some of these coarser fractions were selected because optical microscopic observation and XRD analysis did not identify visible detrital particles. The data confirm, together with all presently available results on nanoparticles extracted from shales (Clauer et al., 1997; Środoń and Clauer, 2001; Honty et al., 2004; Środoń et al., 2006), why separation of pure authigenic illite from associated detrital particles remains especially challenging in shale-type sediments. However, this case study shows that the smallest nanometric illite fractions of shales can also consist only of authigenic crystals, as for most

bentonites and many sandstones.

Of shales and sandstones from the Mahakam Basin

The clay fraction of the shaly/sandy sedimentary sequence beneath the Mahakam Delta (eastern Kalimantan, Indonesia) consists mainly of I-S, with minor kaolinite and/or dickite, discrete detrital illite and chlorite (Clauer et al., 1999). The smectite-to-illite conversion mechanism depends on the lithology of the host rocks, as well as on the identification technique used: it evolves similarly in the shales and the sandstones on the basis of the XRD data of micrometric fractions (<0.4 μm) from surface to about 4000 m depth, but differently for the K-Ar data of the same particles.

The entire stratigraphic interval (from 18 to 0 Ma) shows a pronounced, continuous decrease in the K-A age of the clay fractions with depth from about 80 Ma for the pure detrital end-member at the subsurface to about 20 Ma for the almost pure authigenic <0.4 μm fraction of the sandstones buried at 4000 m. The K-Ar system of the clay material from the associated shales evolves differently as the K-Ar age decreases from about 80 Ma at subsurface to 55 Ma at 1700 m depth, while remaining about constant below (Fig. 20). If the K-Ar age of the progressively buried clay mixtures would have resulted from continuous addition of K and variable release of radiogenic ^{40}Ar in both rock types, as often assumed, it should have decreased continuously until the deepest sample, which is the case for the sandstones, but not for the shales. The almost constant K-Ar pattern of the <0.4 μm fractions in the deeper Mahakam shales has been tentatively explained by a significant decrease in the simulated rates of K addition and radiogenic ^{40}Ar escape, each about 1 %/Ma (Lerman et al., 2007; Clauer and Lerman, 2009). The combined reduction in the K supply to, and radiogenic ^{40}Ar escape from the shales below 1700 m depth, could have resulted from reduction of the porosity and/or permeability due to progressive compaction. Considering that the depleted supply of the sole K cannot explain by itself the almost constant K-Ar ages for illite of the shales in a sediment about 2300 m thick, it would not either support a "steady state" as claimed for the Gulf Coast sediments (Morton, 1985). Application of the K-Ar method is therefore of special interest as it shows that any diagenetic process needs to affect the K and ^{40}Ar contents of both the authigenic and detrital minerals. Here, a continuous diagenetic process is needed to obtain constant K-Ar ages relative to depth, but with limited supply and release rates, and therefore with reduced rock-fluid interactions.

Illite nanometric crystals of two sandstones buried at ~4000 m beneath the Mahakam Delta yield a mean K-Ar age of 15.7 ± 1.6 Ma, which is younger than the stratigraphic age but still slightly biased by minute amounts of discrete detrital illite (Clauer et al., 2004). A model taking into account the occurrence of the discrete detrital illite reduces the K-Ar age to 14.4 ± 0.7 Ma, while the K-Ar ages of the nanometric illite from associated deep shales remain significantly older, above 40 Ma. While the calculated contents of K and radiogenic ^{40}Ar, and therefore the K-Ar ages of the nanofractions, fit with the analytical results in the sandstones, they do so in the shales only if one considers an excess of radiogenic ^{40}Ar from 3000 m depth downwards to fit the analytical data (Fig. 21). This excess of radiogenic ^{40}Ar at depth is intriguing because if it would be only and strictly related to the detrital minerals, it should have decreased with depth because of increasing pervasive alteration of the detrital minerals due to increased burial-related temperature. It is therefore possible that this required excess of radiogenic ^{40}Ar to explain the age differences between nanometric illite of sandstones and shales, does not relate to the occurrence of detrital materials in the size fractions, but rather to an accumulation of radiogenic ^{40}Ar released by the altering detrital minerals, which could not escape from pore space at depth greater than about 3000 m. Combined with the data of the Le Puy illite obtained in the previous section, this calculation confirms that not only can an excess of radiogenic ^{40}Ar be present in shale nanofractions, but also that it could result from its sequestration in the pore system of the rock matrix.

Despite lack of visible detrital material in some nanometric fractions of shales, increasing K-Ar ages with grain size tend to confirm that authigenic crystals could precipitate at the surface of original detrital grains, giving progressively idiomorphic shapes to the crystals on which they crystallized. However, it cannot be denied that these authigenic crystals could also have incorporated radiogenic ^{40}Ar in excess. In favor of this hypothesis is the fact that no observations validate either dissolution of detrital crystals or a solid-state process, refuting in turn a cannibalistic K supply to the authigenic nanocrystals, which had to be limited. Notewothy here is the fact that discrete radiogenic ^{40}Ar in excess has been reported in recent Pacific deep-sea red clays for which confinement is not insured by their compaction, but by their mechanical plasticity (Clauer, 2006).

Of sandstones of the Eastern Paris Basin

961 Middle and Lower Triassic sandstones from the eastern Paris Basin only reached a
962 shallow burial depth of <2500 m and were only subjected to temperatures of <100 °C. Despite
963 this limited depth and crystallization temperatures, these sandstones contain extensive amounts of
964 filamentous illite similar to widely described illite cementation at deeper depth (~3000-5000 m)
965 and higher temperatures (~120-150 °C; Fig. 22). Nanometer-sized illite-rich subfractions
966 extracted from such sandstones buried to 1825-2000 m depth, were analyzed for their chemical
967 and $\delta^{18}O$ isotope compositions, and were dated by the K-Ar and Rb-Sr methods (Blaise et al., in
968 preparation). Illite K-Ar dating reports two crystallization events for the <0.05 μm illite separates,
969 at 179.4 ± 0.8 and 149.4 ± 0.3 Ma, during the Lower and Upper Jurassic, on the basis of an
970 isochron display. Illite separates coarser than 0.05 μm systematically contain detrital minerals
971 that bias the K-Ar ages towards older ages. The $\delta^{18}O$ of the coarser (>0.05 μm) fractions are most
972 often lower than those of the finer fractions, confirming ~~in turn~~ isotopic heterogeneity at this
973 nanometric scale with occurrence of detrital minerals. For the <0.05 μm illite separates, there is
974 also a tendency for $\delta^{18}O$ to decrease with depth, suggesting higher cystallization temperatures,
975 unless the decrease identifies some addition of surface-derived water to the migrating
976 hydrothermal fluids.
977 The nanometric fractions of two samples were dated by Rb-Sr after gentle acidic (1M
978 HAc) leaching of each fraction (Blaise et al., in preparation). For one of the two samples, the Rb-
979 Sr ages are systematically younger than the corresponding K-Ar ages, whereas they are identical
980 for all size fractions of the second sample. Calculated on the basis of the leachate-untreated
981 couples of each fraction, Rb-Sr ages depend essentially on the initial $^{87}Sr/^{86}Sr$ of the obtained
982 arrays that vary narrowly from 0.7108 ± 0.0001 to 0.7134 ± 0.0003 (2σ), which is significantly
983 above the seawater $^{87}Sr/^{86}Sr$ ratio between 0.7068 and 0.7076, during a potential Jurassic illite
984 crystallization (e.g. Jones et al., 1994). For the sample that yields consistent younger Rb-Sr ages
985 than the corresponding K-Ar ages, the difference ~~can be speculated to~~ might be due to increased
986 $^{87}Sr/^{86}Sr$ ratios of the leachates by addition of soluble minerals that were dissolved by leaching.
987 In that case, the Rb-Sr age of the leachate-untreated couples could have been lowered if this
988 soluble mineral phase depleted in Rb contained Sr with an $^{87}Sr/^{86}Sr$ ratio higher than that of the
989 Sr from illite nanocrystals. This difference calls for a crystallization timing necessarily after that
990 of illite. Its solubility would not have allowed it to be resistant to a fluid flow at the thermal
991 conditions of illite crystallization.

Elemental analysis of the acid leachates showed that for the sample with identical Rb-Sr and K-Ar ages, the soluble mineral phase consists of dominant Ca-Mg carbonate in one nanofraction (sample EST-1 in Fig. 23). The soluble mineral phase present in the different fractions of the second sample with similar Rb-Sr and K-Ar ages (sample EST-2 in Fig. 23) is a Ca-phosphate, which could represent partial dissolved detrital apatite detected by XRD and wet chemical analysis. However, as the crystallization temperature of the illite nanocrystals was fairly low at about 100 °C, the hydrothermal fluids that induced illitization did probably not alter significantly the detrital crystals detected in the coarser nanocrystals, their $^{87}Sr/^{86}Sr$ ratio being partly biased by addition of either dissolved detrital P-rich apatite, or carbonates that had to crystallize after illite precipitation.

In summary, illitization was induced by episodic fluid flows related to thermal anomalies that were fueled by the North Atlantic rifting and possibly the initial Rhine-Graben rifting, although these rift systems were located several hundred kilometers away from the eastern Paris Basin. Beyond the fact that the obtained data confirm K-Ar and $\delta^{18}O$ results of nanometric illite crystals from other sandstones, the additional Rb-Sr analysis also highlights the complex relationship between geodynamical events, thermal anomalies and related fluid movements. The combined data especially show that remote tectonic activities may impact crystallization of nanometric illite crystals in quiescent basins through long-distance fluid flows, particularly in sandstones.

A concept for illitization based on isotopic studies of nanometric illite

Differentiation of illite nanocrystals by K-Ar dating of alkylammonium leached crystals

Alkylammonium leaching of K-bearing minerals has the specific advantage of opening the mica-type interlayers and stochiometrically replacing K of dioctahedral micas (Sears et al., 1998; Chaudhuri et al., 1999). This specificity can be used to evaluate K-Ar ages of the tri-octahedral illite from variably sized mixtures, also of nanometric size (Clauer, 2011), especially in the case of shales containing mixtures of authigenic and detrital di- and tri-octahedral illite. The concept is the determination of the K-Ar ages of illite before and after leaching and of calculating the K-Ar ages of the tri-octahedral illite crystals or interlayer domains that were not emptied of their K by the alkylammonium cations. Comparison of the K-Ar ages of untreated and

leached micrometric size fractions from two Early-Cambrian Estonian claystones collected a meter apart showed how precise the procedure could be. Even with strictly identical mineralogical characteristics and similar K-Ar ages of the illite mixture, the illite component of the size fractions collected next to each other consisted in fact of two types of illite crystals, with age differences depending on the amounts of crystals sensitive to alkylammonium cationic exchanges (Chaudhuri et al., 1999). In another experiment, the K-Ar ages of aklyammonium-leached nano- to micrometric illite from two levels of a thick Late-Cretaceous bentonite bed of the Disturbed Belt in Montana (USA) indicated that illite that crystallized first at the rim of the bentonite bed was identical to that from the center of the bed (Clauer, 2011). The same conclusion was obtained for growing nanometric illite crystals of a Middle-Miocene bentonite bed from the East Slovak Basin. Tracing the homogeneity or heterogeneity of pure illite from bentonite beds, and therefore of the interacting fluids is obviously possible.

A general finding of alkylammonium leaching is that varying K-Ar ages, and probably light-element isotope compositions, of nanometric illite crystals from I-S, whether increasing or decreasing, reveal the occurrence of heterogeneous crystals, unless they identify structural defects in the same mineral structures. Whatever the reason for the structural modifications, the variable K-Ar results from alkylammonium-leached illite particles indirectly highlight these changes. In summary, the alkylammonium leaching technique appears very appropriate to distinguish different types of illite crystals mixed in nanometric size fractions, if of different origin.

Timing and duration of crystal nucleation and growth by K-Ar and Rb-Sr dating

Dating illite nanocrystals of bentonite and sandstone units can be successful, often producing geologically meaningful ages. This is not yet the case for shales for which illitization is either mechanically "polluted" by the occurrence of older nanometric particles, or follows a process involving a nucleation on or next to detrital particles preventing separation of the authigenic from detrital crystal, or incorporates some radiogenic ^{40}Ar present in the pore space from alteration of the detrital minerals. Available results from East Slovak Basin show that during burial (= an extended process with progressive temperature increase with or without slow chemical changes in the fluid chemistry), the step between nucleating (<0.02 μm) and growing (0.02-0.2 μm) can be either short (1-2 Ma) or long (>2 Ma) lasting, with a mechanism that can be either a combined nucleation and growth process, or continued nucleation (e.g. in a

supersaturated fluid). The available data have also shown that the finest nanocrystals can be either older or younger than the coarser, and that illitization can be unique or multi-episodic. During a short lasting thermal activity (such as a hydrothermal fluid flow or fault activity), the ages are within analytical uncertainty, without visible distinction for the process unless successive events occurred or changing chemical signatures occurred.

Dating by the Rb-Sr method adds complementary information about the origin of the solutes in interacting fluids with the initial $^{87}Sr/^{86}Sr$ ratio of soluble minerals that can be close or not to those of sea-, meteoric- or hydrothermal waters. The initial Rb-Sr dating attempt was on nanosized illite crystals of the Čičarovče and Trhovište sites in the East Slovak Basin (Clauer et al., 2003). The nanometric fractions were leached with dilute HCl (1M) to distinguish the Sr adsorbed on the exterior surfaces of the illite crystals or trapped in soluble mineral phases such as salts, carbonates, sulfates or oxides, from that trapped in the illite crystals. The $^{87}Sr/^{86}Sr$ ratios of the leachates were found to decrease systematically with increasing particle size that is to say during crystal growth. The straightforward explanation for such a decrease towards seawater $^{87}Sr/^{86}Sr$ ratio is that there was an addition of Sr from outside the bentonite beds into the pore space where smectite crystals were nucleating first, followed by illite nucleation. The $^{87}Sr/^{86}Sr$ ratios of the leachates can therefore be considered to represent mixtures of initial Sr released from precursor minerals between ash deposition and start of the diagenetic alteration of the volcanic glass into smectite with addition of Sr during diagenesis by interstitial fluid diffusion into the bentonite beds, highlighted by light isotope fractionation.

In the case of the nanometric illite crystals from Triassic sandstones of the eastern Paris Basin, the Sr of the leachates has been shown to be a mixture of Sr with varied origins: one of hydrothermal origin trapped by the nucleating illite crystals, and another obviously carried by late migrating fluids that favored crystallization of Ca-Mg carbonates.

More potential for combined Rb-Sr and K-Ar methods applied to illite nanocrystals

The next case study, despite being analytically very limited as applied to only one set of nanometric fractions of one bentonite sample, has been integrated in this review because of its application to nanocrystals of smectite-rich instead of illite-rich I-S, and because of its potential in combining K-Ar and Rb-Sr data (Clauer, unpublished). The following discussion is therefore

to be considered more as preliminary information on initial nanometric illitization; it is still far from aany solid interpretation.

The bentonite core sample belongs to a well drilled into the prolific hydrocarbon-producing Campos Basin from southeastern Brazilian continental offshore margin. There, oil is mainly hosted by Upper-Cretaceous sandstone turbidites that are interbedded with altered volcanic ash beds in the center of the basin (Alves et al., 1993; Caddah et al., 1998). Buried to approximately 2800 m, the selected bentonite bed is of Santonian stratigraphic age (86-83 Ma). It was handled and prepared like those described in the above analytical section for separation of the nanometric sized crystals. The extracted size fractions (<0.02, 0.02-0.05, 0.05-0.1 and 0.1-0.2 μm) were X-rayed and dated by the K-Ar and Rb-Sr methods. The different size fractions consist of a swelling smectite-type mineral with identical air-dried patterns characterized by a peak at about 15 Å. Kaolinite was observed in the coarser fractions, while illite layers were only identified in the finest size fractions. On the basis of the positions of the d_{009} and d_{0010} XRD peaks (Środoń, 1980), an amount of about 5% illite layers was estimated in the smectite-rich I-S. The K_2O contents and expandability of the nanocrystals were also compared to data obtained by Šucha et al. (1993) in the East Slovak Basin to approximate the present-day temperature. This temperature is at about 65-70 °C, which represents the lower limit for illitization, and explains the very limited smectite-to-illite conversion.

The K-Ar ages of the four studied fractions are all younger than the stratigraphic reference, confirming a dominant occurrence of authigenic minerals. Those of the two finest size fractions (<0.02 and 0.02-0.05 μm) range from 19 to 21 Ma, while those of the two coarser fractions (0.05-0.1 and 0.1-0.2 μm) range from 47 to 56 Ma. Plots of these data in a Harper (1970) diagram confirm the two groupings (Fig. 24): the two finest fractions plot on a line intersecting the coordinates at the origin, while the two coarser fractions plot on a second line intersecting the ordinate at a negative value, which indicates an excess of radiogenic ^{40}Ar in the fractions enriched in K. In the isochron diagram, the two finest fractions plot on a line that yields an age of 19.9 $\pm$ 0.7 Ma, with an initial $^{40}Ar/^{36}Ar$ ratio of 300, while the coarser fractions plot along a second line with a higher slope, an age at 51.4 $\pm$ 4.8 Ma and an initial $^{40}Ar/^{36}Ar$ slightly higher at about 304, which could be explained, at least partly, by an excess radiogenic ^{40}Ar scavenged by the newly-formed crystals that was suggested by the data distribution in the Harper (1970) diagram.

The same size fractions were also analyzed for their Rb-Sr system after gentle leaching with dilute HCl (1M). Because these leachates carry Sr that is not constitutive of the clay particles for the reasons already formulated, elements external to the smectite-rich crystals are expected to provide information about the chemical conditions of the inter-particle volumes of the clay particles, while the leached residues are expected to provide the chemical and Sr isotopic composition of the nanocrystals themselves. In this respect, it is appropriate to recall that such gentle acid leaching alters neither the Rb-Sr nor the K-Ar system of the clay particles, regardless of type, size or crystallinity degree (Clauer et al., 1993). It might also be remembered that the data points of the untreated, leached and residue aliquots of a given size fraction normally define arrays on $^{87}Sr/^{86}Sr$ vs. $^{87}Rb/^{86}Sr$ diagrams, depending on the quality of the analytical determinations (e.g. Clauer and Chaudhuri, 1995). The significance of these lines strictly depends on the material studied: a geological meaningful isochron, for instance, can only be claimed if the analyzed material is homogeneously authigenic. If this is not the case, the lines represent mixtures of particles of varied origins.

The Rb-Sr data unexpectedly display two arrays with negative slopes in an isochron diagram for the untreated (U in the figure), residue (R in the figure) and leachate (L in the figure) fractions of the coarser smectite-rich fractions (Fig. 25). Beyond the complex distribution, it can be agreed that the analytical conditions were adequate, as the data points of the L, U and R of the four size fractions fit individual lines. Among the four obtained lines, those of the coarser (0.05-0.1 and 0.1-0.2 μm) separates yield negative slopes with a higher initial intercept at about 0.71098 than the $^{87}Sr/^{86}Sr$ ratios of the residues. Such distribution patterns were already described for clay material of oceanic volcanic deposits (Clauer, 1982; Clauer et al., 2011) and have been reported to be mixing lines. They outline $^{87}Sr/^{86}Sr$ ratios for minerals of volcanic origin, that is to say lower than the ratio of the environmental fluids (= the initial values of the lines) and the authigenic soluble minerals removed by leaching. The initial $^{87}Sr/^{86}Sr$ ratios of the two mixing lines together with the L, U and R data points of the coarser fractions consisting only of smectite is about 0.71098, which is significantly above the seawater $^{87}Sr/^{86}Sr$ ratio (Jones and Jenkyns, 2001). Conversely the line through the two coarse leached smectite fractions (black dots in Fig. 25) has an initial $^{87}Sr/^{86}Sr$ ratio of about 0.70868, which is within the seawater ratio about 20-30 Ma ago, at the time determined by K-Ar dating. Of interest is the fact that this line has a slope giving an age of about 25 Ma. Also, the initial $^{87}Sr/^{86}Sr$ ratio of the line through the more illite-

rich fine (<0.05 and 0.05-0.1 μm) fractions is about 0.71098, which is the initial value of the two mixing lines through the coarser smectite residues. And last but not least, the slope of the line through the two fine-grained residues containing some illite layers provides an age of about 2 Ma.

This dataset can be ~~converted into~~ tentatively explained by the following process: (1) pure smectite (here of the 0.05-0.1 and 0.1-0.2 μm coarse fractions) crystallized from volcanic ash in contact with seawater about 25 Ma ago, age given by the line joining the two residues with an initial seawater $^{87}Sr/^{86}Sr$ ratio, the line being therefore an isochron; and (2) some K was supplied later by different pore fluids having a high $^{87}Sr/^{86}Sr$ of about 0.71098 more typical for sedimentary interstitial fluids that interacted with deposited minerals. The K supply initiated nucleation and growth of illite layers, necessarily in the smallest <0.02 and 0.02-0.05 μm fractions, the line joining the two finer residues being again an isochron. Deposition of the volcanic glass occurring during Santonian time (86-83 Ma), initial smectite might have crystallized during a period between ~51 Ma ago, on the basis of the K-Ar data, and ~25 Ma ago, on the basis of the Rb-Sr data. Nucleation and growth of illite layers could have started at this time (~20 Ma ago on the basis of the K-Ar data), and have ended ~2 Ma ago on the basis of the Rb-Sr data. It looks like the start of illite crystallization was initiated by the changing composition of the interstitial fluid ~25-20 Ma ago.

Such discrete and long-lasting crystallization episodes appear reasonable in the Campos bentonites because available K was limited, while the temperature was at the lower limit of potential illitization. As a complementary remark it must be reiterated that such a scenario remains hypothetical as it is based on a single sample, with the specificity of consisting mostly of dominant smectite with some illite layers. The purpose was to highlight the potential of combined K-Ar and Rb-Sr studies, especially on smectite-rich nanocrystals, for a change.

Thermal conditions of illite nucleation and growth by $\delta^{18}O$ tracing

The initial attempt to analyse $\delta^{18}O$ of nanocrystals was published on illite from Čičarovče and Trhovište sites of the East Slovak Basin (Fig. 26; Clauer et al., 2003). The two sets of size fractions yielded different $\delta^{18}O$ values: those of the illite fractions from Čičarovče are lower than those from Trhovište. When crystal size increases, the former decrease slightly from 12 to 10‰, while those from Trhovište increase slightly, from 16.5 to 18‰,. Together with different K-Ar

ages, the $\delta^{18}O$ trends of the illite nanocrystals of the two sites suggest different nucleation and growth processes occurring only 20 km apart in the same basin. The decrease in $\delta^{18}O$ with increasing particle size at Čičarovče seems to relate to a slow temperature increase during the 3.5-Ma-long illitization process, whereas the almost constant $\delta^{18}O$ with particle size increase at Trhovište seems to relate to an almost constant temperature between 11 and 8 Ma. The $\delta^{18}O$ of the fluids associated with crystal nucleation and growth remained in a similar narrow range for the two populations of fundamental particles, with an overlapping calculated mean $\delta^{18}O$ of 0 $\pm$ 3‰ at Trhovište and of 2 $\pm$ 1.5‰ at Čičarovče on the basis of the temperatures estimated from organic maturation data at about 120 °C at Čičarovče and at about 160 °C at Trhovište. These estimates agree reasonably well with those by Šucha et al. (1993) based on the crystallization temperatures derived from maturation temperature of organic matter in the same East Slovak Basin by Francú et al. (1990). In fact, the differences identified by K-Ar dating are frequently supported by $\delta^{18}O$ data that often allow distinction of probable temperature changes from changes in the fluid chemistry.

Which illitization mechanism in shales?

The systematically older ages for nanometric illite fractions in shales favor the general belief of an occurrence of detrital material, which corresponds to an excess of radiogenic ^{40}Ar relative to the K content. However, these detrital crystals are not "just" mechanically mixed, as is the case in coarser size fractions of sandstones, because their odd shapes would be recognizable by microscope observation, which seems not to be always the case. In fact, these detrital crystals could serve as supports of newly nucleating authigenic crystals with interaction of the most recent fluids with the nearby detrital crystals that alter while authigenic crystals grow on them and possibly modify their shape to become idiomorphic.

Crystallization of Le Puy illite also questions the generally admitted basic "mechanical" mixing of authigenic and detrital particles to explain isotopic ages older than the stratigraphic reference (e.g. Clauer and Chaudhuri, 1995). This "mixing" also occurring at nanometric size clearly discriminates between the isotopic data of nanoparticles of bentonites and sandstones from those of nanoparticles of shales. These consistent results question also the multiphase illitization model of Yates and Rosenberg (1996, 1997, 1998) based on a dissolution-precipitation process following a ripening step in which metastable intermediate phases are transformed into

end-member illite. Not based on the fundamental particle concept (Nadeau et al., 1984), Yates and Rosenberg's model (1996, 1997, 2011) was conceived on the basis of hydrothermal experiments, which do not reproduce natural conditions, as shown again recently in a comparative study of naturally buried and experimentally matured shale rocks and <2 μm fractions (Clauer et al., 2014).

The high number of varied models, including those of Altaner and Bethke (1988) and Altaner and Ylagan (1997), as well as of Rosenberg et al. (1980), Whitney and Northrop (1988), Whitney and Velde (1993) and Ferratge et al. (2011), provide varied explanations for illitization that end up being confusing. The isotopic approach may not yet explain the intimate mechanisms of illitization, but it clearly outlines a process depending on numerous physico-chemical factors that can vary from case to case and even within a ~~study~~ single case. For instance, nucleation can be, but need not to be, followed by growth; it can be unique or multiple and last for varied durations in progressive burial conditions; and it appears "fast" when temperature is significantly above 150 °C. The stable isotope data provide information about the temperature, when the chemical composition of the interacting fluids can be constrained. Alternatively, temperature determination by independent methods allows using the $\delta^{18}O$ signature for interpreting the fluid compositions. In shales, authigenic illite-type crystals seem to equilibrate with fluids faster than the detrital particles, primarily because first nucleated crystals are in equilibrium with fluids whereas larger crystals only equilibrate slowly (Williams and Hervig, 2006). Admittedly, experimental conditions do not mimic natural conditions, as experiments limit environmental variables in order to simplify the interpretation of results. All these aspects may, at least partly, explain why modeling of illitization is somehow confusing with rules that apparently only apply to specific cases.

Light-element isotope tracing of interactions during illitization and organic-matter maturation

Combined thermal maturation of mixtures consisting of clay crystals and organic matter was studied in the Eocene Kreyenhagen Shale from the San Joaquin Basin, California USA, by subjecting the outcrop <2 μm clay fraction from the shale to hydrous-pyrolysis experiments (Clauer et al., 2014a). Intended to alleviate the problem of mineral and chemical variations in the initially deposited rocks of natural sequences in a basin, hydrous pyrolysis experiments of the immature outcrop sample did not induce significant changes in the clay mineral composition in

1239 experiments conducted for 72 h at temperatures from 270 to 365 °C, far from those induced by
1240 natural burial-induced maturation. Interestingly, large amounts of smectite layers remained in the
1241 I-S of the pyrolyzed outcrop <2 μm fraction during the thermal experiments, especially above
1242 310 °C, despite leaching the mineral powders with H_2O_2 before pyrolysis. No K transfer being
1243 noticed into the clay material and therefore no illitization being detected, smectite appears to have
1244 inhibited rather than promoted generation of expelled oil from the decomposition of bitumen.
1245 This hindrance results from bitumen impregnating the smectite interlayer sites, but also from lack
1246 of available K for illitization.

1247 In a recent study, the $\delta^{11}B$ and B content, and the $\delta^{18}O$ and δD of such <2 μm clay and
1248 organic mixtures were determined and compared to the total organic content (TOC) of the
1249 fractions pyrolyzed at temperatures from 270 to 365 °C for 72 h, and at a higher 365 °C step for
1250 216 h (Clauer, Williams, Fallick and Lewan, unpublished). The data show a significant
1251 correlative decrease of the TOC and B contents, 75 and 33% respectively, of the untreated
1252 immature outcrop <2 μm fraction after the initial pyrolysis experiment at 210 °C during 72 h
1253 (Fig. 27). Afterwards, the B and TOC (probably mixed left-over kerogen and bitumen) contents
1254 remained almost constant, while $\delta^{11}B$ decreased continuously, suggesting that B with low $\delta^{11}B$
1255 was released to the fluids. The clay $\delta^{18}O$ value also decreased continuously, quite significantly
1256 after the first pyrolysis step at 210 °C during 72 h, perhaps pointing to a release of oxygen with
1257 high $\delta^{18}O$. To be mentioned is the fact that the $\delta^{18}O$ values were obtained here on a clay fraction
1258 contaminated by kerogen despite H_2O_2 treatment, which may be analytically questionable
1259 because products like COF_2 might have formed during fluorination, and the released O_2 might not
1260 be pure. The yield data are not conclusive on this possibility, but the hypothetical bias induced by
1261 the occurrence of kerogen could be of limited impact, as $\delta^{18}O$ decreases with experimental
1262 temperature increase, whereas clay δD increases (Fig. 27).

1263 The $\delta^{11}B$, $\delta^{18}O$ and δD values all decreased during the further pyrolysis steps. As each
1264 individual pyrolysis experiment started with the same immature outcrop <2 μm fraction, it
1265 becomes apparent that the pyrolysis experiments at 365 °C during 72 h and 216 h (labeled 4 and
1266 5 in figure 27) have an identical impact on the B contents and $\delta^{11}B$. Conversely, the experiments
1267 at 349 and 365 °C during 72 h (labeled 3 and 4 in figure 27) have similar important impacts on
1268 $\delta^{18}O$, while at 365 °C at 216 h (step labeled 5 in figure 27) has a more limited effect. A graphical

outline of the theoretical amount of released B during each pyrolysis experiment can be constructed (Fig. 28), showing that the B released from kerogen becomes isotopically heavier at each higher-temperature step, with an overall release of about 135-140 μg/g at each step and a $\delta^{11}B$ that shifts progressively from -2 to +9‰. Of course, the contents need to be adjusted to the amount of removed TOC if considering that all mobile B is bound to kerogen rather than bitumen. In fact, not much more B is released from organics after the pyrolysis experiment at 270 °C during 72 h (labeled step 1 in figure 28), when taking into account the content of the whole removed TOC, but with increasing $\delta^{11}B$. The data support that most B is stored in the sedimentary organics, and that this B is isotopically light compared to rocks and minerals. Another interesting fact is the correlation between the decreasing $\delta^{18}O$ and the largest removal of TOC during the initial experiment at 270 °C during 72 h. If the occurrence of kerogen has a limited impact on the released $\delta^{18}O$, this finding raises a basic question about the meaning of the $\delta^{18}O$ of clay-sized minerals mixed with organics in naturally maturing sediments. During initial maturation, it is possible that most of the released oxygen with high $\delta^{18}O$ was released by the organics, which would modify the interpretation of oxygen isotope data as thermal tracers of the clay material, if clay is still mixed with some organic material. Van Krevelen (1950) diagrams generally used to assess the origin and maturity of kerogen and petroleum show that both O and H are released from kerogen with increasing thermal maturity, so that the source of oxygen from all minerals and organic compounds in a bulk shale-type rock must be considered quantitatively. At natural thermal conditions above 100 °C, the data suggest that most of the oxygen is retained by the clay material. The δD values increase consistently at each temperature step, supporting that release of proyium (^1H) is energetically favored over deuterium, which needs higher temperature or longer time than protium to be released from organics.

These experimental data confirm that B of illite is isotopically lighter than that in pore fluids, and that the source of the isotopically light B is organic matter. The B data confirm again that the illite tetrahedral B-O bond is as strongly tied as the Si-O bonds with wide isotopic variations. The results on Li contents and isotope compositions of nanocrystals potentially interacting with organics remain scarce, but they outline trends that follow often those of B.

Conclusions

The present review summarizes the innovative aspects of light-element isotopic (δD, δ^7Li, $\delta^{11}B$, $\delta^{18}O$) tracing and isotopic (K-Ar and Rb-Sr) dating of nanometric illite-rich crystals extracted mostly from bentonites, but also from sandstones and shales in diagenetic to anchi-metamorphic conditions. ~~If~~ The study of nanocrystals from bentonite and sandstone beds ~~are~~ is often successful and well under control, but problems remain to separate mechanically authigenic illite-type crystals from detrital components, also at nanometric size of shale units. Mixed authigenic crystallization and detrital alteration complicates deciphering the results, but a way to separate them, at least for the use of the K-Ar method, is alkylammonium leaching of the crystal mixtures. As alkylammonium chains have the specificity of slipping into the interlayers of mica-type sheetsilicates, especially into those of dio-octahedral crystalline organization, and to replace stochiometrically K, this finding is of interest in studying the K-Ar system of di- and tri-octahedral illite mixtures, to potentially differentiate detrital from authigenic crystals.

The initial K-Ar studies in the late 1990s have ~~highlighted~~ pointed to the fact that no age information is lost during crystal nucleation and growth, so that it can be considered that details of the whole illitization process are stored in the illite crystals. By combining K-Ar, Rb-Sr, δD and $\delta^{18}O$ studies, a comparision of nucleating and growing crystals that become illitic allows calculation of reaction rates and process durations, together with crystallization temperatures and fluid chemistry depending on the water/rock ratios. Not only do such studies confirm that illitization is not continuous during burial, but they indicate it can last over extended but variable periods of time, or be episodic, sometimes successively so. The Rb-Sr method provides complementary information about the origin of the solutes from interacting fluids though comparison of the $^{87}Sr/^{86}Sr$ ratio of the nucleating crystals, which depends also on the water/rock ratio, with that of the leached Sr outside of the crystal structures. The δD and $\delta^{18}O$ values of the illite crystals provide information about the nucleation or growth temperature, either increasing during burial or remaining constant during a short-lasting thermal episode. Occurrence of organic matter mixed with the crystals may bias the $\delta^{18}O$ of the crystallizing and growing illite crystals, if the data provided here are not analytically biased, as organics could release oxygen with abnormally high $\delta^{18}O$ during maturation.

A major finding of isotopic studies of nanometric illite crystals relates to B, for which the largest reservoir in sedimentary deposits is the organic material. Most of this organic-derived B yields light $\delta^{11}B$ to fluids upon maturation, and that fixed in illite is isotopically light relative to

1331 the fluids. The heavy ^{11}B preferentially fractionates into bitumen. The B data also confirm that
1332 the illite tetrahedral B-O bonds are as strong as, or stronger than the Si-O bonds with isotopic
1333 variations nearly as great as those of δD. Clay-organic matter interactions in sedimentary
1334 environments can, therefore, be traced by monitoring the B contents and isotope composition of
1335 clays and organics during thermal maturation. The results of Li contents and isotope composition
1336 of nanocrystals remain scarce, appearing more complicated than B due to the multiple phases that
1337 may incorporate Li and also to analytical uncertainties. When interacting with organics, Li
1338 follows trends that are similar to those of B, but the thermal energy for Li release from organics
1339 may differ. If so, these two "heteroatoms" variously released from organic matter under different
1340 thermal conditions, may be useful tracers of organic maturation, which will be readily recorded in
1341 the stable framework of authigenic illite that crystallized in rock volumes where organics
1342 matured.
1343

1344 ## Acknowledgements

1345

1346 We are very deeply indebted to all who contributed to the studies that were referred to
1347 here as having provided support to this review. Jan Środoń, Sam Chaudhuri and Richard L.
1348 Hervig are among those who deserve our gratitude for their contribution and interest. Many of the
1349 nanometric size fractionations, which results were discussed in this review, were completed by
1350 Mrs M. Zielinska of the Geological Institut of Krakow who deserves also special thanks for her
1351 excellent technical contribution. At last, not least, we are very thankful to the two anonymous
1352 reviewers for their thoughtful comments and remarks, which helped improve the submitted
1353 version of this contribution.
1354

1355 ## References

1356

1357 Ahn, J.H. and Peacor, D.R., 1987, Kaolinitization of biotite: TEM data and implications for an
1358 alteration mechanism. American Mineralogist, 72, 353-356.
1359 Aja, S.U., 1995, Thermodynamic properties of some 2:1 layer clay minerals from solution-
1360 equilibration data. European Journal of Mineralogy, 7, 325-333.
1361 Altaner, S.P. and Ylagan, R.F., 1997, Comparison of structural models of mixed-layer

illite/smectite and reaction mechanisms of smectite illitization. Clays and Clay Minerals, 45, 517-533.

Alves, D.B., Mizusaki, A.M.P. and Caddah, L.F.G., 1993. Camadas de cinzas vulcanicas no Santiniano (Cretaceo Superior) da Bacia de Campos, Brasil. Simposio de Geologia do Sudeste, 3, Rio de Janeiro, SBG, Atas, 37-42.

Bird, M.I. and Chivas, A.R., 1988. Stable-isotope evidence for low-temperature kaolinitic weathering and post-formational hydrogen-isotope exchange in Permian kaolinites. Chemical Geology, 72, 249–265.

Blaise et al. - Reconstructing fluid-flow events in Triassic sandstones of the eastern Paris Basin by combined chemical (major and rare-earth elements) and isotopic (oxygen) tracing, and (K-Ar and Rb-Sr) dating of nanometric illite particles. In preparation.

Boles, J.R. and Franks, S.G., 1979, Clay diagenesis in Wilcox sandstones of southwest Texas: Implications of smectite diagenesis on sandstone cementation. Journal of Sedimentary Petrology, 49, 55-70.

Bostick, N.H. and Pawlewicz, M.J., 1984, Paleotemperatures based on vitrinite reflectance of shales and limestones in igneous dike aureoles in the Upper Cretaceous Pierre Shale, Walsenburg, Colorado. In: Woodward, J., Meissner, F.F. and Clayton, J.L., (Eds.), Hydrocarbon Source Rocks of the Greater Rocky Mountain Region, Rocky Mountain Association of Geologists, Denver, Colorado, 387-392.

Bottomly, D.J., Chan, L.H., Katz, A., Starinsky, A. and Clark, I.D., 2003, http://onlinelibrary.wiley.com/doi/10.1111/j.1745-6584.2003.tb02426.x/abstract Lithium isotope geochemistry and origin of Canadian Shield brines. Groundwater, 41, 847-856.

Burley, S.D. and Flisch, M., 1989, K/Ar geochronology and the timing of detrital I/S clay illitization and authigenic illite precipitation in the Piper and Tartan fields, outer Moray Firth, UK North Sea. Clay Minerals, 24, 285-315.

Caddah, L.F.G., Alves, D.B. and A.M. Mizusaki, 1998, Turbidites associated with bentonites in the Upper Cretaceous of the Campos Basin, offshore Brazil. Sedimentary Geology, 115, 175-184.

Chan, L.H. and Edmond, J.M., 1988, Variation of lithium isotope composition in the marine environment: A preliminary report. Geochimica et Cosmochimica Acta, 52, 1711–1717.

Chan, L.H., Alt, J. and Teagle, D.A.H., 2002, Lithium and lithium isotope profiles through the

upper oceanic crust: A study of seawater-basalt exchange at ODP Sites 504B and 896A. Earth and Planetary Science Letters, 201, 187-201.

Chaudhuri, S., Środoń, J. and Clauer, N., 1999, K-Ar dating of illitic fractions of Estonian "Blue Clay" treated with alkylammonium cations. Clays and Clay Minerals, 47, 96-102.

Clauer, N., 1982, Strontium isotopes of Tertiary phillipsites from the Southern Pacific: Timing of the geochemical evolution. Journal of Sedimentary Petrology, 52, 1003-1009.

Clauer, N., 2011, Another insight into the illitization process by K-Ar dating of micro- to nano-metric illite-type particles leached with alkylammonium cations. Clay Minerals, 46, 593-612.

Clauer, N., 2013, The K-Ar and $^{40}Ar/^{39}Ar$ methods revisited for dating fine-grained K-bearing clay minerals. Chemical Geology, 354, 163-185.

Clauer, N., Chaudhuri, S., Kralik, M. and Bonnot-Courtois, C., 1993, Effects of experimental leaching on Rb-Sr and K-Ar isotopic systems and REE contents of diagenetic illite. Chemical Geology, 103, 1-16.

Clauer, N. and Chaudhuri, S., 1995, Clays in Crustal Environments. Isotope Dating and Tracing. Springer Verlag, Heidelberg, New York, 359p.

Clauer, N. and Chaudhuri, S., 1996, Inter-basinal comparison of the diagenetic evolution of illite/smectite minerals in buried shales on the basis of K-Ar systematics. Clays and Clay Minerals, 44, 818-824.

Clauer, N., Środoń, J., Francú, J. and Šucha, V., 1997, K-Ar dating of illite fundamental particles separated from illite/smectite. Clay Minerals, 32, 181-196.

Clauer, N. and Chaudhuri, S., 1998. Isotopic dating of very low-grade metasedimentary and metavolcanic rocks: techniques and methods. In: Frey, M. and Robinson, D. (Eds.), Low-Grade Metamorphism, Blackwell Science, Oxford, 202-226.

Clauer, N., Rinckenbach, T., Weber, F., Sommer, F., Chaudhuri, S. and O'Neil, J.R., 1999, Diagenetic evolution of clay minerals in oil-bearing Neogene sandstones and associated shales from Mahakam Delta Basin (Kalimantan, Indonesia). American Association of Petroleum Geologists Bulletin, 83, 62-87.

Clauer, N., Liewig, N., Pierret, M.C. and Toulkeridis, T., 2003, Crystallization conditions of fundamental particles from mixed-layers illite-smectite of bentonites based on isotopic data (K-Ar, Rb-Sr and $\delta^{18}O$). Clays and Clay Minerals, 51, 664-674.

Clauer, N., Rousset, D. and Środoń, J., 2004, Modeled shale and sandstone burial diagenesis

based on the K-Ar systematics of illite-type fundamental particles. Clays and Clay Minerals, 52, 576-588.

Clauer, N., 2006, Towards an isotopic modeling of the illitization process based on data of illite-type fundamental particles from mixed layered illite-smectite. Clays and Clay Minerals, 54, 119-130.

Clauer, N. and Lerman, A., 2009, A model for potassium gain and radiogenic argon loss during burial illitization based on analytical data. 46th Annual Meeting of The Clay Minerals Society, Billings, MT, June 5-11, 2009, p. 91.

Clauer, N., Williams, L., Honty, M. and Šucha, V., 2009, Li and B isotopic tracing of illite nucleation and growth in bentonite units of the East Slovak Basin. 46th Annual Meeting of the Clay Minerals Society, Billings, MT, June 5-11, 2009, p. 93.

Clauer, N., O'Neil, J.R., Honnorez, J. and Buatier, M., 2011, $^{87}Sr/^{86}Sr$ and $^{18}O/^{16}O$ ratios of clay minerals from a hydrothermal mound near the Galapagos rift as records of origin, crystallization temperature and fluid composition. Marine Geology, 288, 32-42.

Clauer, N., Zwingmann, H., Liewig, N. and Wendling, R. (2012) Comparative $^{40}Ar/^{39}Ar$ and K-Ar dating of illite-type clay minerals: A tentative explanation for the age identities and differences. Earth Sci. Rev., 115, 76-96.

Clauer, N., Fallick, A.E., Eberl, D.D., Honty, M., Huff, W. and Aubert, A., 2013, K-Ar dating and $\delta^{18}O$-δD characterization of nanometric illite from Ordovician K-bentonites of the Appalachians: Illitization and the Acadian-Alleghenian tectonic activity. American Mineralogist, 98, 2144-2154.

Clauer, N., Lewan, M.D., Dolan, M.P., Chaudhuri, S., and Curtis, J.B., 2014a, Mineralogical, chemical and K-Ar isotopic changes in Kreyenhagen Shale whole rocks and <2 μm clay fractions during natural burial and hydrous-pyrolysis experimental maturation. Geochimica et Cosmochimica Acta, doi: 10.1016/j.gca.2014.01.007.

Clauer, N., Honty, M., Fallick, A.E., and Šucha, V., 2014b Regional illitization in bentonite beds from East Slovak Basin based on isotopic characteristics (K-Ar, $\delta^{18}O$ and δD) of illite-type nanoparticles. Clay Minerals, 49, 165-194.

Collins, A.G., 1975, Geochemistry of Oilfield Waters. New York, Elsevier. 496p.

Connolly, C.A., Walter, L.M., Baadsgaard, H. and Longstaffe, F.J., 1990, Origin and evolution of formation waters, Alberta Basin: I, Chemistry. Applied Geochemistry, 5, 375-396.

1455 Dalrymple, G.B. and Lanphere, M.A., 1969, Potassium-Argon Dating. Freeman, San Francisco,
1456 258p.
1457 Dayal, R., 1975, Clay-sea water interaction at elevated pressures: PhD Thesis, Dalhousie
1458 University, Halifax, Nova Scotia, Canada, 234p.
1459 Drits, V.A., Sakharov, B.A., Lindgreen, H. and Salyn, A.L., 1997, Sequential structure
1460 transformation of illite-smectite-vermiculite during diagenesis of Upper Jurassic shales from
1461 the North Sea and Denmark. Clay Minerals, 32, 351-71.
1462 Drits, V.A., Eberl, D.D. and Środoń, J., 1998, XRD measurement of mean thickness, thickness
1463 distribution and strain for illite and illite/smectite crystallites by the Bertaut-Warren-Averbach
1464 technique. Clays and Clay Minerals, 46, 461-475.
1465 Dudek, T., 2001, Diagenetic evolutionof illite/smectite in the Miocene shales from the Prezmyël
1466 area (Carpathian Foredeep). PhD Thesis, Institute of Geological Sciences PAN, Krakow,
1467 Poland, 148p.
1468 Dudek, T., Środoń, J., Eberl, D.D., Elsass F. and Uhlik, P., 2002, Thickness distribution of illite
1469 crystals in shales. Part I: XRD vs. HRTEM measurements. Clays and Clay Minerals, 50, 562-
1470 577.
1471 Eberl, D.D. and Środoń, J., 1988, Ostwald ripening and interparticle-diffraction effects from illite
1472 crystals. American Mineralogist, 73, 1335-1345.
1473 Eberl, D.D., Drits, V., Środoń, J. and Nüesch, R., 1996, MudMaster: A program for calculating
1474 crystallite size distribution and strain from the shapes of X-ray diffraction peaks. U.S.
1475 Geological Survey, Open-File Report, 96-171.
1476 Eberl, D.D., Drits, V. and Srodon, J., 1997, Measurement of Illite Crystallite Thickness by XRD.
1477 Method of Bertaud–Warren–Averbach. Groupe Français des Argiles, 27–28.
1478 Eberl, D.D., Nüesch, R., Šucha, V. and Tsipursky, S., 1998a, Measurement of fundamental illite
1479 particle thickness by X-ray diffraction using PVP-10 intercalation. Clays and Clay Minerals,
1480 46, 89-97.
1481 Eberl, D.D., Drits, V.A. and Środoń, J., 1998b, Deducing growth mechanisms for minerals from
1482 the shapes of crystal size distributions. American Journal of Science, 298, 499-533.
1483 Eberl, D.D., Drits, V.A. and Środoń, J., 2001, User's guide to GALOPER – a program for
1484 simulating the shapes of crystal size distributions – and associated programs. U.S. Geological
1485 Survey, Open-File Report, OF00-505, 44p.

1486 Eberl, D.D., Kile, D.E. and Drits, V.A., 2002, On geological interpretations of crystal size
1487 distributions: Constant vs. proportionate growth. American Mineralogist, 87, 1235-1241.
1488 Eberl, D.D., Blum, A.E. and Serravezza, M., 2011, Anatomy of a metabentonite: Nucleation and
1489 growth of illite crystals and their coalescence into mixed-layer illite/smectite. American
1490 Mineralogist, 96, 586-593.
1491 Ehrenberg, S.N. and Nadeau, P.H., 1989, Formation of diagenetic illite in sandstones of the Garn
1492 Formation, Haltenbanken area, mid-Norwegian Continental Shelf. Clays and Clay Minerals,
1493 24, 233-253.
1494 Elliott, W.C., Aronson, J.L., Matisoff, G. and Gautier, D.L., 1991, Kinetics of the smectite to
1495 illite transformation in the Denver Basin; Clay mineral, K-Ar data and mathematical model
1496 results. American Association of Petroleum Geologists Bulletin, 75, 436-462.
1497 Fallick, A.E., Macaulay, C.I. and Haszeldine, R.S., 1993, Implications of linearly correlated
1498 oxygen and hydrogen isotopic compositions for kaolinite and illite in Magnus Sandstone,
1499 North Sea. Clays and Clay Minerals, 2, 121-137.
1500 Faure, G., 1986, Principles of Isotope Geology, 2nd edn. Wiley, New York.
1501 Ferrage, E., Vidal, O., Mosser-Ruck, R., Cathelineau, M. and Cuadros, J. (2011) A
1502 reinvestigation of smectite illitization in experimental hydrothermal conditions: Results from
1503 X-ray diffraction and transmission electron microscopy. American Mineralogist, 96, 207–223.
1504 Fontes, J.C. and Matray, J.M., 1993, Geochemistry and origin of formation brines from the Paris
1505 Basin. Part 2: Saline solutions associated with oil fields. Chemical Geology, 109, 177-200.
1506 Francú, J., Muller, P., Šucha, V., Zatkaliková, V., 1990. Organic matter and clay minerals as
1507 indicators of thermal history in the Transcarpathian Depression (East Slovakian Neogene
1508 Basin) and the Vienna Basin. Geologica Carpathica, 41, 535-546.
1509 Freed, R.L. and Peacor, D.R., 1992, Diagenesis and the formation of authigenic illite-rich crystals
1510 in Gulf Coast shales: TEM study of clay separates. Journal of Sedimentary Petrology, 62, 220-
1511 234.
1512 Furlan, S., Clauer, N., Chaudhuri, S. and Sommer, F., 1996, K transfer during burial diagenesis in
1513 the Mahakam Delta Basin (Kalimantan, Indonesia). Clays and Clay Minerals, 44, 157-169.
1514 Gabis, V., 1963, Etude minéralogique et géochimique de la série sédimentaire oligocène du
1515 Velay. Bulletin de la Société française de Minéralogie et Cristallographie, 86**,** 315-354.
1516 Girard, J.P. and Barnes, D.A., 1995, Illitization and paleothermal regimes in the Middle

1517 Ordovician St Peter Sandstone, Central Michigan Basin, United States: K-Ar, oxygen
1518 isotopes, and fluid inclusion data. American Association of Petroleum Geologists Bulletin, 79,
1519 49-69.
1520 Glasmann, J.R., Larter, S., Briedis, N.A. and Lundegard, P.D., 1989a, Shale diagenesis in the
1521 Bergen area, North Sea. Clays and Clay Minerals, 37, 97-112.
1522 Glassman, J.R., Lundegard, P.D., Clark, R.A., Penny, B.K. and Collins, I.D., 1989b,
1523 Geochemical evidence for the history of diagenesis and fluid migrations: Brent sandstones,
1524 Heather field, North Sea. Clay Minerals, 24, 255-284.
1525 Harper, C.T., 1970. Graphic solution to the problem of ^{40}Ar loss from metamorphic minerals.
1526 Eclogae Geologicae Helveticae, 63, 119-140.
1527 Harris, N.B., 1992, Burial diagenesis of Brent sandstones: A study of Statfjord, Hutton and Lyell
1528 fields. In: Morton, A.C., Haszeldine, R.S., Giles, M.R. and Brown, S. (Eds.), Geology of the
1529 Brent Group, Geological Society of London, Special Publication, 61, 351-375.
1530 Hingston, F.J., 1964, Reactions between boron and clays. Australian Journal of Soil Research, 2,
1531 83-95.
1532 Honty, M., Uhlik, P., Šucha, V., Caplovicová, M., Francú, J., Clauer, N. and Biroń, A., 2004,
1533 Smectite to illite alteration in salt-bearing bentonites; the East Slovak Basin. Clays and Clay
1534 Minerals, 52, 533-551.
1535 Hower, J., Eslinger, E.V., Hower, M. and Perry, E.A., 1976, Mechanism of burial metamorphism
1536 of argillaceous sediments: 1. Mineralogical and chemical evidence. Geological Society of
1537 America Bulletin, 87, 725-737.
1538 Hunziker, J.C., Frey, M., Clauer, N., Dallmeyer, R.D., Friedrichsen, H., Flehmig, W.,
1539 Hochstrasser, K., Roggwiller, P. and Schwander, H., 1986, The evolution of illite to
1540 muscovite: mineralogical and isotopic data from the Glarus Alps, Switzerland. Contribution to
1541 Mineralogy and Petrology, 92,157-180.
1542 Inoue, A., Kohyama, N., Kitagawa, R. and Watanabe, T., 1987, Chemical and morphological
1543 evidence for the conversion of smectite to illite. Clays and Clay Minerals, 35, 111-120.
1544 Inoue, A., Velde, B., Meunier, A. and Touchard, G., 1988, Mechanism of illite formation during
1545 smectite-to-illite conversion in a hydrothermal system. American Mineralogist, 73, 1325-
1546 1334.
1547 Inoue, A. and Kitagawa, R., 1994, Morphological characteristics of illitic clay minerals from a

1548 hydrothermal system. American Mineralogist, 79, 700-711.
1549 Jackson, M.L., 1975, Soil Chemical Analysis – Advanced Course. Madison, Wisconsin, 386p.
1550 Jennings, S. and Thompson, G.R., 1986, Diagenesis of Plio-Pleistocene sediments of the
1551 Colorado river delta, southern California. Journal of Sedimentary Petrology, 56, 89-98.
1552 Jones, C.E. and Jenkyns, H.C., 2001, Seawater strontium isotopes, oceanic anoxic events, and
1553 seafloor hydrothermal activity in the Jurassic and Cretaceous. American Journal of Sciences,
1554 301, 112-149.
1555 Kotzer, T.G. and Kyser, T.K., 1995, Petrogenesis of the Proterozoic Athabasca basin, Northern
1556 Saskatchewan, Canada, and its relation to diagenesis, hydrothermal uranium mineralization
1557 and paleohydrogeology. Chemical Geology, 120, 45-89.
1558 Land, L.S. and MacPherson, G.L., 1992, Origin of saline formation waters, Cenozoic section,
1559 Gulf of Mexico sedimentary basin. Geochimica et Cosmochimica Acta, 76, 1344-1362.
1560 Lawrence, J.R. and Taylor, H.P. Jr., 1971, Deuterium and oxygen-18 correlation: Clay minerals
1561 and hydroxides in Quaternary soils compared to meteoric waters. Geochimica et
1562 Cosmochimica Acta, 35, 993-1003.
1563 Lawrence, J.R. and Taylor, H.P. Jr., 1972, Hydrogen and oxygen isotope systematics in
1564 weathering profiles. Geochimica et Cosmochimica Acta, 36, 1377-1393.
1565 Lee, J.Y., Marti, K., Severinghaus, J.P., Kawamura, K., Yoo, H.S., Lee, J.B. and Kim, J.S., 2006,
1566 A redetermination of the isotopic abundances of atmospheric Ar. Geochimica et
1567 Cosmochimica Acta, 70, 4507-4512.
1568 Leeman, W.P., Vocke, R.D. and McKibben, M.A., 1992, Boron isotopic fractionations between
1569 coexisting vapor and liquid in natural geothermal systems. In: Kharaka, Y.K. and Maest, A.S.
1570 (Eds.), Proceedings of the 7th International Symposium on Water–Rock Interaction, Balkema,
1571 Rotterdam, 1007-1010.
1572 Lemarchand, D., Gaillardet, J., Lewin, E. and Allègre, C.J., 2000, The influence of rivers on
1573 marine boron isotopes and implications for reconstructing past ocean pH. Nature, 408, 951-
1574 954.
1575 Lemarchand, D., Gaillardet, J., Lewin, E. and Allègre, C.J., 2002, Boron isotope systematics in
1576 large rivers: implications for the marine boron budget and paleo-pH reconstruction over the
1577 Cenozoic. Chemical Geology, 190, 123-140.
1578 Lerman, A., Ray, B.M. and Clauer, N., 2007, Radioactive production and diffusional loss of

radiogenic ^{40}Ar in clays in relation to its flux to the atmosphere. Chemical Geology, 243, 205-224.

Longstaffe, F.K. and Ayalon, A., 1987, Oxygen-isotope studies of clastic diagenesis in the Lower Cretaceous Viking Formation, Alberta: Implications for the role of meteoric water. In: Marshall, J.D. (Ed.), Diagenesis of Sedimentary Sequences, Geological Society of London, Special Publications, 36, 277-296.

Longstaffe, F.J. and Ayalon, A., 1990, Hydrogen-isotope geochemistry of diagenetic clay minerals from Cretaceous sandstones, Alberta, Canada: Evidence for exchange. Applied Geochemistry, 5, 657-668.

Lynch, L.L., 1985, The stoichiometry of the smectite to illite reaction in a contact metamorphic environment. M.S. thesis, Dartmouth College, Hanover, New Hampshire, 84p.

Mark, D.F., Stuart, F.M. and de Podesta, M., 2011, New high-precision measurements of the isotopic composition of atmospheric argon. Geochimica et Cosmochimica Acta, 75, 7494-7501.

McCarty, D.C., Sakharov, B.A. and Drits, V.A., 2008, Early clay diagenesis in Gulf Coast sediments: New insights from X-ray diffraction profile modeling. Clays and Clay Minerals, 56, 359-379.

Meunier, A. and Velde, B., 2004, Illite. Springer, Berlin**,** 286p.

Milliken, K.L., 1992, Chemical behavior of detrital feldspars in mudrocks versus sandstones, Frio Formation (Oligocene), South Texas. Journal of Sedimentary Petrology, 62, 790-801.

Misra, S. and Froelich, P.N., 2012, Lithium isotope history of Cenozoic seawater: Changes in silicate weathering and reverse weathering. Science, 335, 818-823.

Moldovanyi, E.P. and Walter, L.M., 1992, Regional trends in water chemistry, Smackover Formation, southwest Arkansas: Geochemical and physical controls. American Association of Petroleum Geologists Bulletin, 76, 864-894.

Moldovanyi, E.P., Walter, L.M. and Land, L.S., 1993, Strontium, boron, oxygen, and hydrogen isotope geochemistry of brines from basal strata of the Gulf Coast sedimentary basin, USA. Geochimica et Cosmochimica Acta, 57, 2083-2099.

Mossmann, J.R., 1991, K-Ar dating of authigenic illite/smectite material: Application to complex mixtures of mixed-layer assemblages. Clay Minerals, 26, 189-198.

Muttik, N., Kirsimäe, K, Newsom, H.E. and Williams, L.B., 2011, Boron isotope composition of

secondary smectite in suevites at the Ries crater, Germany: Implications for the origin of alteration fluids. Earth and Planetary Science Letters, 310, 244-251.

Nadeau, P.H., Wilson, M.J., McHardy, W.J. and Tait, J.M., 1984, Interstratified clays as fundamental particles. Science, 225, 923-925.

Oi, T., Kawada, K., Hosoe, M. and Kakihana, H., 1991, Fractionation of lithium isotopes in cation exchange chromatography. Separation Science Technology, 26, 1353.

O'Neil, J.R. and Kharaka, Y.K., 1976, Hydrogen and oxygen isotope exchange reactions between clay minerals and water. Geochimica et Cosmochimica Acta, 40, 241-246.

Palmer, M.R. and Sturchio, N.C., 1990, The boron isotope systematics of the Yellowstone National Park (Wyoming) hydrothermal system: A reconnaissance. Geochimica et Cosmochimica Acta, 54, 2811-2815.

Perry, E.A. Jr. and Hower, J., 1970, Burial diagenesis in Gulf Coast pelitic sediments. Clays and Clay Minerals, 18, 165-177.

Pevear, D.R., 1992, Illite age analysis, a new tool for basin thermal history analysis. In: Kharaka, Y.K. and Maest, A.S. (Eds.), Proceedings of the 7th International Symposium on Water-Rock Interaction. Balkema, Rotterdam, Netherlands, 1251-1254.

Pevear, D.R., 1999, Illite and hydrocarbon exploration. Proceedings of the National Academy of Sciences of the United States of America, 96, 3440-3446.

Pollastro, R.M., 1985, Mineralogical and morphological evidence for the formation of illite at the expense of illite/smectite. Clays and Clay Minerals, 33, 265-274.

Pollastro, R.M., 1993, Considerations and applications of the illite/smectite geothermometer in hydrocarbon-bearing rocks of Miocene to Mississippian age. Clays and Clay Minerals, 41, 119-133.

Pytte, A.M. and Reynolds, R.C., 1989, The thermal transformation of smectite to illite. In: Naeser, N.D. and McCulloh, T.H. (Eds.), Thermal History of Sedimentary Basins: Methods and Case Histories, New York, Springer-Verlag, 133-140.

Renac, C. and Meunier, A., 1995, Reconstruction of paleothermal conditions in a passive margin using illite/smectite mixed-layered series (BA1 scientific deep drill-hole, Ardèche, France). Clay Minerals, 30, 107-118.

Reynolds, R.C. Jr., 1985, NEWMOD© a computer program for the calculation of one-dimensional diffraction patterns of mixed-layered clays. Reynolds, R.C. Jr., 8 Brook Rd.,

1641 Hanover, NH.
1642 Robinson, A.G., Coleman, M.L. and Gluyas, J.G., 1993, The age of illite cement growth, Village
1643 field area, southern North Sea: Evidence from K–Ar ages and $^{18}O/^{16}O$ ratios. American
1644 Association of Petroleum Geologists Bulletin, 77, 68-80.
1645 Rosenberg, P.E., 2002, The nature, formation and stability of end-member illite: A hypothesis.
1646 American Mineralogist, 87, 103-107.
1647 Savin, S.M. and Epstein, S., 1970, The oxygen and hydrogen isotope geochemistry of clay
1648 minerals. Geochimica et Cosmochimica Acta, 34, 25-42.
1649 Savin, S.M. and Lee, M., 1988, Isotopic studies of phyllosilicates. In: Bailey, S.W. (Ed.),
1650 Hydrous Phyllosilicates (Exclusive of Micas). Reviews in Mineralogy, 19, 189-223.
1651 Savin, S.M. and Hsieh, J.C.C., 1998, The hydrogen and oxygen isotope geochemistry of
1652 pedogenic clay minerals: Principles and theoretical background. Geoderma, 82, 227-253.
1653 Schwarcz, H.P., Agyei, E.K. and McMullen, C.C., 1969, Boron isotopic fractionation during clay
1654 adsorption from sea-water. Earth and Planetary Science Letters, 6, 1-5.
1655 Sears, S.K., Hesse, R., Vali, H., Elliott, W.C. and Aronson, J.L., 1998. K-Ar ages of 2:1 clay
1656 minerals, MacKenzie delta–Beaufort Sea region, Arctic Canada: Significance of *n*-
1657 alkylammonium exchange. The Canadian Mineralogist, 36, 1507-1524.
1658 Spivack, A.J., Palmer, M.R. and Edmond, J.M., 1987, The sedimentary cycle of the boron
1659 isotopes. Geochimica et Cosmochimica Acta, 51, 1939-1949.
1660 Spivack, A.J., Berndt, M.E. and Seyfried, W.E. Jr., 1990, Boron isotope fractionation during
1661 supercritical phase separation. Geochimica et Cosmochimica Acta, 54, 2337-2339.
1662 Środoń, J., 1980, Precise identification of illite/smectite interstratification by X-ray powder
1663 diffraction. Clay Minerals, 28, 401-411.
1664 Środoń, J., 1999, The use of clay minerals in reconstructing geological processes: Current
1665 advances and some perspectives. Clay Minerals, 34, 27-37.
1666 Środoń, J., 2010, Evolution of boron and nitrogen content during illitization of bentonites. Clays
1667 and Clay Minerals, 58, 743-756.
1668 Środoń, J., Elsass, F., McHardy, W.J. and Morgan, D.J., 1992, Chemistry of illite/smectite
1669 inferred from TEM measurements of fundamental particles. Clay Minerals, 27, 137-158.
1670 Środoń, J. and Clauer, N., 2001, Diagenetic history of Lower Palaeozoic sediments in Pomerania
1671 (northern Poland) traced across the Teisseyre-Tornquist tectonic zone using mixed-layer illite-

1672 smectite. Clay Minerals, 36, 15-27.
1673 Środoń, J., Clauer, N. and Eberl, D.D., 2002, Interpretation of K-Ar dates of illitic clays from
1674 sedimentary rocks aided by modeling. American Mineralogist, 87, 1528-1535.
1675 Środoń, J., Kotarba, M., Biroň, A., Such, P., Clauer, N. and Wojtowicz, A., 2006, Diagenetic
1676 history of the Podhale-Orava Basin and the underlying Tatra sedimentary structural units
1677 (Western Carpathians): Evidence from XRD and K-Ar of illite-smectite. Clay Minerals, 41,
1678 751-774.
1679 Środoń, J., Clauer, N., Huff, W., Dudek, T. and Banas, M., 2009, K-Ar dating of Ordovician
1680 bentonites from the Baltic Basin and the Baltic Shield: Implications for the role of temperature
1681 and time in the illitization of smectite. Clay Minerals, 44, 361-387.
1682 Stueber, A.M., Walter, L.M., Huston, T.J. and Pushkar, P., 1993, Formation waters from
1683 Mississippian-Pennsylvanian reservoirs, Illinois basin, U.S.A: Chemical and isotopic
1684 constraints on evolution and migration. Geochimica et Cosmochimica Acta, 57, 763-784.
1685 Šucha, V., Kraus, I., Gerthofferová, H., Peteš, J. and Sereková, M., 1993, Smectite to illite
1686 conversion in bentonites and shales of the East Slovak Basin. Clay Minerals, 28, 243-253.
1687 Swilhart, G.H., Moore, M.R. and Edmond, J.M., 1986, Boron isotopic composition of marine and
1688 non-marine evaporite borates. Geochimica et Cosmochimica Acta, 50, 1297-1301.
1689 Teng, F.-Z., McDonough, W.F., Rudnick, R.L. and Gao, S., 2004, Lithium isotopic composition
1690 and concentration of the upper continental crust. Geochimica et Cosmochimica Acta, 68,
1691 4167-4178.
1692 Teng, F.-Z., McDonough, W.F., Rudnick, R.L. and Walker, R.J., 2006, Diffusion-driven extreme
1693 lithium isotopic fractionation in country rocks of the Tin Mountain pegmatite. Earth and
1694 Planetary Science Letters, 243, 701-710.
1695 Teng, F.-Z., McDonough, W.F., Rudnick, R.L. and Wing, B.A., 2007, Limited lithium isotopic
1696 fractionation during progressive metamorphic dehydration in metapelites : A case study from
1697 the Onawa contact aureole, Maine. Chemical Geology, 239, 1-12.
1698 Teng, F.-Z, Li, W.-Y. Rudnick, R.L. and Gardner, L.R., 2010, Contrasting lithium and
1699 magnesium fractionation during continental weathering. Earth and Planetary Science Letters,
1700 300, 63-71.
1701 Valley, J.W. and Kita, N.T., 2009, In situ Oxygen Isotope Geochemistry by Ion Microprobe, In:
1702 Fayek, M. (Ed.), Mineralogical Association of Canada Short Course: Secondary Ion Mass

1703 Spectrometry in the Earth Sciences, 41, 19-63.
1704 van Krevelen, D.W., 1950, Graphical-statistical method for the study of structure and reaction
1705 processes of coal. Fuel, 29, 269-84.
1706 Velde, B., 1985, Clay Minerals: A Physico-Chemical Explanation of their Occurrence.
1707 Developments in Sedimentology, Elsevier, Amsterdam, 40, 426p.
1708 Velde, B. and Vasseur, G., 1992, Estimation of the diagenetic smectite to illite transformation in
1709 time-temperature space. American Mineralogist, 77, 967-976.
1710 Velde, B. and Renac, C., 1996, Smectite to illite conversion and K-Ar ages. Clay Minerals, 31,
1711 25-32.
1712 Vengosh, A., Starinsky, A., Kolodny, Y. and Chivas, A.R., 1991a, Boron isotope geochemistry as
1713 a tracer for the evolution of brines and associated hot springs from the Dead Sea, Israel.
1714 Geochimica et Cosmochimica Acta, 55, 1689-1695.
1715 Vengosh, A., Starinsky, A., Kolodny, Y., Chivas, A.R. and McCulloch, M.T., 1991b,
1716 Coprecipitation and isotopic fractionation of boron in modern biogenic carbonates.
1717 Geochimica et Cosmochimica Acta, 55, 2901-2910.
1718 Vengosh, A., Starinsky, A., Kolodny, Y., Chivas, A.R. and Raab, M., 1992, Boron isotope
1719 variations during fractional evaporation of seawater: New constraints on the marine vs.
1720 nonmarine debate. Geology, 20, 799-802.
1721 Vengosh, A., Starinsky, A. and Chivas, A.R., 1994, Boron isotopes in Heletz-Kokhav oilfield
1722 brines, the Coastal Plain Israel. Israel Journal of Earth Sciences, 43, 231-237.
1723 Wasserburg, G.J., Hayden, R.I. and Jensen, K.J., 1956, Ar40-K40 dating of igneous rocks and
1724 sediments. Geochimica et Cosmochimica Acta, 10, 153-165.
1725 Weaver, C.E. and Beck, K.C., 1971, Clay water diagenesis during burial, how mud becomes
1726 gneiss. Geological Society of America, Special Paper, 134, 96p.
1727 Wilkinson, M. and Haszeldine, R.S., 2002, Fibrous illite in oilfield sandstones – a nucleation
1728 kinetic theory of growth. Terra Nova, 14, 56-60.
1729 Williams, L.B. and Ferrell, R.E., 1991, Ammonium substitution in illite during maturation of
1730 organic matter. Clays and Clay Minerals, 39, 400-408.
1731 Williams, L.B., Hervig, R.L., Holloway, J.R. and Hutcheon, I., 2001a, Boron isotope
1732 geochemistry during diagenesis: Part 1. Experimental determination of fractionation during
1733 illitization of smectite. Geochimica et Cosmochimica Acta, 65, 1769-1782.

1734 Williams, L.B., Hervig, R.L. and Hutcheon, I., 2001b, Boron isotope geochemistry during
1735 diagenesis: Part II. Applications to organic-rich sediments. Geochimica et Cosmochimica
1736 Acta, 65, 1783-1794.
1737 Williams, L.B. and Hervig, R.L., 2002, Exploring intra-crystalline B-isotope variations in mixed-
1738 layer illite-smectite. American Mineralogist, 87, 1564-1570.
1739 Williams, L.B. and Hervig, R.L., 2006, Crystal size dependence of illite-smectite isotope
1740 equilibration with changing fluids. Clays and Clay Minerals. 54, 531-540.
1741 Williams, L.B., Turner, A. and Hervig, R.L., 2007, Intracrystalline boron isotope partitioning in
1742 illite-smectite: Testing the geothermometer. American Mineralogist, 92, 1958-1965.
1743 Williams, L.B., Clauer, N. and Hervig R.L., 2012, Light stable isotope microanalysis of clays in
1744 sedimentary rocks. In: Sylvester, P. (Ed.), Quantitative Mineralogy and Microanalysis of
1745 Sediments and Sedimentary Rocks, Mineralogical Association of Canada, Short Course, 42,
1746 55-73.
1747 Williams, L.B., Środoń, J., Huff, W.D., Clauer, N. and Hervig, R.L., 2013. Light element
1748 distributions (N, B, Li) in Baltic Basin bentonites record organic sources. Geochimica et
1749 Cosmochimica Acta, 120, 582-599.
1750 Wilson, R.G., Stevie, F.A. and Magee, C.W., 1989, Secondary-ion mass spectrometry: a practical
1751 handbook for depth profiling and bulk impurity analysis. John Wiley & Sons, New York,
1752 384p.
1753 Wilson, T.P. and Long, D.T., 1993, Geochemistry and isotope chemistry of $CaCl_2$ brine in
1754 Silurian formations of the Michigan Basin. Applied Geochemistry, 8, 507-524.
1755 Yapp, C.J., 1993, Stable isotope geochemistry of low temperature Fe(iii) and Al ‘‘oxides’’ with
1756 implications for continental paleoclimates in climate change. In: Swart, P.K., Lohman, K.C.,
1757 McKenzie, J. and Savin S. (Eds.), Continental Isotopic Records, Geophysical Monographs,
1758 American Geophysical Union, Washington, DC, 78, 285-294.
1759 Yates, D.M. and Rosenberg, P.E., 1996, Formation and stability of endmember illite: I. Solution
1760 equilibration experiments at 100-250°C and $P_{v,soln}$. Geochimica et Cosmochimica Acta, 60,
1761 1873-1883.
1762 Yates, D.M. and Rosenberg, P.E., 2011, A reinvestigation of smectite illitization in experimental
1763 hydrothermal conditions: Results from X-ray diffraction and transmission electron
1764 microcroscopy - Discussion. American Mineralogist, 96, 1901-1902.

You, C.F. and Chan, L.H., 1996, Precise determination of lithium isotopic composition in low concentration natural samples. Geochimica et Cosmochimica Acta, 60, 909-915.

Zwingmann, H., Clauer, N. and Gaupp, R., 1999, Structure-related geochemical (REE) and isotopic (K–Ar, Rb–Sr, $\delta^{18}O$) characteristics of clay minerals from Rotliegend sandstone reservoirs (Permian, Northern Germany). Geochimica et Cosmochimica Acta, 63, 2805-2823.

Captions

Figure 1: Theoretical sketch of illite-smectite mixed layer before and after B and Li introduction during crystal nucleation (from Williams et al., 2013).

Figure 2: Theoretical illitization rates (from Clauer, 2006).

Figure 3: Trigonal, tetrahedral and interlayer $\delta^{11}B$ values of a smectite-illite mixed layer of a bentonite bed, depending on the content of illite layers and the distance to an intrusive basaltic dike (from Williams et al., 2007).

Figure 4: K-Ar ages of nanometric illite-rich fractions from bentonite beds of Trhovište and Čičarovče sites in the East Slovak Basin (from Clauer et al., 1997).

Figure 5: Summary of the K-Ar ages from different bentonite beds of the East Slovak Basin. The nanometric fractions are identified by open symbols and the micrometric fractions by grey symbols (from Clauer et al., 2014b).

Figure 6: $\delta^{18}O$ vs. δD of nanometric (in black symbols) and micrometric (in open symbols) of varied size fractions from bentonite beds of the East Slovak Basin (from Clauer et al., 2014b).

Figure 7: (A): $\delta^{18}O$ vs K-Ar ages of nanometric (in white symbols) and micrometric (grey symbols) size fractions of bentonite beds from East Slovak Basin; and (B) δD vs. K-Ar of the same fractions with the same symbols from the same bentonite beds (from Clauer et al., 2014b).

Figure 8: $\delta^{11}B$ vs. B contents of nanometric size fractions labeled 1 to 3 for increasing size

fractions of different bentonite beds identified by different symbols from East Slovak Basin (from Clauer et al., 2009).

Figure 9: Correlation between $\delta^{11}B$ and present-day temperature in the boreholes of the studied bentonite beds from east Slovak Basin. Each symbol represents a distinct bentonite sample (from Clauer et al., 2009).

Figure 10: $\delta^{7}Li$ vs. Li content of varied nanometric size fractions from different bentonite samples (identified by different symbols) of the East Slovak Basin. T stands for measured temperature in the drill holes and Sm stands for smectite layers in the separated nanometric fractions (from Clauer et al., 2009). The different symbols stand for the different studied samples.

Figure 11: (A) Geographic repartition of the nanometric K-Ar ages of bentonite samples from Baltic Basin; (B) $\delta^{11}B$ and $\delta^{7}Li$ signatures of nanometric size fractions of Baltic bentonites along a SW-NE trend reported on the regional map (from Williams et al., 2013).

Figure 12: $\delta^{11}B$ and $\delta^{7}Li$ of the Cambrian Alum shale depending on the H/C ratio of the organics with identification of oil and gas generation (from Williams et al., 2013).

Figure 13: The α and β^{2} parameters of the different size fractions from Appalachian K-bentonite beds showing that illitization occurred in all fractions by simultaneous nucleation and crystal growth, except for one sample. All Appalachian bentonite size fractions are labeled as grey symbols; the other symbols identify fractions from other studies (see Clauer et al., 2013).

Figure 14: $^{40}Ar/^{36}Ar$ vs. $^{40}K/^{36}Ar$ isochron diagram for the nanometric size fractions of the Appalachian K-bentonite beds. The symbols in grey fit the upper isochron of 319.9 $\pm$ 2.0 Ma with an initial $^{40}Ar/^{36}Ar$ of 271 $\pm$ 66, whereas the open symbols fit the lower isochron of 284.9 $\pm$ 1.2 Ma with an initial $^{40}Ar/^{36}Ar$ of 310 $\pm$ 44, and the black symbols identify the fractions off the two isochrons (from Clauer et al., 2013).

Figure 15: (A) $\delta^{18}O$ vs. δD of the nano- to micrometric illite fractions from Appalachian K-bentonites, and (B) $\delta^{18}O$ of the same bentonite size fractions vs. their K-Ar ages. The increasing lettering in the graph from a to d stand for the increasing sizes of the nanometric fractions; more details are in Clauer et al. (2013).

Figure 16: $\delta^{7}Li$ and $\delta^{11}B$ values of <2 μm illite from the Walsen Dike metabentonite across the 13-m contact with the basaltic dike into the country rock. Maximum temperatures range from ~500 ˚C near the dike to ~200 ˚C in country rock (from Williams et al., 2007).

Figure 17: Theoretical K-Ar age of nanosized illite based on a model based on crystal nucleation followed by growth with two trajectories A and B trending on the basis of different intensities for burial illitization. The numbers at the black dots outline the theoretical K-Ar age depending on the parameters considered (from Środoń et al., 2002).

Figure 18: Harper (1970) diagram with the K-Ar data of varied nanometric and micrometric size fractions of the "Illite du Puy" shale. The trends are given by fine dashed arrays, whereas the tendencies are in full lines (from Clauer, unpublished).

Figure 19: Harper (1970) diagram with all size fractions of the different shale-type samples of the "Illite du Puy". Graphs (A) and (B) detail the same data at different scales (from Clauer, unpublished).

Figure 20: Changing K-Ar ages of <0.4 μm size fractions from shales and sandstones of the buried sedimentary sequence beneath the Mahakam Delta, Indonesia (from Clauer et al., 1999).

Figure 21: Modeled K_2O and radiogenic ^{40}Ar contents of nanometric illite from progressively buried shales and sandstones of the Mahakam Delta, Indonesia. The upper left-hand panel outlines the geographic location of the Handil field from where the core samples were recovered. The expandability of the illite-smectite mixed layer in the lower left-hand panel has been used to model the K and radiogenic ^{40}Ar contents relative to depth in both the sandstones and shales. It turns out that an excess of radiogenic ^{40}Ar starting at depth (~3000 m) is needed to match the analytical data (after Clauer et al., 2004).

Figure 22: SEM photomicrographs of illite shapes from Triassic sandstones of the eastern Paris Basin. (A) Illite filaments and fibers growing on a partly dissolved K-feldspar; (B) typical habitus of illite: hairy growing onto well-crystallized hexagonal plates, which suggests that the hairy morphologies correspond to the last stage of the mineral paragenesis; (C) platy and lathlike illite; (D) magnification of platy to the left and lathlike illite to the right (from Blaise et al., in preparation).

Figure 23: Elemental compositions of the leachates from gentle acidic leaching of the nanometric size fractions of two sandstones (A and B) from the eastern Paris Basin (from Blaise et al., in preparation)

Figure 24: (A) Harper (1970) diagram of the nanometric and micrometric size fraction of a smectite-rich bentonite bed from Campos Basin, offshore Brazil; (B) $^{40}Ar/^{36}Ar$ vs. $^{40}K/^{36}Ar$

1857 isochron of the same size fractions from the same bentonite bed. The data of the finest fraction
1858 have been duplicated in the isochron graph (from Clauer, unpublished).
1859 **Figure 25:** Rb-Sr isochron diagram for the leachates (grey symbols), untreated fractions (white
1860 symbols) and residues (black symbols) of the nanometric and micrometric fractions of the
1861 smectite-rich bentonite bed from Campos Basin, offshore Brazil (from Clauer, unpublished).
1862 **Figure 26:** $\delta^{18}O$ of the nano-sized illite from Trhovište and Čičarovče bentonite beds of the East
1863 Slovak Basin (from Clauer et al., 2003).
1864 **Figure 27:** $\delta^{11}B$, $\delta^{18}O$ and δD of an untreated <2 μm clay fraction and the same fraction from an
1865 oil-bearing shale pyrolyzed at successively higher temperatures (from Clauer, Williams,
1866 Fallick and Lewan, unpublished).
1867 **Figure 28:** Graphic calculation of the removed B content and $\delta^{11}B$ for each pyrolysis step (from
1868 Clauer, Williams, Fallick and Lewan, unpublished).
1869
1870 **Table 1:** K-Ar data of the nanometric and micrometric fractions from five "Illite du Puy" shale-
1871 type samples (from Clauer, unpublished).

Genesis of nanometric illite crystals elucidated by light-element (hydrogen, lithium, boron and oxygen) isotope tracing, and K-Ar and Rb-Sr dating

Norbert Clauer[1], Lynda B. Williams[2] and Anthony E. Fallick[3]

[1] Laboratoire d'Hydrologie et de Géochimie de Strasbourg (CNRS-UdS), 1 rue Blessig, 67084 Strasbourg, France

[2] School of Earth & Space Exploration, Arizona State University, Tempe, AZ 85287-1404, USA

[3] Scottish Universities Environmental Research Centre, East Kilbride, Glasgow G75 0QF, UK

Corresponding author: Dr. Norbert Clauer, Laboratoire d'Hydrologie et de Géochimie de Strasbourg (CNRS/UdS), 1 Rue Blessig, 67084 Strasbourg, France; office phone: 033 390 24 04 33; cell phone: 033 680 01 80 49; fax: 033 390 24 04 02; e-mail: nclauer@unistra.fr

Key words: hydrogen, lithium, boron and oxygen isotope geochemistry, K-Ar and Rb-Sr isotope dating, nanometric fundamental illite particles, illitization

Abstract

Illitization is a widely used tracer for evaluation of the thermal evolution in volcano-sedimentary sequences during burial, metamorphic and tectonic events. However, no agreement exists about how the process proceeds at the crystal scale, which initiated perspectives based on the challenging separation of nanometric "fundamental" illite-rich particles in the mid 1980s. In 1997, the first isotopic study on such nanometric crystals was published, followed by others that

raised new potential to improve understanding of the illitization process.

The present review focuses on the promising and still unsolved aspects of light-element isotopic (δD, δ^{7}Li, δ^{11}B, δ^{18}O) tracing, and K-Ar and Rb-Sr dating of nanometric illite-rich crystals extracted mainly from bentonites, but also from sandstones and shales in diagenetic to low-grade metamorphic conditions. If the study of nanocrystals from bentonite and sandstone beds now appears successful, problems remain in separating mechanically authigenic illite-type crystals from detrital minerals of shales, even at the nanometric size. An indirect way to distinguish the data of these components is alkylammonium leaching, which has the specificity of stochiometrically replacing K in dioctahedral mica-type particles, and therefore to modify significantly their K-Ar system. The overall separation technique for illite nanocrystals is specific with chemical treatments to remove the soluble phases, including organics, that are mixed with illite, "infinite" dispersion, high-speed fluid-flow centrifugation and removal of excess reagent by dialysis. Importantly, the initial K-Ar studies showed that no age information is lost during crystal nucleation and growth, with the whole illitization history apparently retained in the illite particles of different size. Based on combined K-Ar, Rb-Sr, δ^{18}O and δD studies, reaction rates and durations of illitization can be reconstructed, together with changing crystallization temperature and fluid chemistry depending on the water/rock ratio. On the basis of K-Ar dating, nucleation and growth can be continuous during a given period of time, or episodic. The Rb-Sr method complements the information about the origin of the interacting fluids by reconstructing ^{87}Sr/^{86}Sr ratios that depend on the amount of the fluids and their interaction with their pore environment. Combined with oxygen isotope data, such Sr isotope information points to differences in the origin of the solvents (by δ^{18}O) and the solutes (by ^{87}Sr/^{86}Sr). The δ^{18}O values of the illite crystals provide information about nucleation or growth temperature, either increasing during burial, or set abnormally high and constant during thermal episodes, or about changing fluid composition. Occurrence of organic matter could potentially bias the δ^{18}O of nucleating and growing illite crystals, when involved in initial organic maturation.

The largest B reservoir in sedimentary deposits is probably within the organic matter. When released with oil and gas after maturation, most of this organic B is isotopically light in the fluids relative to other natural waters, whereas ^{11}B fractionates preferentially into the bitumen. Put in context with oxygen and hydrogen isotope variations, the B data also confirm that the illite tetrahedral B-O bonds are as strong as the Si-O bonds, thus preserving the large isotopic

variations that occur during thermal maturation of kerogen. The changing clay-organic interactions in sedimentary environments can, therefore, be traced by the B content and isotope composition. The presently limited results on Li contents and isotope composition of nanometric illite crystals that potentially interact with organics outline trends that are similar to those of B.

1. Introduction

Since the middle of the 1960s, direct illite precipitation or smectite to illite conversion, both identified as illitization, are considered to be appropriate tracers for reconstructing the evolution of sedimentary basins, which is mainly driven by temperature increase and interaction with interstitial fluids during progressive burial (e.g. Hower et al., 1976; Velde, 1985; Jennings and Thompson, 1986; Pollastro, 1993; Šucha et al., 1993). The wide application of this tracer improved understanding of diagenetic to low-grade metamorphic mineral and organic-matter alteration in varied deposition environments. As temperature and chemistry of the interstitial fluids directly influence the chemistry of the crystallizing and growing minerals, use of clay minerals, especially illite, for tracing progressive or instantaneous crystallographic-chemical changes is best suited by examining the trend from smectite to illite ordering of illite-smectite crystalline structures. These changes have also been used in hydrocarbon exploration, as the progressive smectite to illite trend agrees fairly well with organic maturation indices and indigenous hydrocarbon grades, as a function of temperature increase.

However, many elemental and isotopic studies have focused, for a long time, on the fact that separation of authigenic illite-rich micrometric (first for <2 μm and later for <0.2 μm) particles from detrital material of any sedimentary host rock, especially shales, remains a tricky challenge (e.g. Weaver and Beck, 1971; Boles and Franks, 1979; Clauer and Chaudhuri, 1995 and references therein; Pevear 1999). This difficulty was partly resolved by attempts to reduce as much as technically possible the size of the separated particles including disaggregation of illite-smectite mixed-layers (labeled I-S hereafter) instead of crushing, and by separating nanometric illite crystals from separated I-S. Such illite-rich nanoparticles with sizes as small as <0.02 μm were characterized by electron microscopy and high-resolution transmission microscopy, and were precisely identified by X-ray diffraction analysis aided by mathematical modeling (e.g. Reynolds, 1985; Drits et al., 1998; Eberl et al., 2002). Precise identification allowed evaluation of

93 the crystal-size distribution of the illite crystals from separated size fractions, identifying the
94 crystallization processes and the crystal-growth trends (e.g. Nadeau et al., 1984; Eberl et al.,
95 1998a). This progress initiated a K-Ar dating attempt (Clauer et al., 1997), later a Rb-Sr
96 application combined with hydrogen and oxygen isotope tracing (Clauer et al., 2003), and more
97 recently boron and lithium isotope studies (Williams et al., 2013). Focus was mainly on bentonite
98 beds to avoid as much as possible the problematic occurrence of detrital "contaminants" (Clauer
99 et al., 1997; Środoń and Clauer, 2001; Clauer et al., 2003; Clauer et al., 2004; Środoń et al., 2006;
100 Środoń et al., 2009).

101 The respective elements of interest in the nanometric fundamental illite crystals are
102 located in tetrahedral sites for B, octahedral sites for Li, interlayer sites for K and its radiogenic
103 daughter ^{40}Ar, as well as for ^{87}Rb and the corresponding radiogenic daughter ^{87}Sr, while oxygen
104 forms the apices of the tetrahedrons and octahedrons, and hydroxyls the edges of the octahedral
105 layers (Fig. 1). The varied locations of these elements in an illite crystal focus attention on the
106 great potential of studies combining them. The following goals were set for the present review of
107 light-element isotope geochemistry, and K-Ar and Rb-Sr geochronology of illite-type
108 nanocrystals: (1) extract the key geochemical information that improves the understanding of
109 illitization in diagenetic to low-grade metamorphic sedimentary rocks; (2) differentiate the
110 potential processes that characterize illitization depending on the rock lithology and the degree of
111 recrystallization; (3) identify potential changes in paleofluid compositions during crystal
112 nucleation and growth; and (4) generate new information for the reconstruction of thermal
113 histories of sedimentary basins. The review starts with a presentation of the illitization concept
114 followed by specific aspects of the analytical and methodological approaches, and the alternative
115 concepts for illitization. The core of the review consists of a detailed discussion of the conceptual
116 nucleation and growth of nanometric crystals on the basis of available studies, with perspectives
117 of improved isotope-based interpretations of the global illitization process.
118

119 ## 2. The illitization process

120

121 Illite has been reported as forming in various environments, from continental soils to
122 deeply buried sediments. Evidence of high temperature promoting the diagenetic formation of
123 illite or the conversion of I-S (defined above) into illite is based mainly on studies of geologic

conditions controlled by constrained geothermal gradients and/or temperature increases resulting from circulation of hydrothermal solutions at depth (e.g. Meunier and Velde, 2004). The formation of illite in different physical and chemical conditions is often attributed to processes such as precipitation favored by dissolution of K-bearing feldspar and micas. The reactions between solute K and clays depleted in or lacking K (e.g. when kaolinite precipitates) are also included, as well as uptake of K ions and structural rearrangement of smectite or I-S crystal lattices into illite. However, these theoretical reactions are often difficult to adjust to natural conditions, because sources of K that are variably attributed to local dissolution of detrital K-feldspars and micas, or to K import from outside the rock volume by migrating fluids, are variably constrained (e.g. Pollastro, 1985; Freed and Peacor, 1992; Milliken, 1992; Furlan et al., 1996).

At this point, it is appropriate to recall that there is no aggrement about how illitization proceeds at the crystal scale. Theoretical models were conceived for varied mechanisms such as dissolution and precipitation in porous host rocks, and solid-state alteration in almost impermeable host rocks (e.g. Velde and Vasseur, 1992; Renac and Meunier, 1995; Altaner and Ylagan, 1997). Also, on the basis of experimental studies, the upper temperature limit of illite stability diverges from 250 to 360 ºC (Yates and Rosenberg, 1996; Rosenberg, 2002). If illitization can be summarized as a nucleation and growth of fine crystals, it is neither by an "Ostwald ripening" (Eberl and Środoń, 1988; Inoue et al, 1988), nor a "permanent recrystallization" (Velde and Renac, 1996), because dissolution of the first nucleated crystals has never been documented. In fact, initial K-Ar studies have shown that no age information is lost during initial nucleation and growth, and that the entire illitization process appears to be retained in the illite particles (e.g. Clauer et al., 1997). This information includes nucleation of initial smectite-rich crystals, then simultaneous nucleation of new illite-type crystals and growth of the initially nucleated crystals by a surface-controlled mechanism, and finally continuous mineral surface-controlled growth without nucleation (Środoń et al., 2002). Noteworthy also is the fact that illitization leads to lognormal crystal thickness distribution (CTD), at least in bentonites (Eberl et al., 1998). In shales, the shape of the CTD is generally asymptotic, which could result from a theoretical dominance of nucleation over growth, but also from the presence of detrital illite (Dudek at al., 2002). Experimental results and thermodynamic databases have also shown variable effects of temperature on K-containing mineral equilibria (Aja, 1995). It is expected that

crystallization of illite induces a lowering of K^+ concentration in the solute, and therefore a decrease of its K^+/H^+ ratio. Yates and Rosenberg (1996) reported such decreasing K^+/H^+ activity ratios in solution at equilibrium between low- and high-K illite phases mixed with kaolinite, during a temperature increase from 100 to 250 ºC. Conversely, not much seems to be known about the impact of pressure on illitization, for instance in oil-bearing sandstone reservoirs. In this context, Dayal (1975) reported a layering of 10-Å illite at the expense of expandable smectite in an I-S when pressure was increased from 1 to 1000 kPa in seawater, at 22 °C.

"Fundamental" nanoparticles of illite (<0.02 μm = <20 nm) are theoretically among the first to nucleate from a supersaturated solution at diagenetic temperatures (Eberl et al., 1998). Also, because the crystal size distribution is normally asymptotic (reflecting constant nucleation) or lognormal (reflecting combined nucleation and growth) in nature, only a small proportion of the initially nucleated particles are expected to continue growing (Eberl et al., 2002). As the initial K-Ar studies of "fundamental" illite particles have suggested that no age information is lost, none of the finest crystals being therefore potentially dissolved, separation of various size fractions or 'bins' of these nanometric particles (e.g. <0.02, 0.02-0.05, 0.05-0.1 μm) is able to provide useful information about the nucleation conditions of a specific clay mineral phase. The chemical and isotopic information in the successively larger size fractions ideally reveals changes in the chemistry of the interacting fluid over time, but that chemical and isotopic heterogeneity with increasing size fraction, of shales especially, can also be due to an increasing addition of detrital minerals to the authigenic ones. Also, if a fluid supersaturated in K relative to illite percolates a rock where illite crystals had already crystallized, a new generation of nucleating crystals may precipitate that are impossible to physically separate from earlier crystallites. Nonetheless, nanometric particle-size separations have been useful in identifying the evolution of fluids during crystal growth (Clauer et al., 1997; Wilkinson and Haszeldine, 2002; Williams and Hervig, 2006; Muttik et al., 2011; Williams et al., 2013).

Illite-type fundamental nanoparticles represent the smallest and finest clay-type crystals that can presently be separated mechanically. Their size is at the nanometer scale with *ab* dimensions of 20 to 30 nanometers and *c* dimensions of 2 to 3 nanometers. The concept implies a process starting with dissolution of the smectite layers of I-S, progressively replaced by nucleating and growing illite layers in the same mixed layering (Nadeau et al., 1984; Inoue et al. 1987; Eberl and Środoń, 1988). Depending on whether the mechanism of illitization was solid-

state transformation or dissolution/precipitation (and also assuming that the particle separation was ideal), different geochemical and isotopic characteristics can be expected for fundamental particles of varied size, especially if nucleation and growth were progressing slowly, such as during burial diagenesis. Growth theoretically depends on temperature, chemical thermodynamic parameters, and accessibility of the interstitial fluid supplying ions to the particles. On the basis of K-Ar age data of nanometric size fractions from I-S separates, different ages associated with progressive crystal growth have been reported (Clauer et al., 1997). As stated, if the first nucleated nanoparticles that did not grow can be separated from coarser ones, they should be the oldest. Alternatively, if crystal growth was not unique but periodic (episodic), the smallest fundamental particles could be younger than the associated coarser fundamental particles. Also, if crystal growth relates to a single fluid migration induced by a short-lasting hydrothermal activity, the fundamental particles of any size should be approximately of the same age. These theoretical aspects of illite crystal-growth were tentatively sketched relative to time on the basis of analytical evidence of I-S nanoparticles from bentonite beds of the East Slovak Basin (Fig. 2; Clauer, 2006).

In fact, clay material of most clastic sedimentary rocks not only consists of first-cycle coarse mica from crystalline parent rocks, but also varied clay-sized material resulting from continental erosion or pedogenetic weathering, in addition to authigenic nucleating and growing illite-type particles. These aspects have been covered in numerous publications (e.g. Perry and Hower, 1970; Burley and Flisch, 1989; Ehrenberg and Nadeau, 1989; Glassman et al., 1989a and b; Mossmann 1991; Freed and Peacor, 1992; Harris, 1992; Pevear, 1992; Girard and Barnes, 1995; Clauer and Chaudhuri, 1996; Clauer et al., 1999). Notwithstanding some successful studies (e.g. Elliott et al., 1991), the mechanism of illitization at the crystal scale is still debated. Published studies clearly show dissolution and precipitation (e.g. Nadeau et al., 1984; Ahn and Peacor, 1987), while others envision solid-state transformations (e.g. Drits et al., 1997). Case studies of both evidential bases can be evaluated: Inoue and Kitagawa (1994), Yates and Rosenberg (1996; 2011), Altaner and Ylagan (1997), Środoń (1999), Środoń et al. (2009) and Ferrage et al. (2011) published on the topic over the last two decades.

On the basis of published K-Ar, Rb-Sr and stable isotope data of nanometer- to micrometer-sized illite crystals of bentonite beds from sedimentary basins (Clauer et al., 1997; Środoń et al., 2002; Clauer et al., 2003; Honty et al., 2004; Środoń et al., 2006), Clauer (2006)

published a simplified conceptual model for the K-Ar and $\delta^{18}O$ characteristics of such nucleating and growing particles during progressive burial. The model envisages different reaction rates and durations, as well as variable temperature increases and impacts of the fluid chemistry as influenced by the water/rock ratio. Nucleating particles that stop growing and remain small yield older K-Ar ages in the particle-size distribution, whereas episodic crystal growth provides potentially younger K-Ar data for the smallest crystals than for the associated coarser micrometer-sized particles, because they nucleate while the earlier (therefore coarser) crystals are growing. Therefore, K-Ar dating of nanometric particles from any bentonite I-S size fraction does not always provide decreasing K-Ar ages when crystal size increases. Dating assemblages of young small particles comprising apparently older coarser sizes may therefore also provide unexpected and misleading results, not because of technical or conceptual problems, but for natural reasons. In any case, "fundamental" nanoparticles are most appropriate for reconstructing the history of bentonite beds, because well-defined illite crystals are not affected by surface sorption nor by particle agglomeration, and their thickness distribution profiles conform to the crystal growth theory (Eberl et al., 2011). However, it cannot be denied that different size fractions of a sample can integrate particles of the same or similar mineral types but of variable ages, resulting from episodic and variable K supply. Such varied mineral types cannot be distinguished by the traditional analytical procedures such as classical X-ray diffraction (XRD) or wet chemical analysis, but they might be by XRD profile modeling (Reynolds, 1985; Eberl et al. 1996; Drits et al. 1998; Eberl et al., 1998b; Eberl et al. 2001; Eberl et al., 2011). And last, but not least, it is appropriate, in dealing with K-Ar ages, to recall that these nanometric particles do not leak any radiogenic ^{40}Ar due to their particle size, as the smallest particles are sometimes older than the coarser ones (e.g. Clauer et al., 1997), which is crucial for the overall application of the K-Ar method being reviewed here.

In addition, K-Ar ages can also record information about the crystal-growth mechanism and associated reaction rate(s). For instance, the crystal-growth rate may have remained constant during the entire process, with or without significant changes in temperature or chemical composition of the interacting fluids (Fig. 2; Clauer, 2006). Depending on fluid temperature and chemical characteristics, the mode of the K-Ar ages of nanocrystals of variable size will locate either: (1) towards the middle of the theoretical illitization time span when the rate was about constant; (2) close to the beginning of the theoretical time span when the rate decreased or was

248 interrupted; or (3) towards the end of the time span when the crystallization rate increased
249 progressively. In summary, K-Ar ages of bentonite illite-type nanoparticles are able to record a
250 complicated illitization history that might have occurred on the basis of constant or varied growth
251 rates, and of one or more successive nucleation/growth episodes. If such scenarios occur in
252 individual bentonite beds of a given stratigraphic age, the interpretation will be necessarily
253 complicated, raising questions about the sample preparation and analysis, but also and more
254 importantly to decrypt how illitization recorded the complex evolution of a whole sedimentary
255 basin, as was attempted in the East Slovak Basin (Clauer et al., 2014b).

256 While electron microscope observations and XRD measurements of nanosized particles
257 are informative about the physical aspects of particle growth, the $\delta^{18}O$ values of the crystal
258 separates can provide information about the nucleation and growth conditions, especially about
259 the fluid-particle interactions (Fig. 4 of Clauer, 2006). A decrease of $\delta^{18}O$ from fine to coarse
260 particles suggests either a temperature increase, a change in the $\delta^{18}O$ of the interacting fluid,
261 and/or a variable water/rock ratio during growth, whereas a $\delta^{18}O$ increase implies the opposite.
262 Only limited information is yet available on hydrogen isotopic data of nanoparticles, perhaps
263 because of the difficulty in separating H from hydroxyl and interlayer water (e.g. Savin and
264 Hsieh, 1998).

265 For completeness, it might be recalled that the label "fundamental" corresponds strictly to
266 an extremely small size of crystals and aggregates that were obtained following a specific sample
267 preparation and particle separation presented below. The term "fundamental" has no connotation
268 other than the fact that the particles are nanometric in size. However, to avoid any rhetorical
269 debate about the meaning of "fundamental" whilst accepting the concept and definition of
270 Nadeau et al. (1984), the term "nanometric" has been adopted hereafter to identify these very fine
271 and small crystals, although it is only partly appropriate because it refers to the thickness of the
272 particles in nanometers, whereas their width can be of micrometric size.

273

274 ## 3. An isotopic concept for a nucleation/growth model of nanometric illite

275

276 The locations of the elements of concern here are of specific and complementary interest
277 in studying the intimate conversion of smectite to illite, as B is hosted by tetrahedral sites where
278 it can replace either Si or Al, Li is integrated in octahedral sites replacing Al, Mg or Fe, K is the

dominant cation in the interlayers, which host also Rb, Sr and radiogenic ^{40}Ar. Oxygen is at the corners of either the tetrahedral or octahedral sites, whereas structural hydrogen is mostly concentrated at the edges of the crystals where the tetrahedral and octahedral sites connect (Fig. 1). Their combined study is a significant opportunity for an improving insight into illitization at crystal size.

3.1. Some basics about stable isotope geochemistry of light elements

Boron has two natural stable isotopes (^{11}B and ^{10}B) that represent respectively about 80 and 20% of the element. Its concentrations and isotopic signatures vary widely in surface environments, especially in natural waters, for which four orders of magnitude in concentration and $\delta^{11}B$ ranges from –16 to +59‰ were reported (Vengosh et al., 1994). B isotopes have been used for about two decades to trace the source of waters (Palmer and Sturchio, 1990), the evolution of brines (Vengosh et al., 1991a, b; Moldovanyi et al., 1993), the origin of evaporites (Vengosh et al., 1992; Swihart et al., 1996; Bottomly and Clark, 2003), and to examine hydrothermal flow systems (Leeman et al., 1992). Lithium has also two naturally stable isotopes (^{7}Li and ^{6}Li) with abundances of 92.5 and 7.5%, respectively. As Li is easily hydrated, it does not occur as a free element on Earth, but represents a minor part of most igneous rocks. It occurs in many natural brines and fractionates isotopically in a wide variety of natural processes involving either mineral precipitation from and alteration by fluids, or ion exchanges (e.g. Chan and Edmond, 1988). Known to substitute for Mg and Fe in octahedral sites of clay minerals, ^{6}Li is incorporated preferentially over ^{7}Li (Teng et al., 2004; 2006; 2007; 2008). As for oxygen and hydrogen examined here, the B and Li isotope compositions are usually expressed as deviations (in ‰) from standard materials (Williams et al., 2012).

The $\delta^{11}B$ of seawater (+39.5 ‰) is enriched in ^{11}B relative to the oceanic and continental crust (Lemarchand et al., 2000; 2002). Although the reason for this is not yet well understood, it is assumed that it is due to a preferential adsorption of aqueous ^{10}B (predominantly from borate anion $^{10}B(OH)_4^-$) onto clay particles. Isotope exchange reactions between the two soluble species $^{11}B(OH)_3^0$ and $^{10}B(OH)_4^-$ control the B isotopic partitioning in solution (Schwarcz et al., 1969). These authors calculated a fractionation enriching ^{10}B in clays by about 30-40 ‰. They also noticed that it is in good agreement with a seawater $\delta^{11}B$ value calculated when assuming a steady state ocean with respect to both the B concentration and isotope composition. This steady

state is approximately maintained by a combined input of B from continental weathered rocks and removal by sediment adsorption and mineral substitutions. Subsequently, Williams et al. (2001a, b) and Williams and Hervig (2002) made laboratory experiments on B fractionation during exchange processes between I-S and water, considering that diagenetic clay nucleation and growth induce incorporation of ^{10}B into illite-type structures (Spivack et al., 1987). They observed that the B-isotope exchange kinetic rates follow mineralogical recrystallization of smectite into illite. However, depletion of B contents in pore waters with increasing $\delta^{11}B$ is not the general rule, especially in the Gulf Coast Basin (Land and Macpherson, 1992; Moldovanyi and Walter, 1992), suggesting another source of ^{10}B in deep basinal environments. In an attempt to identify the source(s) of ^{10}B in deep sedimentary reservoirs, Williams et al. (2001a, b) studied the B isotope composition of organic matter from hydrocarbon reservoirs of the Gulf Coast and found that pore fluids associated with hydrocarbons are B-enriched. As ^{10}B is preferentially taken up by clay minerals, or retained in remnant kerogen, the pore fluid becomes progressively ^{11}B-enriched during fluid migration through clay-rich sediments. Bitumen has been recently shown to contain several hundreds of μg/g B (Williams and Hervig, 2013) that yields isotopic compositions 10‰ heavier than the associated kerogen, with $\delta^{11}B$ <0‰ for kerogen and clays and >0‰ for bitumen. Significant amounts of B are reported in kerogen from coals and oil source rocks, with $\delta^{11}B$ values all less than 0‰, similar to authigenic pore-filling clay minerals in sandstone reservoirs (Williams and Hervig, 2004; Tagahashi et al., 2011). Boron isotopes are also fractionated during hydrothermal mineral crystallization (Oi et al., 1989; Spivack et al., 1990; Leeman et al., 1992). In summary, there is no specific mineral isotopic fractionation for B isotopes, as there is for oxygen, but there is rather an ion-coordination dependence of the fractionation. In diagenetic environments where the pH is buffered to <7, B is dominantly in trigonal coordination in the fluids as $B(OH)_3$ that preferentially accomodate ^{11}B, but it substitutes in tetrahedral sites of authigenic clay crystals, which prefer ^{10}B (Palmer and Swihart, 1996), inducing a major isotope fractionation as a function of temperature (Williams et al., 2001; 2007).

Li is commonly enriched in oilfield brines and saline formation waters of sedimentary basins (Collins, 1975; Connolly et al., 1990; Fontes and Matray, 1993; Moldovanyi et al., 1993; Stueber et al., 1993; Wilson and Long, 1993). Also, because of its long residence time, ocean water is homogeneous in Li concentration (about 180 μg Li/L) and isotopic composition (δ^7Li = 32‰; Chan and Edmond, 1988; You and Chan, 1996). Time-dependent $^6Li/^7Li$ variations in

seawater have also been discussed recently (Misra and Froelich, 2012) based on Li-isotopes of foraminifera. These authors concluded that the δ^7Li of the seawater rose by 9‰ during the last 60 million years, resulting from changes in continental and seafloor weathering. However, evidence for the critical lack of diagenetic alteration in the analyzed foraminiferas that might produce similar trends was not given, and a potential contribution of Li from organic sources was not evaluated. Marine sediments are generally rich in Li with concentrations ranging from about 100 μg/g in pelagic clays to 1 μg/g in carbonates and biogenic silica (Chan et al., 2002).

Oxygen and hydrogen, the latter as OH groups in the crystal structure of clay minerals, were a focus of extensive research on their fractionation between different types of clays and waters at temperatures from Earth's surface to 200 °C (e.g. Savin and Epstein, 1970a; Savin and Lee, 1988). The δD and δ^{18}O values of weathering clays plot on lines nearly parallel to the Meteoric Water Line with slopes close to 8, but with different intercepts. Such δD-δ^{18}O trends were also reported for varied hydroxides and oxy-hydroxides (Yapp, 1993). The relationships between δD and δ^{18}O in clay-water systems indicate that the clays are enriched in ^{18}O and depleted in D in a temperature-dependent fashion. Savin and Epstein (1970a) and Lawrence and Taylor (1971, 1972) also demonstrated that clay crystals are able to retain their isotopic signatures through further processes of erosion, transportation and deposition. Bird and Chivas (1988) showed that oxygen-isotope exchange in kaolinite being negligible, post-formational hydrogen-isotope exchange is possible at temperatures below ~80 °C. From δD and δ^{18}O of diagenetic kaolinite and 10Å clay minerals (illite, illite-smectite), Longstaffe and Ayalon (1990) reported that hydrogen-isotope re-equilibration between diagenetic kaolinite and formation water can be independent of oxygen-isotope exchange at temperatures as low as 40 °C.

Three kinds of water are usually reported in clay minerals: adsorbed on the particle exterior surfaces, held in interlayer positions, and OH groups held in structural sites of the mineral framework. Water held in the interlayer position of coarser clay particles is theoretically lacking in nanocrystals as the smectite-type interlayers of the original I-S were basically dismantled by infinite dispersion. Therefore, the remaining adsorbed water isotopically exchanges with ambient water very fast, in less than a few days. On the other hand, the rates of isotopic exchange between structural and ambient water are often slow and depend on the temperature and type of clay minerals. Unlike the rate of oxygen-isotope exchange, that of hydrogen-isotope exchange between structural hydrogen and hydrogen of ambient water can be

relatively rapid at temperatures as low as 60 °C (O'Neil and Kharaka, 1976). As an impressive application, Longstaffe and Ayalon (1987) reconstructed the evolutionary path for the $\delta^{18}O$ of pore fluids and associated clay minerals of the lower Cretaceous Viking Formation in the Western Canadian Basin. More studies with similar aims are available, on the basis of varied processes at different localities (e.g. Glasmann et al., 1989; Fallick et al., 1993; Robinson et al., 1993; Girard and Barnes, 1995; Kotzer and Kyser, 1995; Clauer et al., 1999; Zwingmann et al., 1999).

3.2. Some basics about K-Ar and Rb-Sr isotopic dating of nanometric illite

The K-Ar method is a pioneer dating technique based on the natural decay of ^{40}K into ^{40}Ar (e.g. Dalrymple and Lanphere, 1969; Faure, 1986), which makes it especially well suited for dating illite- and glauconite-type materials. It has been applied with varied success to dating such low-temperature and fine-grained separates since the attempt by Wasserburg et al. (1956). The method is also appropriate for dating illite-type nanocrystals, especially from bentonites that lack very fine-grained detrital particles (e.g. Clauer et al., 1997), more than the related $^{40}Ar/^{39}Ar$ method, for instance, as it does not need a problematic irradiation with necessary aliquot encapsulation and restoration of the recoiled ^{39}Ar expelled during irradiation of crystals that are smaller than the recoil distance (Clauer et al., 2012; Clauer, 2013). As any other isotopic dating or tracing method, it needs complementary mineralogical, chemical and morphologic information on the separates. Also, closed-system behavior of the selected minerals is required, as for any isotopic dating method, which is especially crucial for Ar trapped in nanosized particles that is not bonded to other atoms or ions in the mineral structure like the cations of the classical isotopic dating methods. Rather it is only held ("squeezed") in interlayer sites without any chemical bonding with the surrounding elements but because of its larger ionic radius than the radioactive ^{40}K. Therefore, it is particularly susceptible to be released by incipient crystal alteration, especially when temperature increases.

The Rb-Sr method, which is another pioneer method, is also well suited for the study of illite-type nanocrystals. The behavior of K and Rb being identical in illite interlayers, it has been shown that in anchi-to-epimetamorphic conditions, the K-Ar and Rb-Sr methods often provide similar ages on the same illite fractions (e.g. Clauer and Chaudhuri, 1998), which is not found systematically in diagenetic environments (e.g. Clauer and Chaudhuri, 1995). Beside the dating

aspect, the Rb-Sr method provides information in differentiating Rb, Sr, and other elements that are either substituted in the mineral structure, or adsorbed on the exterior surfaces and in interlayer sites (Clauer, 1982). This information can be quantified by gentle leaching of various size fractions with dilute acid (e.g. 0.1M HCl or HAc) or other reagents (EDTA, acetates, etc; Clauer et al., 1993), and by separate analysis of the leachates and residues. Differentiating the Sr amounts and $^{87}Sr/^{86}Sr$ ratios from inside and outside the crystals has the advantage of identifying the Sr content and $^{87}Sr/^{86}Sr$ ratio from interstitial fluids that interacted with the nucleating and growing illite-type crystals, or from fluids that percolated through the pore system after mineral nucleation and growth (Clauer et al., 2003).

4. Specific analytical aspects

Illite-type nanometric crystals were first separated, studied, identified and defined by Nadeau et al. (1984). These authors explained their occurrence by dissolution of smectite layers from I-S, followed by crystallization and growth of new illite layers in the same mixed-layers. This model was promoted by Inoue et al. (1987), and Eberl and Środoń (1988). The illite-type layers of such intergrowing mixed layers can be separated after infinite osmotic dispersion by a method briefly described below to become so-called "fundamental" particles. Depending on the exact mechanism of illitization, solid-state transformation or dissolution/precipitation, and assuming that the particle separation was successful, one might expect different isotopic records for crystals that have varied particle thickness depending on the host rock, temperature and duration of the nucleation and growth processes, and the chemistry of the interacting interstitial water.

4.1 Separation of fundamental particles

The whole-rock samples are gently crushed, sieved, mixed with deionized water and disaggregated using either an ultrasonic bath or probe, or the freezing-thawing technique (e.g. Zwingmann et al., 1999). These two methods are recommended instead of crushing to avoid as much as possible communition of detrital grains into the clay-sized fractions, as their occurrence is known to bias the results. The slurries are then treated with dilute sodium-acetate buffer, sodium dithionite and hydrogen peroxide to remove the soluble mineral phases and organic

matter from illitic matrix (Jackson, 1975). The next step consists of separating the <2.0 μm size fraction of the samples by gravimetric sedimentation in deionized water following Stokes' law, and further separating the <0.2 μm fraction by centrifugation. The recovered <0.2 μm fraction is then diluted to a concentration of 1g/40L, to ensure "infinite" osmotic swelling by breaking apart the smectite interlayers, and separated into smaller sub-fractions by continuous-flow high-speed ultra-centrifugation. The finest (<0.02 to <0.03 μm) and coarser (0.02-0.05, 0.05-0.1 μm) fractions are finally removed from corresponding diluted fluids by flocculating the suspended matter with NaCl (1M), and by removing the excess electrolyte by dialysis and repeated centrifugation (Środoń et al., 1992). The accuracy of the crystal separation can be monitored by TEM observations.

The fact that B and Li can also be held in the interlayer sites of I-S makes essential the removal of these interlayer species by cation exchange. The reason for this is the fact that the $\delta^{11}B$ of the interlayer B can be significantly different from that of the illite tetrahedral sites (Williams et al., 2007; Fig. 3). Polyhydric alcohol mannitol is often used as a complexation agent (Hingston, 1964) to remove the surface-adsorbed B, because it strongly binds to these light elements ensuring easy cleaning. It is also recommended to check the purity of the reagents, especially in the case of B and Li isotopic studies, to avoid any potential chemical biases, as B and Li are common impurities in laboratory reagents. The individual size fractions are then ready to be analyzed for their mineralogical-crystallographic characteristics and chemical-isotopic compositions.

4.2 Solid-state analysis

In recent decades, instrumentation has been developed for solid-state analysis of trace elements and of their isotopes at a microscale. In brief, instruments like the Secondary Ion Mass Spectrometer (SIMS) use a primary ion beam (most commonly consisting of O^-, O_2^+ or Cs^+) that is directed towards a flat polished sample at impact energies of a few to more than 20 keV under high vacuum (~10^{-9} Torr) conditions. Because the bond strength of minerals is on the order of a few electron volts (eV), these high-energy collisions break chemical bonds in mineral structures and a cascade of secondary atoms and molecules is ejected from sample surface, referred to as 'sputtering' (Wilson et al., 1989). A few percent of the secondary particles are ionized, and are accelerated away from sample. In most SIMS instruments, the ions are guided through an

electrostatic analyzer followed by a magnetic sector. After mass selection, the ions are detected with either a Faraday cup or an electron multiplier for low intensity signals. Complementary information about this analytical method can be found in Williams et al. (2012).

Relative to traditional mass-spectrometry, SIMS has the advantage of eliminating the necessity for chemical extractions that may bias the isotopic ratios of interest. It can also provide high spatial resolution for examining micro-scale chemical variations. For nanosized crystals, such as fundamental clay particles, the SIMS advantage is the small volume (~10^{11} atoms) consumed for analysis at high precision allowing interpretation of chemical or temperature variations on the various nanometric size fractions (bins) potentially representing stages of crystal growth (Williams et al., 2012). The resolution of these analyses has improved to the point where sub-micron resolution can be achieved and still provide useful precise isotope ratios (Valley and Kita, 2009). However, this resolution does not reach the scale of nanometric clay crystals. Solid-state SIMS analysis of Li and B (content and isotopic composition) has been applied to varied illite-rich nanocrystals from volcanic and sedimentary rocks (Williams et al., 2012), with statistically significant results (e.g. errors <2‰ for a range of values >30‰).

5. Case studies of nanometric illite crystals from bentonites

5.1 Initial K-Ar results and hypotheses

Clauer et al. (1997) dated illite-rich <0.02-0.03 μm fractions from two bentonite beds near Trhovište and Čičarovče in the East Slovak Basin, reporting that the K-Ar age of the finest fractions was either younger (well Trh), or older than the slightly coarser fractions (well Cic; Fig. 4). This result was explained by two potential processes: either nucleation followed by growth, exemplified by coarser fractions younger than the finer, or episodic nucleation and growth with the finest crystals being the youngest. The $\delta^{18}O$ values of the same nanometric fractions, which will be discussed in a later section, appeared also to be different, relatively constant at 18‰ for the nanofractions of well Trh and decreasing from 12 to 10‰ for those of well Cic. In the Trhovište bentonite bed sampled at 3015 m depth, illitization lasted from ~15 Ma when the bentonite reached a temperature of 70-80 °C, to ~7 Ma when it reached a temperature of 150-160 °C. In the Čičarovče core located about 20 km away, illitization started at ~11.5 Ma when the sample buried now at 2495 m depth reached 70-80 °C, and it lasted until the present time at about

120 °C. The data also suggested that different processes can occur in the same type of rocks of the same basin, such as one or several illitization episodes located only about 20 km apart on a horizontal scale and 520 m apart on a vertical scale.

The shales that sandwich the Trhovište and Čičarovče bentonite beds were also sampled for recovery of the illite nanoparticles of their I-S (Clauer et al. 1997; Honty et al. 2004). The K-Ar data of these crystals were systematically older than the stratigraphic age of the respective units, suggesting that the authigenic illite nucleated either on or next to detrital particles that were already present in the rocks when illitization started. This leads to the assumption that the detrital particles were as small and fine as the authigenic crystals in the shale beds. Similar K-Ar ages older than the depositional age of nanometric illite crystals from shales were found in other contexts, supporting the generally admitted occurrence of detrital "contaminating" minerals (Środoń and Clauer, 2001; Środoń et al., 2006). However, it cannot be denied that the authigenic crystals may have, alternatively, incorporated in their structure chemical elements, such as radiogenic ^{40}Ar that were released by dissolution of previous detrital micaceous components in a postulated closed interstitial space where the authigenic crystals nucleated. Not being able to escape, the excess of "detrital" radiogenic ^{40}Ar could have been scavenged by the new illite crystals, as reported for recent deep-sea red clays from Pacific Ocean sediments (Clauer, 2006). However, this explanation is not valid if comparing the results with those from bentonites, which are as impermeable as the nearby shales, containing probably even less interstitial fluids, but also lacking any detrital components. The determining difference at this point is that the nanocrystals of bentonites consist almost exclusively of authigenic illite, whereas those of shales apparently contain also detrital illite nanocrystals.

Concerning illitization in argillaceous sediments, it is probably appropriate to mention a study by McCarty et al. (2008) who showed that nucleation of smectite-rich particles in Gulf Coast sediments occurred on the surface of detrital particles or grains and not in their interlayer sites. This observation could explain, at least partly, the unsuccessful attempts to date authigenic nanometric illite crystals from shales, and why separation of pure authigenic illite from associated detrital particles is especially difficult, if not impossible, in shale-type sediments. It also tends to imply that authigenesis of new illite-type particles in the general smectite-to-illite trend strongly depends on the alteration rate of the deposited detrital material if the trend includes an overall dissolution of the detritus followed by a crystallization of a new generation of I-S.

5.2 In bentonites of the East Slovak Basin

Nanometric illite-type particles of I-S from more cored bentonite beds of the East Slovak Basin were studied after the work by Clauer et al. (1997), to investigate the regional extention of illitization: the physical/chemical conditions during nucleation and growth have been reported on the basis of $\delta^{18}O$ and δD isotope characterization and K-Ar dating (Clauer et al., 2014b). The nanosized particles next to salt-bearing formations showed more advanced illitization, but the duration of the process did not change, whereas the oxygen and hydrogen isotope signatures of the parental brines were modified. A comparison of the stratigraphic ages of the bentonite beds and the onset of illitization based on K-Ar ages showed that illitization was initiated by the regional mid-Miocene subsidence detected in most bentonite beds, from as early as ~17.5 to as late as ~11.5 Ma, depending on its timing at the different geographic locations. Based on age differences in the selected beds, the calculated sedimentation rate was found to vary from less than 300m/Ma to more than 500m/Ma, and the thermal gradient to range from as high as ca. 60 °C/km to less than 50 °C/km. The K-Ar ages also pointed to either short- or long lasting illitization, even in closely located beds: short (less than 2 Ma) when illitization started shortly after sedimentation and long (up to 6-8 Ma) when the onset started long after sedimentation. The K-Ar ages of the nanofractions from eight different bentonite beds indicate episodic pulses that appear to have lasted from as short as 1 million years to as long as 6 million years (Fig. 5). The pattern also suggests episodic illitization at some locations.

Illite $\delta^{18}O$ varies little when crystal size increases, whereas δD ranges widely over almost 100‰, albeit more than half of the data lie within $\pm$15‰ of -45‰ (Fig. 6). These wide δD variations are even more apparent in a diagram comparing them to the K-Ar ages (Fig. 7). As the crystallization temperature did not change significantly during crystal growth in most samples, the observed variations relate to changing interacting fluids, depending on the sample location, immediate environment, timing, and duration of illitization. These local variations in the timing and duration of illitization in bentonite beds contrast with large-scale fluid connectivity, especially in sandstone aquifers. It looks like the stable isotope compositions of nucleating and growing illite-type crystals of bentonite beds that are of limited porosity and permeability, and therefore of reduced fluid-rock ratios, give a local insight into the fluid-temperature regime of sedimentary basins rather than large-scale processes. The key concept is in the effective fluid-

558 rock ratio of the host rocks during nucleation and growth of the authigenic clay material.
559 Illitization appears, therefore, more to be of an episodic diagenetic process lasting variably along
560 different crystallization pathways and to various extents, in closely located samples, but
561 obviously depending on changing conditions that vary even in beds that were considered to be
562 mineralogically and chemically homogeneous.

563 B and Li concentrations and isotopic compositions were also measured in nucleating and
564 growing illite-rich nanocrystals from I-S of the same bentonite beds from the same East Slovak
565 Basin (Clauer et al., 2009). Most of the B contents correlate positively with the $\delta^{11}B$ of the
566 nanometric crystals (Fig. 8). The B content and $\delta^{11}B$ of three analyzed nanofractions of most
567 bentonite beds correlate positively and define a common initial field with a theoretical high B
568 content of about 475 μg/g and a $\delta^{11}B$ of about +7‰. This "reservoir" could correspond to B-rich
569 minerals, for instance of evaporitic origin (Swilhart et al., 1986; Vengosh et al., 1992; Bottomly
570 and Clark, 2003), as such were described in the basin (Honty et al., 2004). These evaporites could
571 have dissolved during the progressive burial diagenesis with slightly increasing temperature, and
572 have released some of the scavenged B that was scavenged by the nucleating illite crystals. The
573 second B-rich reservoir, with much lower contents of about 30 μg/g and a $\delta^{11}B$ of -5‰ or of
574 about 100 μg/g with a $\delta^{11}B$ of -17‰, could correspond to organic matter that is a common
575 component of almost all sedimentary sequences. When sediment layers are interbedded with
576 bentonite beds, their fluids that carry organic matter-derived components are able to migrate into
577 the bentonite layers (Williams et al., 2013). Such a transfer of organic-derived B into bentonite
578 beds was also reported by Środoń (2010). If the transfer is continuous during burial-induced
579 illitization, the coarser growing illite nanocrystals should be enriched in B relative to the initial
580 nucleating illite. However, this is not always true, as shown in the illite nanofractions of bentonite
581 beds studied here (Fig. 8). When growing, the data points of the nanofractions (numbered 1 to 3
582 from finest to coarsest) that are identified with distinct symbols for each sample, do not
583 systematically trend towards a "reservoir" containing high B amounts with high $\delta^{11}B$ (in the
584 upper right area of the figure). The B contents can also remain about constant, which is the case
585 for the nanofractions of three samples (fractions 1 to 3 of the open squares, the full squares and
586 the open circles). In the case of the three fractions of another sample (identified by grey squares),
587 the trend is again towards high B contents, but with low $\delta^{11}B$.

588 The influence of temperature on the $\delta^{11}B$ of the <0.02 μm fractions is also visible from

correlations between present-day temperature determined in the wells and the $\delta^{11}B$ of five out of seven <0.02 μm illite fractions (Fig. 9). Five data points fit a correlation line with a $\delta^{11}B$ close to 0‰ for the lower temperature of ~120 °C and $\delta^{11}B$ of -12‰ for the higher temperature of 165 °C. The two other fractions plot along a second correlation line indicating lower $\delta^{11}B$ values of -13.5 ‰ at 95 °C and -15.5‰ at 135 °C. This distribution suggests the input of more isotopically light ^{10}B derived from kerogen, as temperature increases.

At the highest temperatures (>130 °C), most of the illite-rich nanofractions yield positive $\delta^{7}Li$ values (up to ~12‰), while the Li contents are systematically low, below 20 μg/g. At lower temperatures (<115 °C), the size fractions yield systematically negative $\delta^{7}Li$ values and most have higher Li concentrations (up to 140 μg/g; Fig. 10). This relationship suggests that increasing temperature fractionates ^{7}Li from organic matter into the fluids. Comparing the Li contents and $\delta^{7}Li$ of the studied nanofractions indicates the major correlations. The less thermally mature sediments contain clays that are characterized by a Li content of 10 μg/g with a $\delta^{7}Li$ of -16‰, a Li content of 40 μg/g with a $\delta^{7}Li$ of about -13‰, or a Li content of about 140 μg/g with a $\delta^{7}Li$ of -22‰. This decreasing $\delta^{7}Li$ with increasing Li concentration suggests that higher Li organic-rich sediments preferentially derive ^{6}Li from organics, while ^{7}Li goes preferentially into fluids during thermal maturation.

5.3 In bentonites of the Baltic Basin

The distribution of Li and B (and N) was examined in I-S from Ordovician-Silurian K-bentonites of the Baltic Basin (Williams et al., 2013). These elements are linked to thermal maturation of organic matter with fluid signatures that are distinct from those resulting from usual burial of sediments or from those migrating through basement rocks. Boron and Li-isotope variations (>10‰) of three illite nanofractions (<0.02, 0.02–0.05 and 0.05–0.2 μm) relate mainly to changes in the fluid composition during illite growth and in the temperature gradient across the basin (SW to NE) induced by tectonic activity during the Caledonian orogen (Środoń et al., 2009).

The K-bentonite beds mark stratigraphic timelines (Late Ordovician-Early Silurian), and were correlated across the basin (Huff et al., 2002), while illitization ages of these K-bentonite beds reflect either the timing of a tectonic-related temperature gradient, or that of deep burial.

619 The K-Ar data define a central zone of mostly older ages (392-382 Ma) that extend from
620 Denmark to Estonia, and are bordered to the northwest and southeast by bentonite beds having
621 younger ages (362-302 Ma) because of a slower burial (Fig. 11A). Based on its oxygen isotope
622 composition, illite from the slowly buried bentonites precipitated from different (isotopically
623 lighter) fluids than that of the central basin.

624 In the central Baltic Basin, bentonites were deposited on a carbonate platform near
625 Estonia, grading to deep shales near Denmark and Poland. Compositional variations in illite of
626 the K-bentonite beds reflect fluids from different sources. High B (>250 μg/g) and Li (>100
627 μg/g) contents were observed in bentonite illite of northeastern Estonia. Identified trends follow a
628 thermal gradient for illitization with high tectonically induced temperatures near Poland (200 ˚C)
629 to low temperatures (90 ˚C) in northeastern Estonia. The B- and Li- isotope ratios of illite also
630 show significant trends across this thermal gradient: $\delta^{11}B$ decreases from southwest (+18‰) to
631 northeast (-4‰), while $\delta^{7}Li$ increases from -10‰ near Poland to +32‰ (seawater value) near
632 Estonia (Fig. 11B).

633 The Cambrian Alum shale, which is a hydrocarbon source rock of the Baltic Basin, is an
634 adequate potential source for interpretation of isotopically light B and Li in the migrating
635 hydrocarbon-related fluids associated with illitization of the bentonite beds. More than 50% of
636 the B and Li from the Alum shale are associated with organic matter. Organics released from
637 kerogen during thermal maturation created a fluid that mixed the isotopically light B and Li
638 derived from hydrocarbon generation (with high B and Li concentrations), with the B and Li
639 from basement (plutonic) sources near Estonia. With increasing thermal maturity, illite $\delta^{11}B$ and
640 $\delta^{7}Li$ of the Alum shale varied by ~15‰ (Fig. 12). The $\delta^{11}B$ of illite was istotopically light at gas-
641 generation thermal grades, while the $\delta^{7}Li$ was isotopically heavier, however still lighter than
642 seawater $\delta^{7}Li$. This suggests a difference in the bonding of ^{10}B and ^{6}Li in the kerogen and
643 therefore differences in the release temperatures of these atoms during thermal maturation. The
644 trends (magnitude of isotopic change) observed in the Alum shale source rock being similar to
645 those measured in the overlying bentonite beds, it can be concluded that organic sources of B, Li
646 (and N) dominated in fluids that migrated through the bentonites beds from the southwestern
647 Baltic Basin, while basement-derived fluids dominated in those of the northeastern basin. The B
648 and Li contents and isotope compositions record paleofluid changes during illization, and they
649 can be used to identify regional pathways of chemically distinct oil and gas related fluids on the

650 basis of careful consideration of local chemical inputs.
651
652 *5.4. In bentonites of the Appalachian orogen*
653 Nanometric illite particles from <0.02 to 0.2 μm of K-bentonites from northwestern
654 Georgia (USA) were studied for their oxygen and hydrogen isotope geochemistry, and their K-Ar
655 isotopic dating for a better constraint of the tectono-thermal history of the Appalachian orogen in
656 the northern American Mid-Continent (Clauer et al., 2013). The crystal population is ordered I-S
657 with very homogeneous crystal thickness distributions in each sample, but with different
658 crystallite thickness ranges depending on the location of the samples. The volume-weighted and
659 area-weighted mean thicknesses of the crystallites were calculated according to the Bertaud-
660 Warren-Averbach theory (Eberl et al., 1997), as well as the parameters α (= mean of the natural
661 logarithms of the thicknesses) and β^2 (= variance of the natural logarithms of the thicknesses). On
662 the basis of these parameters, illitization occurred in all size fractions, except for one sample, by
663 simultaneous nucleation and crystal growth (Fig. 13). In that specific sample, simultaneous
664 nucleation and growth was followed by growth without nucleation.
665 The K-Ar ages of the nanofractions organize into two isochrons at 319.9 ± 2.0 Ma with an
666 initial $^{40}Ar/^{36}Ar$ ratio of 271 ± 66, and at 284.9 ± 1.2 Ma with an initial $^{40}Ar/^{36}Ar$ ratio of 310 ±
667 44 (Fig. 14). One data point above the older isochron and three between the two isochrons
668 suggest some detrital contamination for the former and a possible supplementary generation of
669 nanoparticles for the three others. Those with the older crystallization age consist of illite and
670 illite-rich I-S, whereas those with the younger age contain only I-S, mainly with expandable
671 interlayers. The two K-Ar isochron ages fit the age ranges published previously for similar K-
672 bentonites with age patterns from 240 to 270 Ma in the southwestern region, from 270 to 300 Ma
673 in the central and the southern Appalachians, and from 315 to 370 Ma to the north.
674 The two K-Ar dated generations of illite crystals yield very consistent $\delta^{18}O$ values at +17
675 ± 1‰ for the older and at +21 ± 1‰ for the younger (Fig. 15A), while the δD values do not show
676 any trend. A comparison between $\delta^{18}O$ and age confirms the correlation with the K-Ar ages (Fig.
677 15B). If crystallization temperatures of the nanometric illite were between 100 and 200 °C, on the
678 basis of complementary microthermometric determinations, the hydrothermal fluids had $\delta^{18}O$
679 values of 4 to 8 ± 1‰ at the lower temperature of 100 °C, and of 11 to 15 ± 1‰ in the same
680 locations at the higher temperature of 200 °C. Apparently, the $\delta^{18}O$ of the fluids remained

681 unchanged during local illitization, but varied depending on the timing and geographic location
682 of the samples.
683
684 *5.5 In Walsen Dike metabentonite*
685 The Cretaceous Pierre Shale near Walsenburg (Colorado, USA) is an organic-rich shale
686 containing bentonite beds that was cross-cut normal to bedding by a basaltic dike known as the
687 Walsen Dike (Johnson, 1964). The thermal gradient across the contact metamorphic zone
688 provides an ideal natural example of smectite illitization in the bentonite bed. This contact-
689 metamorphosed bentonite has been used to model illitization in response to the thermal pulse
690 (Lynch, 1985; Pytte and Reynolds, 1989), reaction kinetics of NH_4 fixation in the illite interlayer
691 (Williams and Ferrell, 1991), timing of B substitution in the tetrahedral sites (Williams et al.,
692 2007) and of Li in octahedral sites of the authigenic illite (Williams et al., 2006). Illitization of
693 smectite was shown to have occurred from 500 ˚C at the contact with the basaltic dike
694 (lamprophyre) to 200 ˚C in the buried country rock.
695 Using vitrinite reflectance, Bostick and Pawlewicz (1984) determined the thermal
696 maturity of the Pierre Shale organic matter. The temperature zone that generated mature
697 hydrocarbons (equivalent to the "oil window") occurred between 8 and 25 m away from the
698 shale/dike contact. Both B and Li showed a maximum substitution in authigenic illite of this oil
699 window with highest concentrations of 75 μg/g tetrahedral B (Williams et al., 2007) and 40 μg/g
700 octahedral Li (Williams et al., 2012). B-isotope values in the bulk Walsen Dike metabentonite
701 range from +8 to -17‰ when approaching the dike (~500 ˚C). However, the tetrahedral-B values
702 (after removal of the interlayer-B) scatter less, from -2 to -17‰, with $\delta^{11}B$ increasing up to +8‰
703 about 10 m away from dike contact (Fig. 16). This $\delta^{11}B$ value of +8‰ in the tetrahedral site is
704 maintained in the country rock away from dike. On the basis of the temperature gradient, the
705 water $\delta^{11}B$ composition decreased from ~16‰ to 4‰ as temperature and organic maturity
706 increased in the oil window. Again, addition of ^{10}B to the pore fluids at high temperatures was
707 interpreted as resulting from release of B from the surrounding thermally matured organic matter.
708 The $\delta^{7}Li$ values of the same <2.0 μm I-S fraction increase from country rock toward the
709 dike contact from -15 to -5‰ (Fig. 16). The isotopic composition in the shale is light away from
710 dike, potentially influenced by the organic-rich source of light B and Li (Williams et al., 2012;
711 2013). It is also possible that the more positive $\delta^{7}Li$ near the dike has been biased by some ^{7}Li

712 introduced by migrating metasomatic fluids. Assuming that the first illite crystals precipitated at
713 ~80 ˚C in the country rocks, which is common in deeply buried sediments, the δ^7Li composition
714 of the water was initially ~22‰ (Williams et al., 2012). If the water composition remained
715 constant during temperature increasing to 200 ˚C, the coarse illite would be expected to have a
716 δ^7Li of +9‰. No reasonable temperature can be calculated, given the local geological constraints
717 that could produce the observed δ^7Li of –10.5‰ for illite crystals precipitated from a fluid with a
718 +22‰ δ^7Li value. An external source of ^{6}Li that lowered the δ^7Li value of the pore water is
719 therefore required. The decreasing δ^7Li value away from dike is consistent with ^{6}Li diffusion
720 away from heat source. If all of the illite grew at the maximum regional temperature of 200 ˚C,
721 the water would have had an initial δ^7Li composition of +15‰, decreasing to 3‰ as illite grew.
722 This scenario could be explained by diffusion of Li away from the igneous heat source, with the
723 light isotope diffusing faster than the heavy isotope.
724 Within the 13-m contact metamorphic aureole of the dike, the B and Li isotope trends are
725 parallel, convincingly proving that the minerals generated during one fluid event. Also to be
726 mentioned is the change in δ^7Li from +3 to -11‰ in progressively coarser crystals of the
727 bentonite from the contact zone (Williams et al., 2012). Such change could reflect the declining
728 temperature as the dike cooled, considering a constant water composition.
729

730 ## 6. Studies of nanometric illite crystals of shales and sandstones

731

732 *6.1 In shales of the East Slovak Basin*

733 The initial test of K-Ar dating illite-rich nanoparticles from shales was made as a
734 comparison with nanocrystals from nearby bentonite beds in the East Slovak Basin (Clauer et al.,
735 1997). The age differences were significant among the shale and bentonite nanometric separates
736 of identical stratigraphic age: the K-Ar age of the <0.02 μm fractions of the Cic 1/20 bentonite
737 was at 7.4 ± 2.4 Ma, while that of the nearby Cic 1/16 shale gave 39.0 ± 1.9 Ma. The K-Ar age of
738 the shale fractions increased to about 68 Ma for the 0.02-0.05 and 0.05-0.1 μm sizes, while those
739 of the corresponding bentonite remained similar at 3.8 ± 2.0 Ma. The coarser 0.1-0.3 μm fraction
740 of the shale even continued to increase to ~109 Ma relative to a constant 5.1 ± 1.2 Ma age for the
741 equivalent size fraction of the bentonite. Significantly older than the 13-Ma deposition timing
742 (Lower Sarmatian), the K-Ar ages of the shale-bearing nanoparticles require the generally

743 admitted occurrence of detrital crystals or mineral fragments. In summary, the K-Ar age of the
744 nanoparticles extracted from shales continuously increased from 39.0 $\pm$ 1.9 to 108.8 $\pm$ 3.0 Ma,
745 while those of the nearby bentonite unit remained at about 5.0 $\pm$ 2.0 Ma. Considering the age of
746 the detrital nanoparticles at ~110 Ma and that of the authigenic nanoparticles at ~5 Ma, a rough
747 calculation suggests that the finest nanoparticles of the shale unit already consisted of one third
748 of detrital components, and that this amount increased to two thirds of the total nanocrystals in
749 the coarser 0.02-0.1 μm size.

750 Somehow disappointing, this initial result did not raise much concern to look more into
751 abnormally high K-Ar ages of diagenetic nanocrystals from shales. The belief that nanofractions
752 of shales consistently represent mixtures of detrital and authigenic crystals that are not separable
753 by the available techniques did obviously not encourage further studies on the topic. However, if
754 a physical separation of both, the authigenic and detrital clay crystals appears impossible, an
755 independent analysis of the authigenic and detrital crystals is not. In fact, a way for a separate
756 analysis of both in any size fraction is possible by subjecting illite mixtures to alkylammonium
757 leaching (Chaudhuri et al., 1999; Clauer, 2011) based on the specificity of alkalammonium
758 cations of replacing stochiometrically K in dioctahedral micas, not in trioctahedral micas. If the
759 detrital illite of the leached mixture is di-octahedral, the K-Ar age of the residue after
760 alkylammonium leaching will be indicative of the crystallization age of the tri-octahedral
761 authigenic illite. Conversely, if the authigenic illite is di-octahedral, the K-Ar age of the residue
762 after leaching will be close to that of the detrital supply. For completeness, another way to
763 overcome an impossible mechanical separation of authigenic and detrital illite nanocrystals was
764 explored by mathematical simulations combining the changing K-Ar systems of aggrading
765 authigenic and degrading detrital minerals (Lerman et al., 2007; Clauer and Lerman, 2009).

766 In studying flysch material from Podhale-Orava Basin in the Western Carpathians, Środoń
767 et al. (2006) reported that nanometric mineral assemblages only homogenize completely their K-
768 Ar system when subjected to low-grade metamorphic conditions, from 125 to 180 °C, which
769 confirmed earlier conclusions of Środoń and Clauer (2001) in a similar study on nanoparticles
770 across the Teisseyre-Tornquist tectonic zone of Pomerania (Poland). However, no information is
771 yet available about how authigenesis of nucleating crystals and altering detrital crystals combine
772 chemically. Środoń et al. (2002) provided a theoretical simulation of the illitization process using
773 a nucleation and growth mechanism, but they did not take into account the progressive alteration

774 of the detrital components. Interestingly, a fast burial followed by a slow burial provides older K-
775 Ar ages for the nanocrystals than the reverse, a slow burial followed by a fast burial (Fig. 17),
776 which is not necessarily the expected result if considering temperature increase as the main
777 driving parameter.
778
779 *6.2 In Paleogene shales of the French Massif Central*
780 Nanofractions of the well-known "Illite du Puy" were also analyzed for their K-Ar
781 systematic (Clauer, unpublished; data in Table 1). Interestingly, this illite described first in an 80-
782 m thick Late Eocene (Ludian; 40-34 Ma) argillite-type horizon covering the plutonic basement of
783 the French Massif Central (Gabis, 1963) also consists of mixtures of authigenic and detrital
784 nanocrystals. Five shale samples were collected near Brives-Charensac in the center of the Puy-
785 en-Velay basin to document further the authigenic-detrital relationship of nanometric illite-rich
786 shale separates.
787 The samples were subjected to the specific nanoparticle separation including chemical
788 treatments, infinite dispersion and high-speed flow-through centrifugation. The size fractions
789 consist of the 1Md illite polytype in sample 2, with some kaolinite in the coarser fractions of
790 sample 5, and some authigenic K-feldspar in sample 1. Coarse size fractions (>10 μm) of four
791 samples were also separated and purified, identified by XRD and K-Ar dated to establish the ages
792 and origin of their components. The >10 μm fractions of samples 4 and 5 were selected because
793 they consisted almost exclusively of recognizable detrital quartz, micas, K-feldspars and
794 plagioclases with a small amount of secondary quartz. Conversely, the coarser >10 μm fractions
795 of samples 1 and 2 were selected because XRD analysis did not detect detrital components, nor
796 were the usual odd shapes observed by microscope (e.g. Hunziker et al., 1986).
797 Several fractions (<0.03, 0.03-0.05, 0.05-0.1, 0.1-0.3, 0.3-2 μm and >10 μm) of the
798 selected samples were K-Ar dated, with individual ages ranging from 42.8 $\pm$ 1.4 Ma for the <0.03
799 μm fraction of sample 3 to 269.0 $\pm$ 6.0 Ma for the >10 μm fraction of sample 5 (Table 1). The K-
800 Ar ages are positively correlated with size increase of the fractions, supporting the rule of
801 increasing content of detrital material when size increases. The four finest <0.03 μm fractions
802 plot on a line that cuts both coordinates at the origin in the Harper (1970) diagram precisely
803 relating the K_2O and the radiogenic ^{40}Ar contents (Fig. 18). These data points being apparently
804 representative of crystals for which the radiogenic ^{40}Ar relates strictly to the ^{40}K content without

805 any excess in radiogenic ^{40}Ar from detritals, the extracted ages can be considered to be
806 geologically meaningful as shown repeatedly in the literature (e.g. references in Clauer and
807 Chaudhuri, 1995). The stratigraphic age of the host rocks is therefore close to ~46 Ma, which is
808 slightly older than the attributed Upper Eocene deposition timing (40-34 Ma). At this point, either
809 the dating technique or the attributed stratigraphic age should be reconsidered.
810 In addition to the ^{40}K and radiogenic ^{40}Ar equilibrium line cutting the coordinates at zero,
811 noteworthy is the almost vertical array including the four size fractions of sample 3 and the
812 coarse >10 μm fraction of samples 4 and 5 (Fig. 18). This vertical array suggests that the
813 authigenic illite is mechanically mixed with detrital illitic material without any detectable
814 interaction between both, the detrital illite having an identical K_2O content of about 6 wt% and an
815 older K-Ar age of 260 $\pm$ 10 Ma. This older age corresponds to an already identified Upper
816 Permian tectono-thermal episode that affected the Hercynian plutonic basement on which the
817 Cenozoic sedimentary sequence was deposited, suggesting that the detrital illite of the Upper
818 Eocene sedimentary sequence represents communition micas from nearby Hercynian plutons. A
819 second sub-vertical line fits through three data points of sample 2, suggesting the same
820 mechanical mixture without crystal interaction in similar size fractions. Also, the K-Ar system of
821 the detrital components of the vertical lines appears not to have been affected by the 46-Ma
822 diagenesis that induced authigenesis of nanometric illite.
823 Of interest is also the fact that this second vertical array fitting the data points of the finer
824 fractions of sample 2 deviates into an oblique line towards higher K contents including either the
825 coarser fractions of sample 2 or most fractions of sample 1 (Fig. 18). A similar oblique line joins
826 the finest fraction of sample 5 with the highest K content to the coarsest fraction of sample 5 that
827 consists only of detrital particles. In fact, the diagram outlines three major arrays: (1) an oblique
828 line fitting through the data points of the pure authigenic illite nanocrystals, and providing the age
829 of these authigenic crystals; (2) a vertical line corresponding to an addition of detrital particles
830 characterized by an excess of radiogenic ^{40}Ar for constant K content; and (3) oblique trajectories
831 that combine addition of variable amounts of K and radiogenic ^{40}Ar, which is well illustrated by
832 the data points of sample 5. Based on the finest nanometric fraction of sample 5, which basically
833 does not contain detrital particles, the K increase is induced by nucleation and growth of
834 authigenic crystals. This hypothesis is supported by the other data points of sample 5 that trend
835 towards the detrital end-member pole with the same K content as the other detrital crystals of

similar size. Depending on individual sample evolution, the mechanical mixing of detrital and authigenic nanocrystals should also be affected by some alteration of the detritals that could have released K accumulating in an almost "closed" shale-type pore context. And last, but not least, it cannot be excluded that the age difference between the stratigraphic and isotopic K-Ar ages of the finest illite nanocrystals at 46 Ma, instead of the expected 34-40 Ma, was biased by a minute amount of detrital material. An alternative discrete addition of radiogenic ^{40}Ar in excess due to in situ alteration of detrital minerals can be discarded as the data points of the authigenic and detrital crystal mixtures plot on the expected trends drawn through the authigenic and detrital end-members.

Further information is provided by the $^{40}Ar/^{36}Ar$ vs. $^{40}K/^{36}Ar$ isochron diagram that displays an array through the two finest nanofractions of samples 3 and 5 (Fig. 19A). This array has an initial $^{40}Ar/^{36}Ar$ value of ~300, which matches the atmospheric $^{40}Ar/^{36}Ar$ ratio (Lee et al., 2006; Mark et al., 2011), therefore qualifying this line as an isochron with a meaningful age at 45.0 $\pm$ 2.2 Ma. This isochron, whose age does not match the stratigraphy for reasons just discussed, precisely includes the data points of the four finest nanofractions. The other feature to consider is the unique trend for the data points of all fractions between 0.03 and 10 μm that intersects the $^{40}Ar/^{36}Ar$ ordinate at a significantly negative value (Fig. 19B). As the initial $^{40}Ar/^{36}Ar$ ratio of any mineral can never be negative, this trend confirms the mixing of detrital and authigenic particles as demonstrated by Clauer and Chaudhuri (1995). The <0.03 μm fractions consist of 1Md illite without detectable contaminating particles of any type, and yield close individual K-Ar ages from 42.8 $\pm$ 1.4 to 48.2 $\pm$ 1.5 Ma (Table 1). When these fractions become larger, they appear to be progressively mixed with a detrital component, despite the fact that some of these coarser fractions were selected because optical microscopic observation and XRD analysis did not identify visible detrital particles. The data confirm, together with all presently available results on nanoparticles extracted from shales (Clauer et al., 1997; Środoń and Clauer, 2001; Honty et al., 2004; Środoń et al., 2006), why separation of pure authigenic illite from associated detrital particles remains especially challenging in shale-type sediments. However, this case study shows that the smallest illite nanofractions of shales can also consist exclusively of authigenic crystals, as for most bentonites and many sandstones.

6.3 Of shales and sandstones from the Mahakam Basin

867 The clay fraction of the shaly/sandy sedimentary sequence beneath the Mahakam Delta
868 (eastern Kalimantan, Indonesia) consists mainly of I-S, with minor kaolinite and/or dickite,
869 discrete detrital illite and chlorite (Clauer et al., 1999). The smectite-to-illite conversion
870 mechanism depends on the lithology of the host rocks, as well as on the identification technique
871 used: it evolves similarly in the shales and the sandstones on the basis of the XRD data of
872 micrometric fractions (<0.4 μm) from surface to about 4000 m depth, but differently for the K-Ar
873 data of the same particles.
874 The entire stratigraphic interval (from 18 to 0 Ma) shows a pronounced, continuous
875 decrease in the K-A age of the <0.4 μm clay fractions with depth from ~80 Ma for the pure
876 detrital end-member at the subsurface to ~20 Ma for the almost pure authigenic fraction of the
877 sandstones buried at 4000 m. The K-Ar system of the clay material from the associated shales
878 evolves differently as the K-Ar age decreases from ~80 Ma at subsurface to 55 Ma at 1700 m
879 depth, while remaining about constant below (Fig. 20). If the K-Ar age of the progressively
880 buried clay mixtures would have resulted from continuous addition of K and variable release of
881 radiogenic ^{40}Ar in both rock types, as often assumed, it should have decreased continuously until
882 the deepest sample, which is the case for the sandstones, but not for the shales. The almost
883 constant K-Ar pattern of the <0.4 μm fractions in the deeper Mahakam shales has been
884 tentatively explained by a significant decrease in the simulated rates of K addition and radiogenic
885 ^{40}Ar escape, each about 1 %/Ma (Lerman et al., 2007; Clauer and Lerman, 2009). The combined
886 reduction in the K supply to, and radiogenic ^{40}Ar escape from the shales below 1700 m depth,
887 could have resulted from reduction of the porosity and/or permeability due to progressive
888 compaction. Considering that the depleted supply of the sole K cannot explain by itself the
889 almost constant K-Ar ages for illite of the shales in a sediment about 2300 m thick, it would not
890 either support a "steady state" as claimed for the Gulf Coast sediments (Morton, 1985).
891 Application of the K-Ar method is therefore of special interest as it shows that any diagenetic
892 process needs to affect the K and ^{40}Ar contents of both the authigenic and detrital minerals. Here,
893 a continuous diagenetic process is needed to obtain constant K-Ar ages relative to depth, but with
894 limited supply and release rates, and therefore with reduced rock-fluid interactions.
895 Illite nanocrystals of two sandstones buried at ~4000 m beneath the Mahakam Delta yield a
896 mean K-Ar age of 15.7 $\pm$ 1.6 Ma, which is younger than the stratigraphic age but still slightly
897 biased by minute amounts of discrete detrital illite (Clauer et al., 2004). A model taking into

account the occurrence of discrete detrital illite reduces the K-Ar age to 14.4 ± 0.7 Ma, while the K-Ar ages of the nanometric illite from associated deep shales remain significantly older, above 40 Ma. While the calculated contents of K and radiogenic ^{40}Ar, and therefore the K-Ar ages of the nanofractions, fit with the analytical results in the sandstones, they do so in the shales only if one considers an excess of radiogenic ^{40}Ar from 3000 m depth downwards to fit the analytical data (Fig. 21). This excess of radiogenic ^{40}Ar at depth is intriguing because if it would be only and strictly related to the detrital minerals, it should have decreased with depth because of increasing pervasive alteration of the detrital minerals due to increased burial-related temperature. It is therefore possible that this required excess of radiogenic ^{40}Ar to explain the age differences between nanometric illite of sandstones and shales, does not relate to the classical occurrence of detrital materials in the size fractions, but rather to an accumulation of radiogenic ^{40}Ar released by the altering detrital minerals, which could not escape from pore space at depth greater than about 3000 m. Combined with the data of the Le-Puy illite obtained in the previous section, this calculation confirms that not only can an excess of radiogenic ^{40}Ar be present in shale nanofractions, but also that it could result from its sequestration in the pore system of the rock matrix.

Despite lack of visible detrital material in some nanofractions of shales, increasing K-Ar ages with grain size tend to confirm that authigenic crystals could precipitate at the surface of original detrital grains, giving progressively idiomorphic shapes to the crystals on which they crystallized. However, it cannot be denied that these authigenic crystals could also have incorporated radiogenic ^{40}Ar in excess. In favor of this hypothesis is the fact that no observation validates either dissolution of detrital crystals or solid-state process, refuting in turn a cannibalistic K supply to the authigenic nanocrystals . Notewothy here is the fact that discrete radiogenic ^{40}Ar in excess has been reported in recent Pacific deep-sea red clays for which confinement is not completed by their compaction, but by their mechanical plasticity (Clauer, 2006).

6.4 Of sandstones from the Eastern Paris Basin

Middle and Lower Triassic sandstones from the eastern Paris Basin only reached shallow burial depths of <2500 m and were only subjected to temperatures of <100 °C. Despite this limited depths and crystallization temperatures, these sandstones contain extensive amounts of

929 filamentous illite similar to widely described illite cementation at deeper depths (~3000-5000 m)
930 and higher temperatures (~120-150 °C; Fig. 22). Illite-rich nanofractions extracted from such
931 sandstones buried at 1825-2000 m were analyzed for their chemical and $\delta^{18}O$ isotope
932 compositions, and were dated by the K-Ar and Rb-Sr methods (Blaise et al., in preparation). Illite
933 K-Ar dating reports two crystallization events for the <0.05 μm illite separates, at 179.4 ± 0.8 and
934 149.4 ± 0.3 Ma, during the Lower and Upper Jurassic, on the basis of an isochron display. Illite
935 separates coarser than 0.05 μm systematically contain detrital minerals that bias the K-Ar ages
936 towards older values. The $\delta^{18}O$ of the coarser (>0.05 μm) fractions are most often lower than
937 those of the finer fractions, confirming an isotopic heterogeneity at this nanometric scale due to
938 addition of detrital minerals. For the <0.05 μm illite separates, there is also a tendency for $\delta^{18}O$ to
939 decrease with depth, suggesting higher cystallization temperatures, unless the decrease identifies
940 some addition of surface-derived water to the migrating hydrothermal fluids.
941 The nanofractions of two samples were dated by Rb-Sr after gentle acidic (1M HAc)
942 leaching of each fraction (Blaise et al., in preparation). For one of the two samples, the Rb-Sr
943 ages are systematically younger than the corresponding K-Ar ages, whereas they are identical for
944 all nanofractions of the second sample. Calculated on the basis of the leachate-untreated couples
945 of each fraction, the Rb-Sr ages depend essentially on the initial $^{87}Sr/^{86}Sr$ of the obtained arrays
946 that vary narrowly from 0.7108 $\pm$ 0.0001 to 0.7134 $\pm$ 0.0003 (2σ), which is significantly above
947 the seawater $^{87}Sr/^{86}Sr$ ratio at 0.7068-0.7076, assuming a potential Jurassic illite crystallization
948 (e.g. Jones et al., 1994). For the sample with consistent younger Rb-Sr ages than the
949 corresponding K-Ar ages, the difference might be due to increased $^{87}Sr/^{86}Sr$ ratios of the leached
950 soluble minerals. In that case, the Rb-Sr age of the leachate-untreated couples could have been
951 lowered if this soluble mineral phase depleted in Rb contained Sr with an $^{87}Sr/^{86}Sr$ ratio higher
952 than that of the Sr from illite nanocrystals. This difference calls for a crystallization timing of the
953 soluble mineral phase necessarily after that of illite. Its solubility would not have allowed it to be
954 resistant to a fluid flow at the thermal conditions of illite crystallization.
955 Elemental analysis of the acid leachates showed that for the sample with identical Rb-Sr
956 and K-Ar ages, the soluble mineral phase is dominantly a Ca-Mg carbonate (sample EST-1 in
957 Fig. 23). The soluble mineral phase of the second sample with younger Rb-Sr than K-Ar ages
958 (sample EST-2 in Fig. 23) is a Ca-phosphate, potentially a partially dissolved detrital apatite
959 detected by XRD and wet chemical analysis. However, as the crystallization temperature of illite

nanocrystals was fairly low at ~100 °C, the interacting hydrothermal fluids did probably not alter significantly the detrital micaceous fragments detected in the coarser nanocrystals, their $^{87}Sr/^{86}Sr$ ratio being partly biased by addition of either partly dissolved detrital apatite, or carbonates that crystallized after illite precipitation.

In summary, illitization was induced by episodic fluid flows related to thermal anomalies that were fueled by the North Atlantic rifting and possibly the initial Rhine-Graben rifting, although these rift systems were located several hundred kilometers away from the eastern Paris Basin. Beyond the fact that the obtained data confirm K-Ar and $\delta^{18}O$ results of illite nanocrystals from other sandstones, the additional Rb-Sr analysis also highlights the complex relationship between geodynamic events, thermal anomalies and related fluid movements. The combined data especially show that remote tectonic activities may impact crystallization of illite nanocrystals in quiescent basins through long-distance fluid flows, particularly in sandstones.

7. A concept for illitization based on isotopic studies of nanometric illite

7.1 Timing and duration of crystal nucleation and growth by K-Ar and Rb-Sr dating

Dating illite nanocrystals of bentonite and sandstone units can be successful, often producing geologically meaningful ages. This is not yet the case for shales for which authigenic illite crystals are either mechanically "polluted" by the occurrence of older nanoparticles, following a process that involves a nucleation on or next to detrital particles preventing an separation of the authigenic from detrital crystals, or by an incorporation of some radiogenic ^{40}Ar present in the pore space release during alteration of the detrital minerals. Available results from East Slovak Basin show that during burial (= an extended process with progressive temperature increase with or without slow chemical changes in the fluid chemistry), the step between nucleating (<0.02 μm) and growing (0.02-0.2 μm) can be either short (1-2 Ma) or long (>2 Ma) lasting, with a mechanism that can be either a combined nucleation and growth process, or continued nucleation (e.g. in a supersaturated fluid). Slow and long lasting processes could have favored trapping of radiogenic ^{40}Ar released into the pore space of impermeable shale-type host-rocks by alteration of their detrital nanocrystals. Of course, this explanation does not stand for bentonite beds that are devoid of detrital fragments. Conversely, nanocrystals that precipitated or recrystallized during a short lasting thermal activity (such as a hydrothermal fluid flow or fault

991 activity) have expelled the excess of radiogenic ^{40}Ar , which apparently escaped from pore space
992 of the rocks as the ages of the different size fractions are often within analytical uncertainty.
993 Dating by the Rb-Sr method adds complementary information about the origin of the
994 solutes in the interacting fluids with the initial $^{87}Sr/^{86}Sr$ ratio of the soluble minerals that can be
995 close or not to those of sea-, meteoric- or hydrothermal waters. The initial Rb-Sr dating attempt
996 was on nanosized illite crystals of the Čičarovče and Trhovište sites in the East Slovak Basin
997 (Clauer et al., 2003). The nanofractions were leached with dilute HCl (1M) to distinguish the Sr
998 adsorbed on the exterior surfaces of the illite crystals or trapped in soluble mineral phases such as
999 salts, carbonates, sulfates or oxides, from that trapped in the illite crystals. The $^{87}Sr/^{86}Sr$ ratios of
1000 the leachates were found to decrease systematically with increasing particle size that is to say
1001 during crystal growth. The straightforward explanation for such a decrease towards seawater
1002 $^{87}Sr/^{86}Sr$ ratio is that there was an addition of Sr from outside the bentonite beds into the pore
1003 space where smectite crystals were nucleating first, followed by illite nucleation. The $^{87}Sr/^{86}Sr$
1004 ratios of the leachates can therefore be considered to represent mixtures of initial Sr from
1005 volcanic precursor glass between ash deposition and start of the diagenetic alteration into
1006 smectite with Sr of interstitial fluids that diffused into the bentonite beds.
1007 In the case of the illite nanocrystals from Triassic sandstones of the eastern Paris Basin,
1008 the Sr of the leachates has been shown to be a mixture of Sr with varied origins: one of
1009 hydrothermal origin trapped by the nucleating illite crystals, and another obviously carried by late
1010 migrating fluids that favored precipitation of Ca-Mg carbonates.
1011
1012 *7.2 More potential for combined Rb-Sr and K-Ar methods applied to illite nanocrystals*
1013 The next case study, despite being analytically very limited as applied to nanofractions of
1014 one single bentonite sample, has been integrated in this review because of its application to
1015 smectite-rich instead of illite-rich nanocrystals, and because of its potential in combining K-Ar
1016 and Rb-Sr data (Clauer, unpublished). The following discussion is therefore to be considered
1017 more as preliminary information on initial nanometric illitization; it is still far from a solid
1018 interpretation.
1019 The bentonite core sample belongs to a well drilled into the prolific hydrocarbon-
1020 producing Campos Basin from southeastern Brazilian continental offshore margin. There, oil is
1021 mainly hosted by Upper-Cretaceous sandstone turbidites that are interbedded with altered

volcanic ash beds in the center of the basin (Alves et al., 1993; Caddah et al., 1998). Buried to approximately 2800 m, the selected bentonite bed is of Santonian stratigraphic age (86-83 Ma). It was handled and prepared following the procedure described in the above analytical section for separation of nanosized crystals. The extracted fractions (<0.02, 0.02-0.05, 0.05-0.1 and 0.1-0.2 μm) were X-rayed and dated by the K-Ar and Rb-Sr methods. The different size fractions consist of a swelling smectite-type mineral with identical air-dried patterns characterized by a peak at ~15 Å. Kaolinite was observed in the coarser nanofractions, while illite layers were only identified in the finest size fractions. On the basis of the positions of the d_{009} and d_{0010} XRD peaks (Środoń, 1980), ~5% illite layers were estimated in the smectite-rich I-S. The K_2O contents and expandability of the nanocrystals were also compared to data obtained by Šucha et al. (1993) in the East Slovak Basin to approximate the present-day temperature. This temperature is at about 65-70 °C, which represents the lower limit for illitization, and explains the very limited smectite-to-illite conversion.

The K-Ar ages of the four studied nanofractions are all younger than the stratigraphic reference, confirming a dominant occurrence of authigenic crystals. Those of the two finest fractions (<0.02 and 0.02-0.05 μm) range from 19 to 21 Ma, while those of the two coarser fractions (0.05-0.1 and 0.1-0.2 μm) range from 47 to 56 Ma. Plots of these data in a Harper (1970) diagram confirm the two groupings (Fig. 24): the two finest fractions plot on a line intersecting the coordinates at the origin, while the two coarser fractions plot on a second line intersecting the ordinate at a negative value, which indicates an excess of radiogenic ^{40}Ar in the fractions enriched in K. In the isochron diagram, the two finest fractions plot on a line that yields an age of 19.9 $\pm$ 0.7 Ma, with an initial $^{40}Ar/^{36}Ar$ ratio of ~300, while the coarser fractions plot along a second line with a higher slope, an age at 51.4 $\pm$ 4.8 Ma and an initial $^{40}Ar/^{36}Ar$ slightly higher at ~304, which could be explained, at least partly, by an excess radiogenic ^{40}Ar scavenged by the newly-formed crystals that was suggested by the data distribution in the Harper (1970) diagram.

The same size fractions were also analyzed for their Rb-Sr systematics after gentle leaching with dilute HCl (1M). Because these leachates carry Sr that is not constitutive of the clay particles for the reasons already formulated, elements external to the smectite-rich crystals are expected to provide information about the chemical conditions of the inter-particle volumes of the clay particles, while the leached residues are expected to provide the chemical and Sr

1053 isotopic composition of the nanocrystals themselves. In this respect, it is appropriate to recall that
1054 the gentle acid leaching applied here alters neither the Rb-Sr nor the K-Ar system of the clay
1055 crystals, regardless of type, size or crystallinity degree (Clauer et al., 1993). It might also be
1056 remembered that the data points of the untreated, leached and residue aliquots of a given size
1057 fraction normally define arrays on $^{87}Sr/^{86}Sr$ vs. $^{87}Rb/^{86}Sr$ diagrams, depending on the quality of
1058 the analytical determinations (e.g. Clauer and Chaudhuri, 1995). The significance of these lines
1059 strictly depends on the material studied: a geological meaningful isochron, for instance, can only
1060 be claimed if the analyzed material is homogeneously authigenic. If this is not the case, the lines
1061 represent mixtures of particles of varied origins.
1062 The Rb-Sr data unexpectedly display two arrays with negative slopes in an isochron
1063 diagram for the untreated (U in the figure), residue (R in the figure) and leachate (L in the figure)
1064 fractions of the coarser smectite-rich nanofractions (Fig. 25). Beyond the complex distribution, it
1065 can be agreed that the analytical conditions were adequate, as the data points of the L, U and R of
1066 the four size fractions fit individual lines. Among the four obtained lines, those of the coarser
1067 (0.05-0.1 and 0.1-0.2 μm) separates yield negative slopes with a higher initial intercept at
1068 ~0.71098 than the $^{87}Sr/^{86}Sr$ ratios of the residues. Such distribution patterns were already
1069 described for clay material of oceanic volcanic deposits (Clauer, 1982; Clauer et al., 2011) and
1070 have been reported to be mixing lines. They outline $^{87}Sr/^{86}Sr$ ratios for minerals of volcanic
1071 origin, that is to say lower than the ratio of the environmental fluids (= the initial values of the
1072 lines) and the authigenic soluble minerals removed by leaching. The initial $^{87}Sr/^{86}Sr$ ratios of the
1073 two mixing lines together with the L, U and R data points of the coarser nanofractions consisting
1074 only of smectite is ~0.71098, which is significantly above the seawater $^{87}Sr/^{86}Sr$ ratio (Jones and
1075 Jenkyns, 2001). Conversely the line through the two coarse leached smectite nanofractions (black
1076 dots in Fig. 25) has an initial $^{87}Sr/^{86}Sr$ ratio of ~0.70868, which is within the seawater ratio about
1077 20-30 Ma ago, at the time determined by K-Ar dating. Of interest is the fact that this line has a
1078 slope giving an age of ~25 Ma. Also, the initial $^{87}Sr/^{86}Sr$ ratio of the line through the more illite-
1079 rich fine (<0.05 and 0.05-0.1 μm) nanofractions is ~0.71098, which is the initial value of the two
1080 mixing lines through the coarser smectite residues. And last but not least, the slope of the line
1081 through the two fine-grained residues containing some illite layers provides an age of ~2 Ma.
1082 This dataset can be tentatively explained by the following process: (1) pure smectite (here
1083 of the 0.05-0.1 and 0.1-0.2 μm coarse nanofractions) crystallized from volcanic ash in contact

with seawater ~25 Ma ago, age given by the line joining the two residues with an initial seawater $^{87}Sr/^{86}Sr$ ratio, the line being therefore an isochron; and (2) some K was supplied later by different pore fluids having a high $^{87}Sr/^{86}Sr$ of ~0.71098 more typical for sedimentary interstitial fluids that interacted with deposited minerals. The K supply initiated nucleation and growth of illite layers, necessarily in the smallest <0.02 and 0.02-0.05 μm nanofractions, the line joining the two finer residues being again an isochron. Deposition of the volcanic glass occurring during Santonian time (86-83 Ma), initial smectite might have crystallized during a period between ~51 Ma ago, on the basis of the K-Ar data, and ~25 Ma ago, on the basis of the Rb-Sr data. Nucleation and growth of illite layers could have started at this time (~20 Ma ago on the basis of the K-Ar data), and have ended ~2 Ma ago on the basis of the Rb-Sr data. It looks like the start of illite crystallization was initiated by the changing composition of the interstitial fluid ~25-20 Ma ago.

Such discrete and long-lasting crystallization episodes appear reasonable in the Campos bentonites because available K was limited, while the temperature was at the lower limit of potential illitization. Again, it must be reiterated that such a scenario remains hypothetical as it is based on a single sample, with the specificity of consisting mostly of dominant smectite with some illite layers. The purpose was to highlight the potential of combined K-Ar and Rb-Sr studies, especially on smectite-rich and not illite-rich nanocrystals.

7.3 Thermal conditions of illite nucleation and growth by $\delta^{18}O$ tracing

The initial attempt to analyse $\delta^{18}O$ of nanocrystals was published on illite from Čičarovče and Trhovište sites of the East Slovak Basin (Fig. 26; Clauer et al., 2003). The two sets of nanofractions yielded different $\delta^{18}O$ values: those of the illite fractions from Čičarovče were lower than those from Trhovište. When crystal size increases, the former decreased slightly from 12 to 10‰, while those from Trhovište increased slightly, from 16.5 to 18‰. Together with different K-Ar ages, the $\delta^{18}O$ trends of the illite nanocrystals of the two sites suggest different nucleation and growth processes occurring only 20 km apart in the same basin. The decrease in $\delta^{18}O$ with increasing particle size at Čičarovče seems to relate to a slow temperature increase during the 3.5-Ma-long illitization process, whereas the almost constant $\delta^{18}O$ with particle size increase at Trhovište seems to relate to an almost constant temperature between 11 and 8 Ma. The $\delta^{18}O$ of the fluids associated with crystal nucleation and growth remained in a similar narrow

range for the two populations of fundamental particles, with an overlapping calculated mean $\delta^{18}O$ of 0 ± 3‰ at Trhovište and of 2 ± 1.5‰ at Čičarovče on the basis of the temperatures estimated from organic maturation data at ~120 °C at Čičarovče and at ~160 °C at Trhovište. These estimates agree reasonably well with those by Šucha et al. (1993) based on the crystallization temperatures derived from maturation temperature of organic matter in the same basin by Francú et al. (1990). In fact, the differences identified by K-Ar dating are frequently supported by $\delta^{18}O$ data that often allow distinction of probable temperature changes from changes in the fluid chemistry.

7.4 Which illitization mechanism in shales?

The systematically older ages for illite nanofractions of shales favor the general belief of an excess of radiogenic ^{40}Ar relative to the K content, which is often explained by the addition of detrital material. However, these detrital crystals are not "just" mechanically mixed, as is the case in coarser size fractions of sandstones, because their odd shapes would be recognizable by microscope observation, which seems not to be always the case. In fact, these detrital crystals could serve as supports of newly nucleating authigenic crystals resulting from interaction of recent fluids with the detrital crystals that alter while authigenic crystals grow on them and possibly modify their shape to become idiomorphic.

Crystallization of Le Puy illite also questions the generally admitted basic "mechanical" mixing of authigenic and detrital particles to explain isotopic ages older than the stratigraphic reference (e.g. Clauer and Chaudhuri, 1995). This "mixing" also occurring at nanosize clearly discriminates between isotopic data of nanoparticles of bentonites and sandstones from those of nanoparticles of shales. These consistent results question also the multiphase illitization model of Yates and Rosenberg (1996, 1997, 1998) based on a dissolution-precipitation process following a ripening step in which metastable intermediate phases are transformed into illite. Not based on the fundamental particle concept (Nadeau et al., 1984), Yates and Rosenberg's model (1996, 1997, 2011) was conceived on the basis of hydrothermal experiments, which do not reproduce natural conditions, as shown again recently in a comparative study of naturally buried and experimentally matured shale rocks and <2 μm fractions (Clauer et al., 2014).

The high number of varied models, including those of Altaner and Bethke (1988) and Altaner and Ylagan (1997), as well as of Rosenberg et al. (1980), Whitney and Northrop (1988),

Whitney and Velde (1993) and Ferratge et al. (2011), provide varied explanations for illitization that end up being confusing. The isotopic approach may not yet explain the intimate mechanisms of illitization, but it clearly outlines a process depending on numerous physico-chemical factors that can vary from case to case and even within a single case. For instance, nucleation can be, but need not to be, followed by growth; it can be unique or multiple and last for varied durations in progressive burial conditions; it also appears "fast" when temperature is significantly above 150 °C. The stable isotope data provide information about the temperature, when the chemical composition of the interacting fluids can be constrained. Alternatively, temperature determination by independent methods allows using the $\delta^{18}O$ signature for interpreting the fluid compositions. In shales, authigenic illite-type crystals seem to equilibrate with fluids faster than the altering detrital particles, primarily because first nucleated crystals are in equilibrium with fluids whereas larger crystals only equilibrate slowly (Williams and Hervig, 2006). Admittedly, experimental conditions do not mimic natural conditions, as experiments limit environmental variables in order to simplify the interpretation of results. All these aspects may, at least partly, explain why modeling of illitization is somehow confusing with rules that apparently only apply to specific cases.

7.5. Light-element isotope tracing of mineral and organic-matter interactions

Combined thermal maturation of mixtures consisting of clay crystals and organic matter was studied in the Eocene Kreyenhagen Shale from the San Joaquin Basin, California USA, by subjecting the outcrop <2 μm clay fraction to hydrous-pyrolysis experiments (Clauer et al., 2014a). Intended to alleviate the problem of mineral and chemical variations in the initially deposited rocks of natural sequences in a basin, hydrous pyrolysis experiments of the immature outcrop sample did not induce significant changes in the clay mineral composition in experiments conducted for 72 h at temperatures from 270 to 365 °C, far from those induced by natural burial-induced maturation. Interestingly, large amounts of smectite layers coated by organic material remained in the I-S of the pyrolyzed outcrop <2 μm fraction during the thermal experiments, especially above 310 °C, despite leaching the mineral powders with H_2O_2 before pyrolysis. Almost no K transfer being noticed into the clay material and therefore no illitization being detected, smectite appears to have inhibited rather than promoted generation of expelled oil from the decomposition of bitumen. This hindrance is believed to have resulted from bitumen

impregnating the smectite interlayer sites, but also from lack of available K for illitization.

In a study in progress, the $\delta^{11}B$ and B content, and the $\delta^{18}O$ and δD of such <2 μm clay and organic mixtures were determined and compared to the total organic content (TOC) of the fractions pyrolyzed at temperatures from 270 to 365 °C for 72 h, and at the higher 365 °C step for 216 h (Clauer, Williams, Fallick and Lewan, unpublished). The data show a significant correlative decrease of the TOC and B contents, by 75 and 33% respectively, of the untreated immature outcrop <2 μm fraction after the initial pyrolysis experiment at 210 °C during 72 h (Fig. 27). Afterwards, the B and TOC (probably mixed left-over kerogen and bitumen) contents remained almost constant, while $\delta^{11}B$ decreased continuously, suggesting that B with low $\delta^{11}B$ was released to the fluids. The clay $\delta^{18}O$ value also decreased continuously, quite significantly after the first pyrolysis step at 210 °C during 72 h, perhaps pointing to a release of oxygen with high $\delta^{18}O$. To be mentioned is the fact that the $\delta^{18}O$ values were determined on a clay fraction contaminated by organics despite H_2O_2 treatment, which may be analytically questionable because products like COF_2 might have formed during fluorination, and the released O_2 might not be pure. The yield data are not conclusive on this possibility, but the hypothetical bias induced by the occurrence of organics could be of limited impact, as $\delta^{18}O$ decreases with experimental temperature increase, whereas clay δD increases (Fig. 27).

The $\delta^{11}B$, $\delta^{18}O$ and δD values all decreased during the further pyrolysis steps. As each individual pyrolysis experiment started with the same immature outcrop <2 μm fraction, it is apparent that the pyrolysis experiments at 365 °C during 72 h and 216 h (labeled 4 and 5 in figure 27) have an identical impact on the B contents and $\delta^{11}B$. Conversely, the experiments at 349 and 365 °C during 72 h (labeled 3 and 4 in figure 27) have similar important impacts on $\delta^{18}O$, while that at 365 °C at 216 h (step labeled 5 in figure 27) has a more limited effect. A graphical outline of the theoretical amount of released B during each pyrolysis experiment shows that the B released from organics becomes isotopically heavier at each higher-temperature step, with an overall release of about 135-140 μg/g at each step and a $\delta^{11}B$ that shifts progressively from -2 to +9‰ (Fig. 28). Of course, the contents need to be adjusted to the amount of removed TOC if considering that all mobile B is bound to kerogen rather than bitumen. In fact, not much more B is released from organics after the pyrolysis experiment at 270 °C during 72 h (labeled step 1 in figure 28), but with an increasing $\delta^{11}B$, when taking into account the content of the whole

removed TOC. The data support that most B is stored in the sedimentary organics, and that this B is isotopically light compared to rocks and minerals.

Another interesting fact is the correlation between the decreasing $\delta^{18}O$ and the largest removal of TOC during the initial experiment at 270 °C during 72 h. If the occurrence of organics has a limited impact on the released $\delta^{18}O$, this finding raises a basic question about the meaning of the $\delta^{18}O$ of clay-sized minerals in naturally maturing organic-bearing sediments. During initial maturation, it is possible that most of the released oxygen with high $\delta^{18}O$ was released by the organics, which would modify the interpretation of oxygen isotope data as thermal tracers of the mixed clay material. Van Krevelen (1950) diagrams generally used to assess the origin and maturity of kerogen and petroleum show that both O and H are released from kerogen with increasing thermal maturity, so that the source of oxygen from all minerals and organic compounds in a bulk shale-type rock must be considered quantitatively. At natural thermal conditions above 100 °C, the data suggest that most of the oxygen is retained by the clay material. The δD values increase consistently at each temperature step, supporting that release of proyium (^{1}H) is energetically favored over deuterium, which needs higher temperature or longer time than protium to be released from organics.

These experimental data confirm that B of illite is isotopically lighter than that in pore fluids, and that the source of the isotopically light B is organic. The B data confirm again that the illite tetrahedral B-O bond is as strongly tied as the Si-O bonds with wide isotopic variations. The results on Li contents and isotope compositions of nanocrystals potentially interacting with organics remain scarce, but they outline trends that follow often those of B.

8. Conclusions

The present review summarizes the innovative aspects of light-element isotopic (δD, $\delta^{7}Li$, $\delta^{11}B$, $\delta^{18}O$) tracing and isotopic (K-Ar and Rb-Sr) dating of nanometric illite-rich crystals extracted mostly from bentonites, but also from sandstones and shales in diagenetic to anchi-metamorphic conditions. The study of nanocrystals from bentonite and sandstone beds is often successful and well under control, but problems remain to separate mechanically authigenic illite-type crystals from detrital components, also at nanosize of shale units. Mixed authigenic crystallization and detrital alteration complicates deciphering the results, but a way to separate

1238 them, at least for the use of the K-Ar method, is alkylammonium leaching of the crystal mixtures.
1239 As alkylammonium chains have the specificity of slipping into the interlayers of mica-type
1240 sheetsilicates, especially into those of dio-octahedral crystalline organization, and to replace
1241 stochiometrically K, this finding is of interest in studying K-Ar systematics of di- and tri-
1242 octahedral illite mixtures, to potentially differentiate detrital from authigenic crystals.

1243 The initial K-Ar studies in the late 1990s have pointed to the fact that no age information
1244 is lost during crystal nucleation and growth, so that it can be considered that details of the whole
1245 illitization process are stored in the illite crystals. By combining K-Ar, Rb-Sr, δD and $\delta^{18}O$
1246 studies, a comparision of nucleating and growing crystals that become illitic allows calculation of
1247 reaction rates and process durations, together with crystallization temperatures and fluid
1248 chemistry depending on the water/rock ratios. Not only do such studies confirm that illitization is
1249 not continuous during burial, but they indicate it can last over extended but variable periods of
1250 time, or be episodic, sometimes successively so. The Rb-Sr method provides complementary
1251 information about the origin of the solutes from interacting fluids through comparison of the
1252 $^{87}Sr/^{86}Sr$ ratio of the nucleating crystals, which depends also on the water/rock ratio, with that of
1253 the leached Sr outside of the crystal structures. The δD and $\delta^{18}O$ values of the illite crystals
1254 provide information about the nucleation or growth temperature, either increasing during burial
1255 or being abnormally high but constant during a short-lasting thermal episode. Occurrence of
1256 organic matter mixed with illite crystals may bias the $\delta^{18}O$ of the crystallizing and growing
1257 crystals, if the few data provided here are not analytically biased, as organics could release
1258 oxygen with abnormally high $\delta^{18}O$ during maturation.

1259 A major finding of isotopic studies of nanometric illite crystals relates to B, for which the
1260 largest reservoir in sedimentary deposits is the organic matter. Most of this organic-derived B
1261 yields light $\delta^{11}B$ to fluids upon maturation, and that fixed in illite is isotopically light relative to
1262 the fluids. The heavy ^{11}B preferentially fractionates into bitumen. The B data also confirm that
1263 the illite tetrahedral B-O bonds are as strong as, or stronger than the Si-O bonds with isotopic
1264 variations nearly as great as those of δD. Clay-organic matter interactions in sedimentary
1265 environments can, therefore, be traced by monitoring the B contents and isotope composition of
1266 clays and organics during thermal maturation. The results of Li contents and isotope composition
1267 of nanocrystals remain scarce, appearing more complicated than B due to the multiple phases that
1268 may incorporate Li, and also to analytical uncertainties. When interacting with organics, Li

follows trends that are similar to those of B, but the thermal energy for Li release from organics may differ. If so, these two "heteroatoms" variously released from organic matter under different thermal conditions, may be useful tracers of organic maturation, which will be readily recorded in the stable framework of authigenic illite that crystallized in rock volumes where organics matured.

9. Acknowledgements

We are very deeply indebted to all who contributed to the studies that are referred to here as having provided support to this review. Jan Środoń, Sam Chaudhuri and Richard L. Hervig are among those who deserve our gratitude for their contribution and interest. Many of the nanometric size fractionations, which results were discussed in this review, were completed by Mrs M. Zielinska of the Geological Institut of Krakow who deserves also special thanks for her excellent technical contribution. At last, not least, we are very thankful to the two anonymous reviewers for their thoughtful comments and remarks, which helped improve the previous version of this contribution.

10. References

Ahn, J.H. and Peacor, D.R., 1987, Kaolinitization of biotite: TEM data and implications for an alteration mechanism. American Mineralogist, 72, 353-356.

Aja, S.U., 1995, Thermodynamic properties of some 2:1 layer clay minerals from solution-equilibration data. European Journal of Mineralogy, 7, 325-333.

Altaner, S.P. and Ylagan, R.F., 1997, Comparison of structural models of mixed-layer illite/smectite and reaction mechanisms of smectite illitization. Clays and Clay Minerals, 45, 517-533.

Alves, D.B., Mizusaki, A.M.P. and Caddah, L.F.G., 1993. Camadas de cinzas vulcanicas no Santiniano (Cretaceo Superior) da Bacia de Campos, Brasil. Simposio de Geologia do Sudeste, 3, Rio de Janeiro, SBG, Atas, 37-42.

Bird, M.I. and Chivas, A.R., 1988. Stable-isotope evidence for low-temperature kaolinitic weathering and post-formational hydrogen-isotope exchange in Permian kaolinites. Chemical

Geology, 72, 249–265.

Blaise et al. - Reconstructing fluid-flow events in Triassic sandstones of the eastern Paris Basin by combined chemical (major and rare-earth elements) and isotopic (oxygen) tracing, and (K-Ar and Rb-Sr) dating of nanometric illite particles. In preparation.

Boles, J.R. and Franks, S.G., 1979, Clay diagenesis in Wilcox sandstones of southwest Texas: Implications of smectite diagenesis on sandstone cementation. Journal of Sedimentary Petrology, 49, 55-70.

Bostick, N.H. and Pawlewicz, M.J., 1984, Paleotemperatures based on vitrinite reflectance of shales and limestones in igneous dike aureoles in the Upper Cretaceous Pierre Shale, Walsenburg, Colorado. In: Woodward, J., Meissner, F.F. and Clayton, J.L., (Eds.), Hydrocarbon Source Rocks of the Greater Rocky Mountain Region, Rocky Mountain Association of Geologists, Denver, Colorado, 387-392.

Bottomly, D.J., Chan, L.H., Katz, A., Starinsky, A. and Clark, I.D., 2003, http://onlinelibrary.wiley.com/doi/10.1111/j.1745-6584.2003.tb02426.x/abstract Lithium isotope geochemistry and origin of Canadian Shield brines. Groundwater, 41, 847-856.

Burley, S.D. and Flisch, M., 1989, K/Ar geochronology and the timing of detrital I/S clay illitization and authigenic illite precipitation in the Piper and Tartan fields, outer Moray Firth, UK North Sea. Clay Minerals, 24, 285-315.

Caddah, L.F.G., Alves, D.B. and A.M. Mizusaki, 1998, Turbidites associated with bentonites in the Upper Cretaceous of the Campos Basin, offshore Brazil. Sedimentary Geology, 115, 175-184.

Chan, L.H. and Edmond, J.M., 1988, Variation of lithium isotope composition in the marine environment: A preliminary report. Geochimica et Cosmochimica Acta, 52, 1711–1717.

Chan, L.H., Alt, J. and Teagle, D.A.H., 2002, Lithium and lithium isotope profiles through the upper oceanic crust: A study of seawater-basalt exchange at ODP Sites 504B and 896A. Earth and Planetary Science Letters, 201, 187-201.

Chaudhuri, S., Środoń, J. and Clauer, N., 1999, K-Ar dating of illitic fractions of Estonian “Blue Clay” treated with alkylammonium cations. Clays and Clay Minerals, 47, 96-102.

Clauer, N., 1982, Strontium isotopes of Tertiary phillipsites from the Southern Pacific: Timing of the geochemical evolution. Journal of Sedimentary Petrology, 52, 1003-1009.

Clauer, N., 2011, Another insight into the illitization process by K-Ar dating of micro- to nano-

metric illite-type particles leached with alkylammonium cations. Clay Minerals, 46, 593-612.

Clauer, N., 2013, The K-Ar and $^{40}Ar/^{39}Ar$ methods revisited for dating fine-grained K-bearing clay minerals. Chemical Geology, 354, 163-185.

Clauer, N., Chaudhuri, S., Kralik, M. and Bonnot-Courtois, C., 1993, Effects of experimental leaching on Rb-Sr and K-Ar isotopic systems and REE contents of diagenetic illite. Chemical Geology, 103, 1-16.

Clauer, N. and Chaudhuri, S., 1995, Clays in Crustal Environments. Isotope Dating and Tracing. Springer Verlag, Heidelberg, New York, 359p.

Clauer, N. and Chaudhuri, S., 1996, Inter-basinal comparison of the diagenetic evolution of illite/smectite minerals in buried shales on the basis of K-Ar systematics. Clays and Clay Minerals, 44, 818-824.

Clauer, N., Środoń, J., Francú, J. and Šucha, V., 1997, K-Ar dating of illite fundamental particles separated from illite/smectite. Clay Minerals, 32, 181-196.

Clauer, N. and Chaudhuri, S., 1998. Isotopic dating of very low-grade metasedimentary and metavolcanic rocks: techniques and methods. In: Frey, M. and Robinson, D. (Eds.), Low-Grade Metamorphism, Blackwell Science, Oxford, 202-226.

Clauer, N., Rinckenbach, T., Weber, F., Sommer, F., Chaudhuri, S. and O'Neil, J.R., 1999, Diagenetic evolution of clay minerals in oil-bearing Neogene sandstones and associated shales from Mahakam Delta Basin (Kalimantan, Indonesia). American Association of Petroleum Geologists Bulletin, 83, 62-87.

Clauer, N., Liewig, N., Pierret, M.C. and Toulkeridis, T., 2003, Crystallization conditions of fundamental particles from mixed-layers illite-smectite of bentonites based on isotopic data (K-Ar, Rb-Sr and $\delta^{18}O$). Clays and Clay Minerals, 51, 664-674.

Clauer, N., Rousset, D. and Środoń, J., 2004, Modeled shale and sandstone burial diagenesis based on the K-Ar systematics of illite-type fundamental particles. Clays and Clay Minerals, 52, 576-588.

Clauer, N., 2006, Towards an isotopic modeling of the illitization process based on data of illite-type fundamental particles from mixed layered illite-smectite. Clays and Clay Minerals, 54, 119-130.

Clauer, N. and Lerman, A., 2009, A model for potassium gain and radiogenic argon loss during burial illitization based on analytical data. 46th Annual Meeting of The Clay Minerals Society,

1362 Billings, MT, June 5-11, 2009, p. 91.
1363 Clauer, N., Williams, L., Honty, M. and Šucha, V., 2009, Li and B isotopic tracing of illite
1364 nucleation and growth in bentonite units of the East Slovak Basin. 46th Annual Meeting of the
1365 Clay Minerals Society, Billings, MT, June 5-11, 2009, p. 93.
1366 Clauer, N., O'Neil, J.R., Honnorez, J. and Buatier, M., 2011, $^{87}Sr/^{86}Sr$ and $^{18}O/^{16}O$ ratios of clay
1367 minerals from a hydrothermal mound near the Galapagos rift as records of origin,
1368 crystallization temperature and fluid composition. Marine Geology, 288, 32-42.
1369 Clauer, N., Zwingmann, H., Liewig, N. and Wendling, R., 2012, Comparative $^{40}Ar/^{39}Ar$ and K-
1370 Ar dating of illite-type clay minerals: A tentative explanation for the age identities and
1371 differences. Earth Sci. Rev., 115, 76-96.
1372 Clauer, N., Fallick, A.E., Eberl, D.D., Honty, M., Huff, W. and Aubert, A., 2013, K-Ar dating
1373 and $\delta^{18}O$-δD characterization of nanometric illite from Ordovician K-bentonites of the
1374 Appalachians: Illitization and the Acadian-Alleghenian tectonic activity. American
1375 Mineralogist, 98, 2144-2154.
1376 Clauer, N., Lewan, M.D., Dolan, M.P., Chaudhuri, S., and Curtis, J.B., 2014a, Mineralogical,
1377 chemical and K-Ar isotopic changes in Kreyenhagen Shale whole rocks and <2 μm clay
1378 fractions during natural burial and hydrous-pyrolysis experimental maturation. Geochimica et
1379 Cosmochimica Acta, doi: 10.1016/j.gca.2014.01.007.
1380 Clauer, N., Honty, M., Fallick, A.E., and Šucha, V., 2014b Regional illitization in bentonite beds
1381 from East Slovak Basin based on isotopic characteristics (K-Ar, $\delta^{18}O$ and δD) of illite-type
1382 nanoparticles. Clay Minerals, 49, 165-194.
1383 Collins, A.G., 1975, Geochemistry of Oilfield Waters. New York, Elsevier. 496p.
1384 Connolly, C.A., Walter, L.M., Baadsgaard, H. and Longstaffe, F.J., 1990, Origin and evolution of
1385 formation waters, Alberta Basin: I, Chemistry. Applied Geochemistry, 5, 375-396.
1386 Dalrymple, G.B. and Lanphere, M.A., 1969, Potassium-Argon Dating. Freeman, San Francisco,
1387 258p.
1388 Dayal, R., 1975, Clay-sea water interaction at elevated pressures: PhD Thesis, Dalhousie
1389 University, Halifax, Nova Scotia, Canada, 234p.
1390 Drits, V.A., Sakharov, B.A., Lindgreen, H. and Salyn, A.L., 1997, Sequential structure
1391 transformation of illite-smectite-vermiculite during diagenesis of Upper Jurassic shales from
1392 the North Sea and Denmark. Clay Minerals, 32, 351-71.

1393 Drits, V.A., Eberl, D.D. and Środoń, J., 1998, XRD measurement of mean thickness, thickness
1394 distribution and strain for illite and illite/smectite crystallites by the Bertaut-Warren-Averbach
1395 technique. Clays and Clay Minerals, 46, 461-475.
1396 Dudek, T., 2001, Diagenetic evolutionof illite/smectite in the Miocene shales from the Prezmyël
1397 area (Carpathian Foredeep). PhD Thesis, Institute of Geological Sciences PAN, Krakow,
1398 Poland, 148p.
1399 Dudek, T., Środoń, J., Eberl, D.D., Elsass F. and Uhlik, P., 2002, Thickness distribution of illite
1400 crystals in shales. Part I: XRD vs. HRTEM measurements. Clays and Clay Minerals, 50, 562-
1401 577.
1402 Eberl, D.D. and Środoń, J., 1988, Ostwald ripening and interparticle-diffraction effects from illite
1403 crystals. American Mineralogist, 73, 1335-1345.
1404 Eberl, D.D., Drits, V., Środoń, J. and Nüesch, R., 1996, MudMaster: A program for calculating
1405 crystallite size distribution and strain from the shapes of X-ray diffraction peaks. U.S.
1406 Geological Survey, Open-File Report, 96-171.
1407 Eberl, D.D., Drits, V. and Srodon, J., 1997, Measurement of Illite Crystallite Thickness by XRD.
1408 Method of Bertaud–Warren–Averbach. Groupe Français des Argiles, 27–28.
1409 Eberl, D.D., Nüesch, R., Šucha, V. and Tsipursky, S., 1998a, Measurement of fundamental illite
1410 particle thickness by X-ray diffraction using PVP-10 intercalation. Clays and Clay Minerals,
1411 46, 89-97.
1412 Eberl, D.D., Drits, V.A. and Środoń, J., 1998b, Deducing growth mechanisms for minerals from
1413 the shapes of crystal size distributions. American Journal of Science, 298, 499-533.
1414 Eberl, D.D., Drits, V.A. and Środoń, J., 2001, User's guide to GALOPER – a program for
1415 simulating the shapes of crystal size distributions – and associated programs. U.S. Geological
1416 Survey, Open-File Report, OF00-505, 44p.
1417 Eberl, D.D., Kile, D.E. and Drits, V.A., 2002, On geological interpretations of crystal size
1418 distributions: Constant vs. proportionate growth. American Mineralogist, 87, 1235-1241.
1419 Eberl, D.D., Blum, A.E. and Serravezza, M., 2011, Anatomy of a metabentonite: Nucleation and
1420 growth of illite crystals and their coalescence into mixed-layer illite/smectite. American
1421 Mineralogist, 96, 586-593.
1422 Ehrenberg, S.N. and Nadeau, P.H., 1989, Formation of diagenetic illite in sandstones of the Garn
1423 Formation, Haltenbanken area, mid-Norwegian Continental Shelf. Clays and Clay Minerals,

24, 233-253.

Elliott, W.C., Aronson, J.L., Matisoff, G. and Gautier, D.L., 1991, Kinetics of the smectite to illite transformation in the Denver Basin; Clay mineral, K-Ar data and mathematical model results. American Association of Petroleum Geologists Bulletin, 75, 436-462.

Fallick, A.E., Macaulay, C.I. and Haszeldine, R.S., 1993, Implications of linearly correlated oxygen and hydrogen isotopic compositions for kaolinite and illite in Magnus Sandstone, North Sea. Clays and Clay Minerals, 2, 121-137.

Faure, G., 1986, Principles of Isotope Geology, 2nd edn. Wiley, New York.

Ferrage, E., Vidal, O., Mosser-Ruck, R., Cathelineau, M. and Cuadros, J. (2011) A reinvestigation of smectite illitization in experimental hydrothermal conditions: Results from X-ray diffraction and transmission electron microscopy. American Mineralogist, 96, 207–223.

Fontes, J.C. and Matray, J.M., 1993, Geochemistry and origin of formation brines from the Paris Basin. Part 2: Saline solutions associated with oil fields. Chemical Geology, 109, 177-200.

Francú, J., Muller, P., Šucha, V., Zatkaliková, V., 1990. Organic matter and clay minerals as indicators of thermal history in the Transcarpathian Depression (East Slovakian Neogene Basin) and the Vienna Basin. Geologica Carpathica, 41, 535-546.

Freed, R.L. and Peacor, D.R., 1992, Diagenesis and the formation of authigenic illite-rich crystals in Gulf Coast shales: TEM study of clay separates. Journal of Sedimentary Petrology, 62, 220-234.

Furlan, S., Clauer, N., Chaudhuri, S. and Sommer, F., 1996, K transfer during burial diagenesis in the Mahakam Delta Basin (Kalimantan, Indonesia). Clays and Clay Minerals, 44, 157-169.

Gabis, V., 1963, Etude minéralogique et géochimique de la série sédimentaire oligocène du Velay. Bulletin de la Société française de Minéralogie et Cristallographie, 86**,** 315-354.

Girard, J.P. and Barnes, D.A., 1995, Illitization and paleothermal regimes in the Middle Ordovician St Peter Sandstone, Central Michigan Basin, United States: K-Ar, oxygen isotopes, and fluid inclusion data. American Association of Petroleum Geologists Bulletin, 79, 49-69.

Glasmann, J.R., Larter, S., Briedis, N.A. and Lundegard, P.D., 1989a, Shale diagenesis in the Bergen area, North Sea. Clays and Clay Minerals, 37, 97-112.

Glassman, J.R., Lundegard, P.D., Clark, R.A., Penny, B.K. and Collins, I.D., 1989b, Geochemical evidence for the history of diagenesis and fluid migrations: Brent sandstones,

Heather field, North Sea. Clay Minerals, 24, 255-284.

Harper, C.T., 1970. Graphic solution to the problem of ^{40}Ar loss from metamorphic minerals. Eclogae Geologicae Helveticae, 63, 119-140.

Harris, N.B., 1992, Burial diagenesis of Brent sandstones: A study of Statfjord, Hutton and Lyell fields. In: Morton, A.C., Haszeldine, R.S., Giles, M.R. and Brown, S. (Eds.), Geology of the Brent Group, Geological Society of London, Special Publication, 61, 351-375.

Hingston, F.J., 1964, Reactions between boron and clays. Australian Journal of Soil Research, 2, 83-95.

Honty, M., Uhlik, P., Šucha, V., Caplovicová, M., Francú, J., Clauer, N. and Biroń, A., 2004, Smectite to illite alteration in salt-bearing bentonites; the East Slovak Basin. Clays and Clay Minerals, 52, 533-551.

Hower, J., Eslinger, E.V., Hower, M. and Perry, E.A., 1976, Mechanism of burial metamorphism of argillaceous sediments: 1. Mineralogical and chemical evidence. Geological Society of America Bulletin, 87, 725-737.

Hunziker, J.C., Frey, M., Clauer, N., Dallmeyer, R.D., Friedrichsen, H., Flehmig, W., Hochstrasser, K., Roggwiller, P. and Schwander, H., 1986, The evolution of illite to muscovite: mineralogical and isotopic data from the Glarus Alps, Switzerland. Contribution to Mineralogy and Petrology, 92,157-180.

Inoue, A., Kohyama, N., Kitagawa, R. and Watanabe, T., 1987, Chemical and morphological evidence for the conversion of smectite to illite. Clays and Clay Minerals, 35, 111-120.

Inoue, A., Velde, B., Meunier, A. and Touchard, G., 1988, Mechanism of illite formation during smectite-to-illite conversion in a hydrothermal system. American Mineralogist, 73, 1325-1334.

Inoue, A. and Kitagawa, R., 1994, Morphological characteristics of illitic clay minerals from a hydrothermal system. American Mineralogist, 79, 700-711.

Jackson, M.L., 1975, Soil Chemical Analysis – Advanced Course. Madison, Wisconsin, 386p.

Jennings, S. and Thompson, G.R., 1986, Diagenesis of Plio-Pleistocene sediments of the Colorado river delta, southern California. Journal of Sedimentary Petrology, 56, 89-98.

Jones, C.E. and Jenkyns, H.C., 2001, Seawater strontium isotopes, oceanic anoxic events, and seafloor hydrothermal activity in the Jurassic and Cretaceous. American Journal of Sciences, 301, 112-149.

1486 Kotzer, T.G. and Kyser, T.K., 1995, Petrogenesis of the Proterozoic Athabasca basin, Northern
1487 Saskatchewan, Canada, and its relation to diagenesis, hydrothermal uranium mineralization
1488 and paleohydrogeology. Chemical Geology, 120, 45-89.
1489 Land, L.S. and MacPherson, G.L., 1992, Origin of saline formation waters, Cenozoic section,
1490 Gulf of Mexico sedimentary basin. Geochimica et Cosmochimica Acta, 76, 1344-1362.
1491 Lawrence, J.R. and Taylor, H.P. Jr., 1971, Deuterium and oxygen-18 correlation: Clay minerals
1492 and hydroxides in Quaternary soils compared to meteoric waters. Geochimica et
1493 Cosmochimica Acta, 35, 993-1003.
1494 Lawrence, J.R. and Taylor, H.P. Jr., 1972, Hydrogen and oxygen isotope systematics in
1495 weathering profiles. Geochimica et Cosmochimica Acta, 36, 1377-1393.
1496 Lee, J.Y., Marti, K., Severinghaus, J.P., Kawamura, K., Yoo, H.S., Lee, J.B. and Kim, J.S., 2006,
1497 A redetermination of the isotopic abundances of atmospheric Ar. Geochimica et
1498 Cosmochimica Acta, 70, 4507-4512.
1499 Leeman, W.P., Vocke, R.D. and McKibben, M.A., 1992, Boron isotopic fractionations between
1500 coexisting vapor and liquid in natural geothermal systems. In: Kharaka, Y.K. and Maest, A.S.
1501 (Eds.), Proceedings of the 7th International Symposium on Water–Rock Interaction, Balkema,
1502 Rotterdam, 1007-1010.
1503 Lemarchand, D., Gaillardet, J., Lewin, E. and Allègre, C.J., 2000, The influence of rivers on
1504 marine boron isotopes and implications for reconstructing past ocean pH. Nature, 408, 951-
1505 954.
1506 Lemarchand, D., Gaillardet, J., Lewin, E. and Allègre, C.J., 2002, Boron isotope systematics in
1507 large rivers: implications for the marine boron budget and paleo-pH reconstruction over the
1508 Cenozoic. Chemical Geology, 190, 123-140.
1509 Lerman, A., Ray, B.M. and Clauer, N., 2007, Radioactive production and diffusional loss of
1510 radiogenic ^{40}Ar in clays in relation to its flux to the atmosphere. Chemical Geology, 243,
1511 205-224.
1512 Longstaffe, F.K. and Ayalon, A., 1987, Oxygen-isotope studies of clastic diagenesis in the Lower
1513 Cretaceous Viking Formation, Alberta: Implications for the role of meteoric water. In:
1514 Marshall, J.D. (Ed.), Diagenesis of Sedimentary Sequences, Geological Society of London,
1515 Special Publications, 36, 277-296.
1516 Longstaffe, F.J. and Ayalon, A., 1990, Hydrogen-isotope geochemistry of diagenetic clay

1517 minerals from Cretaceous sandstones, Alberta, Canada: Evidence for exchange. Applied
1518 Geochemistry, 5, 657-668.
1519 Lynch, L.L., 1985, The stoichiometry of the smectite to illite reaction in a contact metamorphic
1520 environment. M.S. thesis, Dartmouth College, Hanover, New Hampshire, 84p.
1521 Mark, D.F., Stuart, F.M. and de Podesta, M., 2011, New high-precision measurements of the
1522 isotopic composition of atmospheric argon. Geochimica et Cosmochimica Acta, 75, 7494-
1523 7501.
1524 McCarty, D.C., Sakharov, B.A. and Drits, V.A., 2008, Early clay diagenesis in Gulf Coast
1525 sediments: New insights from X-ray diffraction profile modeling. Clays and Clay Minerals,
1526 56, 359-379.
1527 Meunier, A. and Velde, B., 2004, Illite. Springer, Berlin**,** 286p.
1528 Milliken, K.L., 1992, Chemical behavior of detrital feldspars in mudrocks versus sandstones, Frio
1529 Formation (Oligocene), South Texas. Journal of Sedimentary Petrology, 62, 790-801.
1530 Misra, S. and Froelich, P.N., 2012, Lithium isotope history of Cenozoic seawater: Changes in
1531 silicate weathering and reverse weathering. Science, 335, 818-823.
1532 Moldovanyi, E.P. and Walter, L.M., 1992, Regional trends in water chemistry, Smackover
1533 Formation, southwest Arkansas: Geochemical and physical controls. American Association of
1534 Petroleum Geologists Bulletin, 76, 864-894.
1535 Moldovanyi, E.P., Walter, L.M. and Land, L.S., 1993, Strontium, boron, oxygen, and hydrogen
1536 isotope geochemistry of brines from basal strata of the Gulf Coast sedimentary basin, USA.
1537 Geochimica et Cosmochimica Acta, 57, 2083-2099.
1538 Mossmann, J.R., 1991, K-Ar dating of authigenic illite/smectite material: Application to complex
1539 mixtures of mixed-layer assemblages. Clay Minerals, 26, 189-198.
1540 Muttik, N., Kirsimäe, K, Newsom, H.E. and Williams, L.B., 2011, Boron isotope composition of
1541 secondary smectite in suevites at the Ries crater, Germany: Implications for the origin of
1542 alteration fluids. Earth and Planetary Science Letters, 310, 244-251.
1543 Nadeau, P.H., Wilson, M.J., McHardy, W.J. and Tait, J.M., 1984, Interstratified clays as
1544 fundamental particles. Science, 225, 923-925.
1545 Oi, T., Kawada, K., Hosoe, M. and Kakihana, H., 1991, Fractionation of lithium isotopes in
1546 cation exchange chromatography. Separation Science Technology, 26, 1353.
1547 O'Neil, J.R. and Kharaka, Y.K., 1976, Hydrogen and oxygen isotope exchange reactions between

clay minerals and water. Geochimica et Cosmochimica Acta, 40, 241-246.

Palmer, M.R. and Sturchio, N.C., 1990, The boron isotope systematics of the Yellowstone National Park (Wyoming) hydrothermal system: A reconnaissance. Geochimica et Cosmochimica Acta, 54, 2811-2815.

Perry, E.A. Jr. and Hower, J., 1970, Burial diagenesis in Gulf Coast pelitic sediments. Clays and Clay Minerals, 18, 165-177.

Pevear, D.R., 1992, Illite age analysis, a new tool for basin thermal history analysis. In: Kharaka, Y.K. and Maest, A.S. (Eds.), Proceedings of the 7th International Symposium on Water-Rock Interaction. Balkema, Rotterdam, Netherlands, 1251-1254.

Pevear, D.R., 1999, Illite and hydrocarbon exploration. Proceedings of the National Academy of Sciences of the United States of America, 96, 3440-3446.

Pollastro, R.M., 1985, Mineralogical and morphological evidence for the formation of illite at the expense of illite/smectite. Clays and Clay Minerals, 33, 265-274.

Pollastro, R.M., 1993, Considerations and applications of the illite/smectite geothermometer in hydrocarbon-bearing rocks of Miocene to Mississippian age. Clays and Clay Minerals, 41, 119-133.

Pytte, A.M. and Reynolds, R.C., 1989, The thermal transformation of smectite to illite. In: Naeser, N.D. and McCulloh, T.H. (Eds.), Thermal History of Sedimentary Basins: Methods and Case Histories, New York, Springer-Verlag, 133-140.

Renac, C. and Meunier, A., 1995, Reconstruction of paleothermal conditions in a passive margin using illite/smectite mixed-layered series (BA1 scientific deep drill-hole, Ardèche, France). Clay Minerals, 30, 107-118.

Reynolds, R.C. Jr., 1985, NEWMOD© a computer program for the calculation of one-dimensional diffraction patterns of mixed-layered clays. Reynolds, R.C. Jr., 8 Brook Rd., Hanover, NH.

Robinson, A.G., Coleman, M.L. and Gluyas, J.G., 1993, The age of illite cement growth, Village field area, southern North Sea: Evidence from K–Ar ages and $^{18}O/^{16}O$ ratios. American Association of Petroleum Geologists Bulletin, 77, 68-80.

Rosenberg, P.E., 2002, The nature, formation and stability of end-member illite: A hypothesis. American Mineralogist, 87, 103-107.

Savin, S.M. and Epstein, S., 1970, The oxygen and hydrogen isotope geochemistry of clay

1579 minerals. Geochimica et Cosmochimica Acta, 34, 25-42.
1580 Savin, S.M. and Lee, M., 1988, Isotopic studies of phyllosilicates. In: Bailey, S.W. (Ed.),
1581 Hydrous Phyllosilicates (Exclusive of Micas). Reviews in Mineralogy, 19, 189-223.
1582 Savin, S.M. and Hsieh, J.C.C., 1998, The hydrogen and oxygen isotope geochemistry of
1583 pedogenic clay minerals: Principles and theoretical background. Geoderma, 82, 227-253.
1584 Schwarcz, H.P., Agyei, E.K. and McMullen, C.C., 1969, Boron isotopic fractionation during clay
1585 adsorption from sea-water. Earth and Planetary Science Letters, 6, 1-5.
1586 Sears, S.K., Hesse, R., Vali, H., Elliott, W.C. and Aronson, J.L., 1998. K-Ar ages of 2:1 clay
1587 minerals, MacKenzie delta–Beaufort Sea region, Arctic Canada: Significance of *n*-
1588 alkylammonium exchange. The Canadian Mineralogist, 36, 1507-1524.
1589 Spivack, A.J., Palmer, M.R. and Edmond, J.M., 1987, The sedimentary cycle of the boron
1590 isotopes. Geochimica et Cosmochimica Acta, 51, 1939-1949.
1591 Spivack, A.J., Berndt, M.E. and Seyfried, W.E. Jr., 1990, Boron isotope fractionation during
1592 supercritical phase separation. Geochimica et Cosmochimica Acta, 54, 2337-2339.
1593 Środoń, J., 1980, Precise identification of illite/smectite interstratification by X-ray powder
1594 diffraction. Clay Minerals, 28, 401-411.
1595 Środoń, J., 1999, The use of clay minerals in reconstructing geological processes: Current
1596 advances and some perspectives. Clay Minerals, 34, 27-37.
1597 Środoń, J., 2010, Evolution of boron and nitrogen content during illitization of bentonites. Clays
1598 and Clay Minerals, 58, 743-756.
1599 Środoń, J., Elsass, F., McHardy, W.J. and Morgan, D.J., 1992, Chemistry of illite/smectite
1600 inferred from TEM measurements of fundamental particles. Clay Minerals, 27, 137-158.
1601 Środoń, J. and Clauer, N., 2001, Diagenetic history of Lower Palaeozoic sediments in Pomerania
1602 (northern Poland) traced across the Teisseyre-Tornquist tectonic zone using mixed-layer illite-
1603 smectite. Clay Minerals, 36, 15-27.
1604 Środoń, J., Clauer, N. and Eberl, D.D., 2002, Interpretation of K-Ar dates of illitic clays from
1605 sedimentary rocks aided by modeling. American Mineralogist, 87, 1528-1535.
1606 Środoń, J., Kotarba, M., Biroň, A., Such, P., Clauer, N. and Wojtowicz, A., 2006, Diagenetic
1607 history of the Podhale-Orava Basin and the underlying Tatra sedimentary structural units
1608 (Western Carpathians): Evidence from XRD and K-Ar of illite-smectite. Clay Minerals, 41,
1609 751-774.

1610 Środoń, J., Clauer, N., Huff, W., Dudek, T. and Banas, M., 2009, K-Ar dating of Ordovician
1611 bentonites from the Baltic Basin and the Baltic Shield: Implications for the role of temperature
1612 and time in the illitization of smectite. Clay Minerals, 44, 361-387.
1613 Stueber, A.M., Walter, L.M., Huston, T.J. and Pushkar, P., 1993, Formation waters from
1614 Mississippian-Pennsylvanian reservoirs, Illinois basin, U.S.A: Chemical and isotopic
1615 constraints on evolution and migration. Geochimica et Cosmochimica Acta, 57, 763-784.
1616 Šucha, V., Kraus, I., Gerthofferová, H., Peteš, J. and Sereková, M., 1993, Smectite to illite
1617 conversion in bentonites and shales of the East Slovak Basin. Clay Minerals, 28, 243-253.
1618 Swilhart, G.H., Moore, M.R. and Edmond, J.M., 1986, Boron isotopic composition of marine and
1619 non-marine evaporite borates. Geochimica et Cosmochimica Acta, 50, 1297-1301.
1620 Teng, F.-Z., McDonough, W.F., Rudnick, R.L. and Gao, S., 2004, Lithium isotopic composition
1621 and concentration of the upper continental crust. Geochimica et Cosmochimica Acta, 68,
1622 4167-4178.
1623 Teng, F.-Z., McDonough, W.F., Rudnick, R.L. and Walker, R.J., 2006, Diffusion-driven extreme
1624 lithium isotopic fractionation in country rocks of the Tin Mountain pegmatite. Earth and
1625 Planetary Science Letters, 243, 701-710.
1626 Teng, F.-Z., McDonough, W.F., Rudnick, R.L. and Wing, B.A., 2007, Limited lithium isotopic
1627 fractionation during progressive metamorphic dehydration in metapelites : A case study from
1628 the Onawa contact aureole, Maine. Chemical Geology, 239, 1-12.
1629 Teng, F.-Z, Li, W.-Y. Rudnick, R.L. and Gardner, L.R., 2010, Contrasting lithium and
1630 magnesium fractionation during continental weathering. Earth and Planetary Science Letters,
1631 300, 63-71.
1632 Valley, J.W. and Kita, N.T., 2009, In situ Oxygen Isotope Geochemistry by Ion Microprobe, In:
1633 Fayek, M. (Ed.), Mineralogical Association of Canada Short Course: Secondary Ion Mass
1634 Spectrometry in the Earth Sciences, 41, 19-63.
1635 van Krevelen, D.W., 1950, Graphical-statistical method for the study of structure and reaction
1636 processes of coal. Fuel, 29, 269-84.
1637 Velde, B., 1985, Clay Minerals: A Physico-Chemical Explanation of their Occurrence.
1638 Developments in Sedimentology, Elsevier, Amsterdam, 40, 426p.
1639 Velde, B. and Vasseur, G., 1992, Estimation of the diagenetic smectite to illite transformation in
1640 time-temperature space. American Mineralogist, 77, 967-976.

1641 Velde, B. and Renac, C., 1996, Smectite to illite conversion and K-Ar ages. Clay Minerals, 31,
1642 25-32.
1643 Vengosh, A., Starinsky, A., Kolodny, Y. and Chivas, A.R., 1991a, Boron isotope geochemistry as
1644 a tracer for the evolution of brines and associated hot springs from the Dead Sea, Israel.
1645 Geochimica et Cosmochimica Acta, 55, 1689-1695.
1646 Vengosh, A., Starinsky, A., Kolodny, Y., Chivas, A.R. and McCulloch, M.T., 1991b,
1647 Coprecipitation and isotopic fractionation of boron in modern biogenic carbonates.
1648 Geochimica et Cosmochimica Acta, 55, 2901-2910.
1649 Vengosh, A., Starinsky, A., Kolodny, Y., Chivas, A.R. and Raab, M., 1992, Boron isotope
1650 variations during fractional evaporation of seawater: New constraints on the marine vs.
1651 nonmarine debate. Geology, 20, 799-802.
1652 Vengosh, A., Starinsky, A. and Chivas, A.R., 1994, Boron isotopes in Heletz-Kokhav oilfield
1653 brines, the Coastal Plain Israel. Israel Journal of Earth Sciences, 43, 231-237.
1654 Wasserburg, G.J., Hayden, R.I. and Jensen, K.J., 1956, Ar40-K40 dating of igneous rocks and
1655 sediments. Geochimica et Cosmochimica Acta, 10, 153-165.
1656 Weaver, C.E. and Beck, K.C., 1971, Clay water diagenesis during burial, how mud becomes
1657 gneiss. Geological Society of America, Special Paper, 134, 96p.
1658 Wilkinson, M. and Haszeldine, R.S., 2002, Fibrous illite in oilfield sandstones – a nucleation
1659 kinetic theory of growth. Terra Nova, 14, 56-60.
1660 Williams, L.B. and Ferrell, R.E., 1991, Ammonium substitution in illite during maturation of
1661 organic matter. Clays and Clay Minerals, 39, 400-408.
1662 Williams, L.B., Hervig, R.L., Holloway, J.R. and Hutcheon, I., 2001a, Boron isotope
1663 geochemistry during diagenesis: Part 1. Experimental determination of fractionation during
1664 illitization of smectite. Geochimica et Cosmochimica Acta, 65, 1769-1782.
1665 Williams, L.B., Hervig, R.L. and Hutcheon, I., 2001b, Boron isotope geochemistry during
1666 diagenesis: Part II. Applications to organic-rich sediments. Geochimica et Cosmochimica
1667 Acta, 65, 1783-1794.
1668 Williams, L.B. and Hervig, R.L., 2002, Exploring intra-crystalline B-isotope variations in mixed-
1669 layer illite-smectite. American Mineralogist, 87, 1564-1570.
1670 Williams, L.B. and Hervig, R.L., 2006, Crystal size dependence of illite-smectite isotope
1671 equilibration with changing fluids. Clays and Clay Minerals. 54, 531-540.

1672 Williams, L.B., Turner, A. and Hervig, R.L., 2007, Intracrystalline boron isotope partitioning in
1673 illite-smectite: Testing the geothermometer. American Mineralogist, 92, 1958-1965.
1674 Williams, L.B., Clauer, N. and Hervig R.L., 2012, Light stable isotope microanalysis of clays in
1675 sedimentary rocks. In: Sylvester, P. (Ed.), Quantitative Mineralogy and Microanalysis of
1676 Sediments and Sedimentary Rocks, Mineralogical Association of Canada, Short Course, 42,
1677 55-73.
1678 Williams, L.B., Środoń, J., Huff, W.D., Clauer, N. and Hervig, R.L., 2013. Light element
1679 distributions (N, B, Li) in Baltic Basin bentonites record organic sources. Geochimica et
1680 Cosmochimica Acta, 120, 582-599.
1681 Wilson, R.G., Stevie, F.A. and Magee, C.W., 1989, Secondary-ion mass spectrometry: a practical
1682 handbook for depth profiling and bulk impurity analysis. John Wiley & Sons, New York,
1683 384p.
1684 Wilson, T.P. and Long, D.T., 1993, Geochemistry and isotope chemistry of $CaCl_2$ brine in
1685 Silurian formations of the Michigan Basin. Applied Geochemistry, 8, 507-524.
1686 Yapp, C.J., 1993, Stable isotope geochemistry of low temperature Fe(iii) and Al ‘‘oxides’’ with
1687 implications for continental paleoclimates in climate change. In: Swart, P.K., Lohman, K.C.,
1688 McKenzie, J. and Savin S. (Eds.), Continental Isotopic Records, Geophysical Monographs,
1689 American Geophysical Union, Washington, DC, 78, 285-294.
1690 Yates, D.M. and Rosenberg, P.E., 1996, Formation and stability of endmember illite: I. Solution
1691 equilibration experiments at 100-250°C and $P_{v,soln}$. Geochimica et Cosmochimica Acta, 60,
1692 1873-1883.
1693 Yates, D.M. and Rosenberg, P.E., 2011, A reinvestigation of smectite illitization in experimental
1694 hydrothermal conditions: Results from X-ray diffraction and transmission electron
1695 microcroscopy - Discussion. American Mineralogist, 96, 1901-1902.
1696 You, C.F. and Chan, L.H., 1996, Precise determination of lithium isotopic composition in low
1697 concentration natural samples. Geochimica et Cosmochimica Acta, 60, 909-915.
1698 Zwingmann, H., Clauer, N. and Gaupp, R., 1999, Structure-related geochemical (REE) and
1699 isotopic (K–Ar, Rb–Sr, $\delta^{18}O$) characteristics of clay minerals from Rotliegend sandstone
1700 reservoirs (Permian, Northern Germany). Geochimica et Cosmochimica Acta, 63, 2805-2823.
1701
1702

Captions

Figure 1: Theoretical sketch of illite-smectite mixed layer before and after B and Li introduction during crystal nucleation (from Williams et al., 2013).

Figure 2: Theoretical illitization rates (from Clauer, 2006).

Figure 3: Trigonal, tetrahedral and interlayer $\delta^{11}B$ values of a smectite-illite mixed layer of a bentonite bed, depending on the content of illite layers and the distance to an intrusive basaltic dike (from Williams et al., 2007).

Figure 4: K-Ar ages of nanometric illite-rich fractions from bentonite beds of Trhovište and Čičarovče sites in the East Slovak Basin (from Clauer et al., 1997).

Figure 5: Summary of the K-Ar ages from different bentonite beds of the East Slovak Basin. The nanometric fractions are identified by open symbols and the micrometric fractions by grey symbols (from Clauer et al., 2014b).

Figure 6: $\delta^{18}O$ vs. δD of nanometric (in black symbols) and micrometric (in open symbols) of varied size fractions from bentonite beds of the East Slovak Basin (from Clauer et al., 2014b).

Figure 7: (A): $\delta^{18}O$ vs K-Ar ages of nanometric (in white symbols) and micrometric (grey symbols) size fractions of bentonite beds from East Slovak Basin; and (B) δD vs. K-Ar of the same fractions with the same symbols from the same bentonite beds (from Clauer et al., 2014b).

Figure 8: $\delta^{11}B$ vs. B contents of nanometric size fractions labeled 1 to 3 for increasing size fractions of different bentonite beds identified by different symbols from East Slovak Basin (from Clauer et al., 2009).

Figure 9: Correlation between $\delta^{11}B$ and present-day temperature in the boreholes of the studied bentonite beds from east Slovak Basin. Each symbol represents a distinct bentonite sample (from Clauer et al., 2009).

Figure 10: $\delta^{7}Li$ vs. Li content of varied nanometric size fractions from different bentonite samples (identified by different symbols) of the East Slovak Basin. T stands for measured temperature in the drill holes and Sm stands for smectite layers in the separated nanometric fractions (from Clauer et al., 2009). The different symbols stand for the different studied

samples.

Figure 11: (A) Geographic repartition of the nanometric K-Ar ages of bentonite samples from Baltic Basin; (B) $\delta^{11}B$ and $\delta^{7}Li$ signatures of nanometric size fractions of Baltic bentonites along a SW-NE trend reported on the regional map (from Williams et al., 2013).

Figure 12: $\delta^{11}B$ and $\delta^{7}Li$ of the Cambrian Alum shale depending on the H/C ratio of the organics with identification of oil and gas generation (from Williams et al., 2013).

Figure 13: The α and β^2 parameters of the different size fractions from Appalachian K-bentonite beds showing that illitization occurred in all fractions by simultaneous nucleation and crystal growth, except for one sample. All Appalachian bentonite size fractions are labeled as grey symbols; the other symbols identify fractions from other studies (see Clauer et al., 2013).

Figure 14: $^{40}Ar/^{36}Ar$ vs. $^{40}K/^{36}Ar$ isochron diagram for the nanometric size fractions of the Appalachian K-bentonite beds. The symbols in grey fit the upper isochron of 319.9 $\pm$ 2.0 Ma with an initial $^{40}Ar/^{36}Ar$ of 271 $\pm$ 66, whereas the open symbols fit the lower isochron of 284.9 $\pm$ 1.2 Ma with an initial $^{40}Ar/^{36}Ar$ of 310 $\pm$ 44, and the black symbols identify the fractions off the two isochrons (from Clauer et al., 2013).

Figure 15: (A) $\delta^{18}O$ vs. δD of the nano- to micrometric illite fractions from Appalachian K-bentonites, and (B) $\delta^{18}O$ of the same bentonite size fractions vs. their K-Ar ages. The increasing lettering in the graph from a to d stand for the increasing sizes of the nanometric fractions; more details are in Clauer et al. (2013).

Figure 16: $\delta^{7}Li$ and $\delta^{11}B$ values of <2 μm illite from the Walsen Dike metabentonite across the 13-m contact with the basaltic dike into the country rock. Maximum temperatures range from ~500 ˚C near the dike to ~200 ˚C in country rock (from Williams et al., 2007).

Figure 17: Theoretical K-Ar age of nanosized illite based on a model based on crystal nucleation followed by growth with two trajectories A and B trending on the basis of different intensities for burial illitization. The numbers at the black dots outline the theoretical K-Ar age depending on the parameters considered (from Środoń et al., 2002).

Figure 18: Harper (1970) diagram with the K-Ar data of varied nanometric and micrometric size fractions of the "Illite du Puy" shale. The trends are given by fine dashed arrays, whereas the tendencies are in full lines (from Clauer, unpublished).

Figure 19: Harper (1970) diagram with all size fractions of the different shale-type samples of the "Illite du Puy". Graphs (A) and (B) detail the same data at different scales (from Clauer,

unpublished).

Figure 20: Changing K-Ar ages of <0.4 μm size fractions from shales and sandstones of the buried sedimentary sequence beneath the Mahakam Delta, Indonesia (from Clauer et al., 1999).

Figure 21: Modeled K_2O and radiogenic ^{40}Ar contents of nanometric illite from progressively buried shales and sandstones of the Mahakam Delta, Indonesia. The upper left-hand panel outlines the geographic location of the Handil field from where the core samples were recovered. The expandability of the illite-smectite mixed layer in the lower left-hand panel has been used to model the K and radiogenic ^{40}Ar contents relative to depth in both the sandstones and shales. It turns out that an excess of radiogenic ^{40}Ar starting at depth (~3000 m) is needed to match the analytical data (after Clauer et al., 2004).

Figure 22: SEM photomicrographs of illite shapes from Triassic sandstones of the eastern Paris Basin. (A) Illite filaments and fibers growing on a partly dissolved K-feldspar; (B) typical habitus of illite: hairy growing onto well-crystallized hexagonal plates, which suggests that the hairy morphologies correspond to the last stage of the mineral paragenesis; (C) platy and lathlike illite; (D) magnification of platy to the left and lathlike illite to the right (from Blaise et al., in preparation).

Figure 23: Elemental compositions of the leachates from gentle acidic leaching of the nanometric size fractions of two sandstones (A and B) from the eastern Paris Basin (from Blaise et al., in preparation)

Figure 24: (A) Harper (1970) diagram of the nanometric and micrometric size fraction of a smectite-rich bentonite bed from Campos Basin, offshore Brazil; (B) $^{40}Ar/^{36}Ar$ vs. $^{40}K/^{36}Ar$ isochron of the same size fractions from the same bentonite bed. The data of the finest fraction have been duplicated in the isochron graph (from Clauer, unpublished).

Figure 25: Rb-Sr isochron diagram for the leachates (grey symbols), untreated fractions (white symbols) and residues (black symbols) of the nanometric and micrometric fractions of the smectite-rich bentonite bed from Campos Basin, offshore Brazil (from Clauer, unpublished).

Figure 26: $\delta^{18}O$ of the nano-sized illite from Trhovište and Čičarovče bentonite beds of the East Slovak Basin (from Clauer et al., 2003).

Figure 27: $\delta^{11}B$, $\delta^{18}O$ and δD of an untreated <2 μm clay fraction and the same fraction from an oil-bearing shale pyrolyzed at successively higher temperatures (from Clauer, Williams,

Fallick and Lewan, unpublished).

Figure 28: Graphic calculation of the removed B content and $\delta^{11}B$ for each pyrolysis step (from Clauer, Williams, Fallick and Lewan, unpublished).

Table 1: K-Ar data of the nanometric and micrometric fractions from five "Illite du Puy" shale-type samples (from Clauer, unpublished).

Figure

Click here to download high resolution image

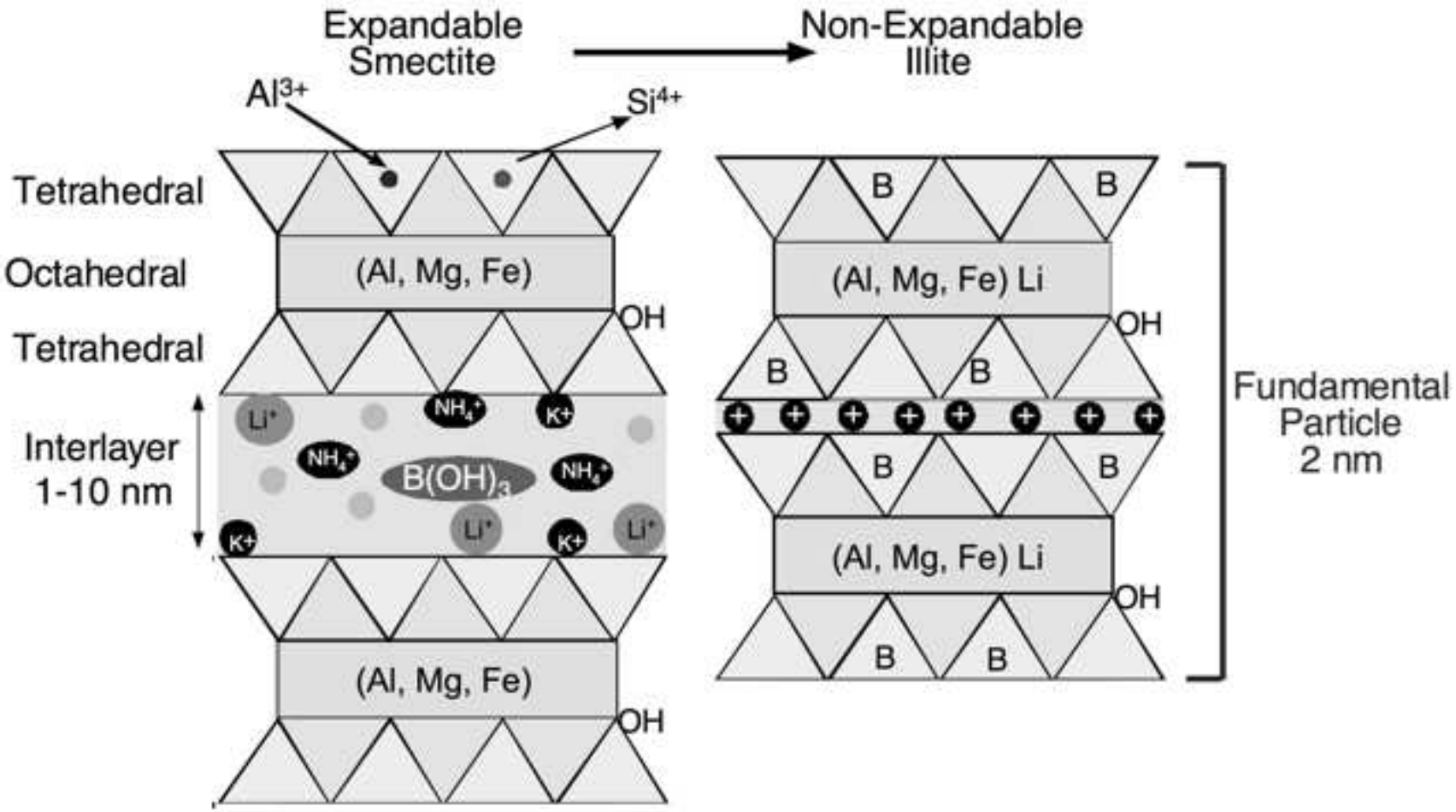

Figure
Click here to download high resolution image

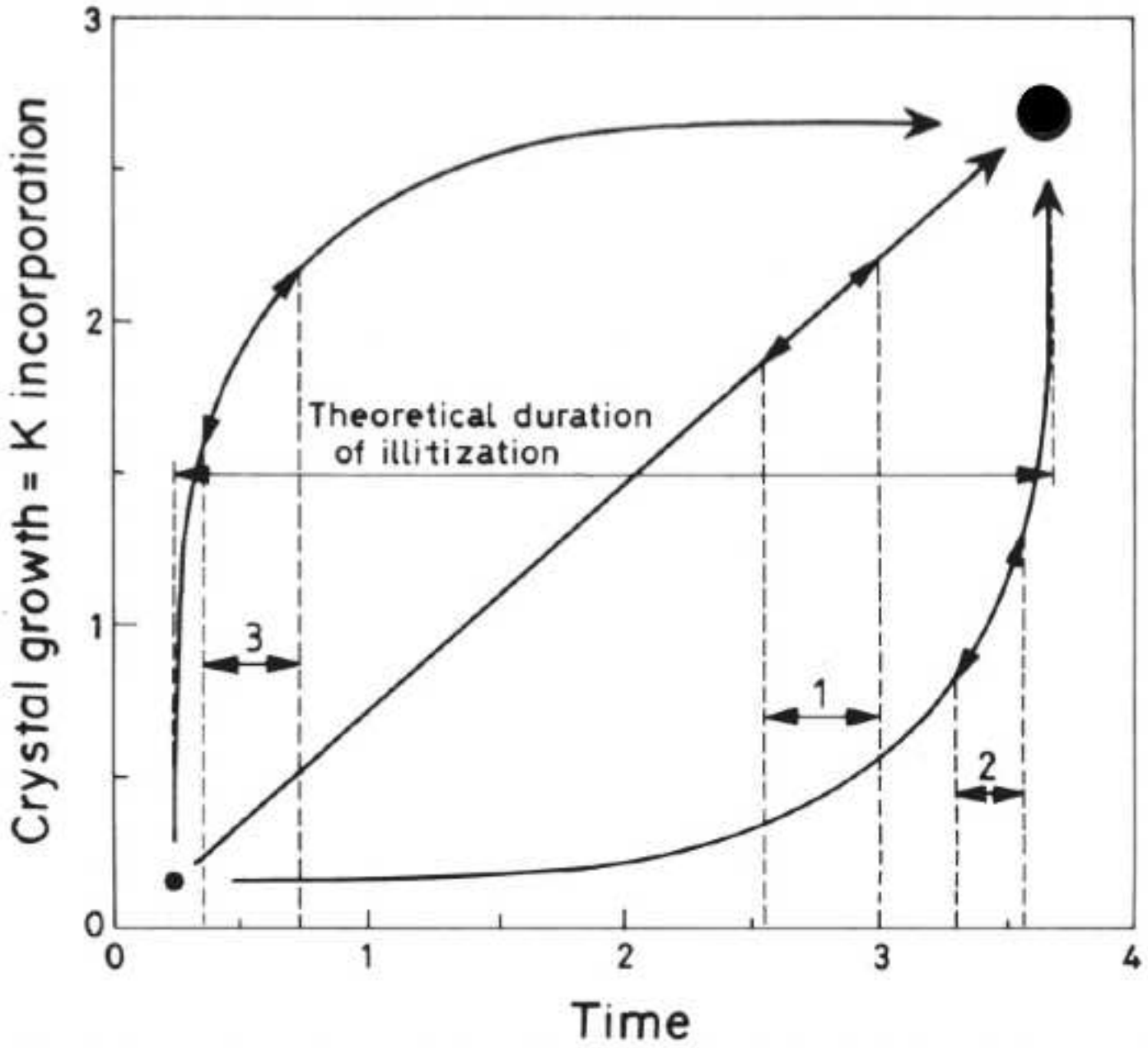

Figure
Click here to download high resolution image

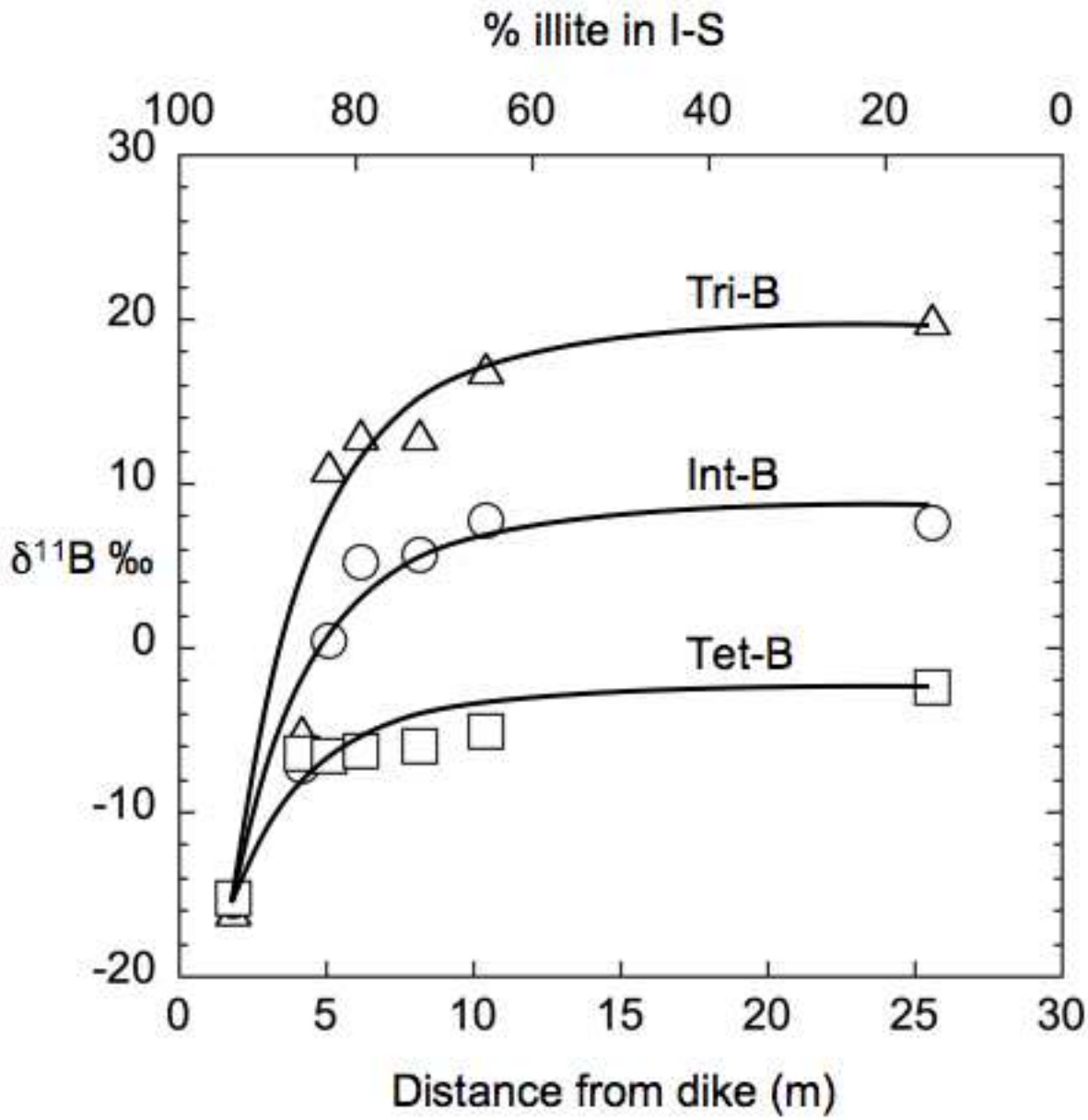

Figure
Click here to download high resolution image

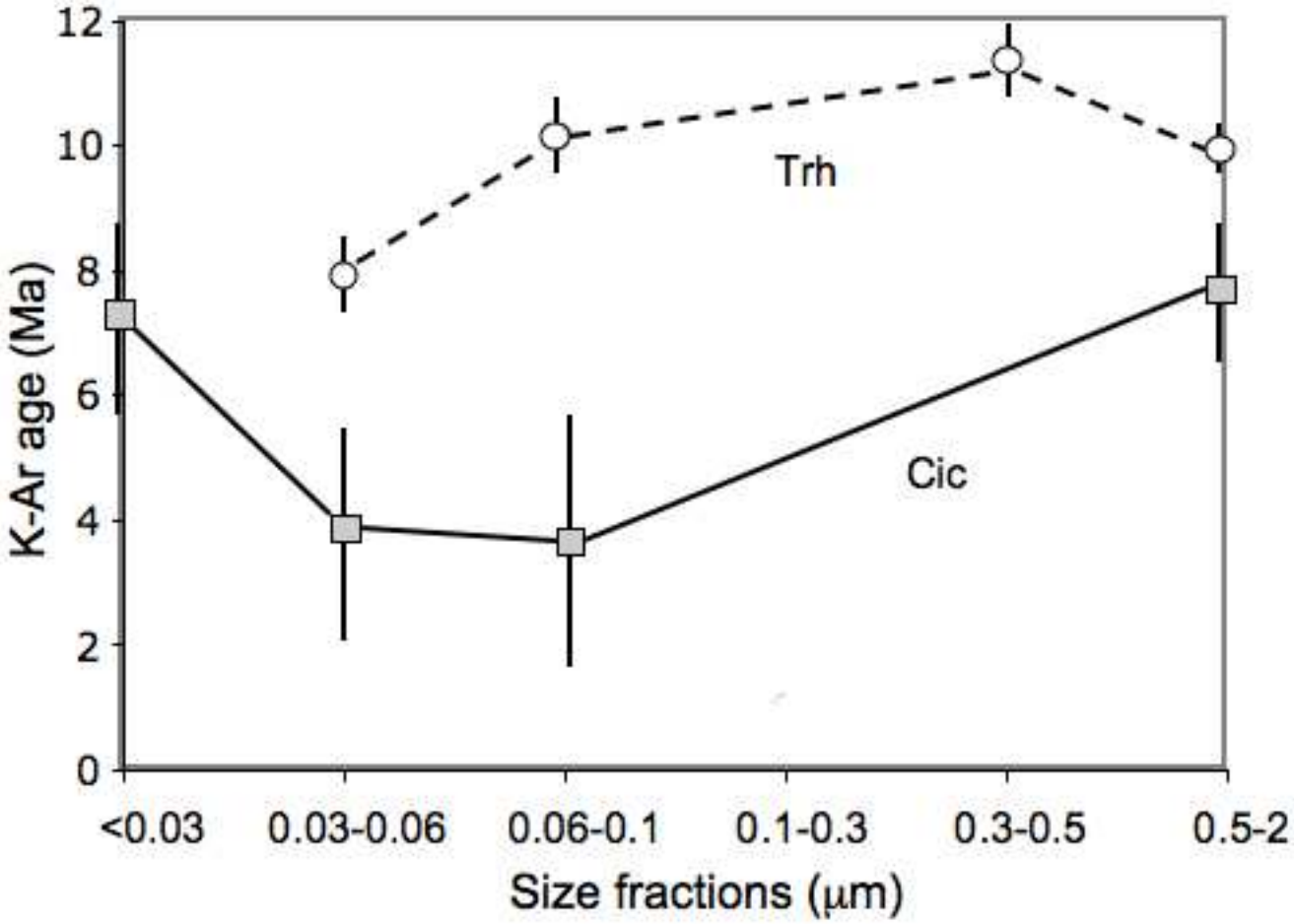

Figure

Click here to download high resolution image

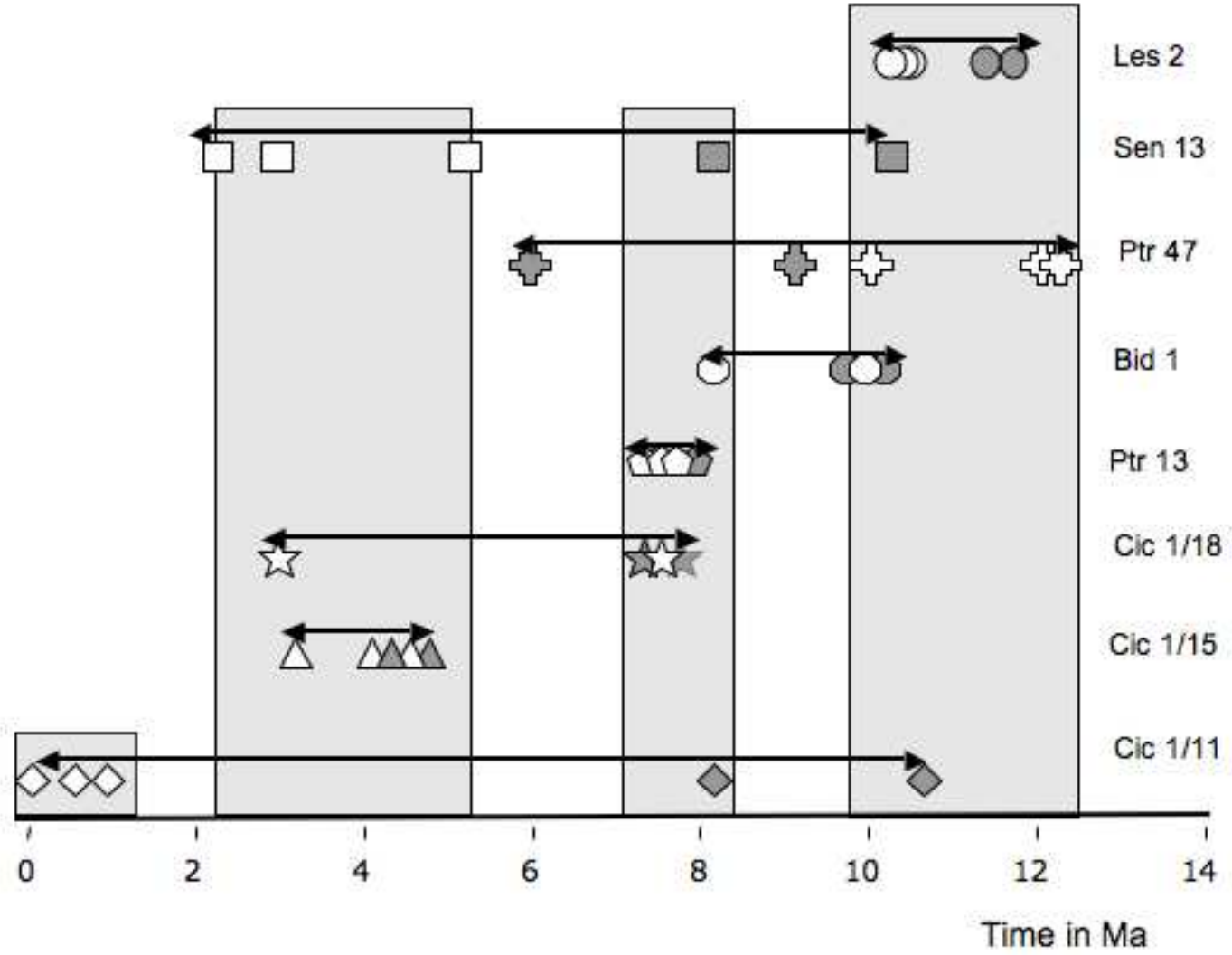

Figure
Click here to download high resolution image

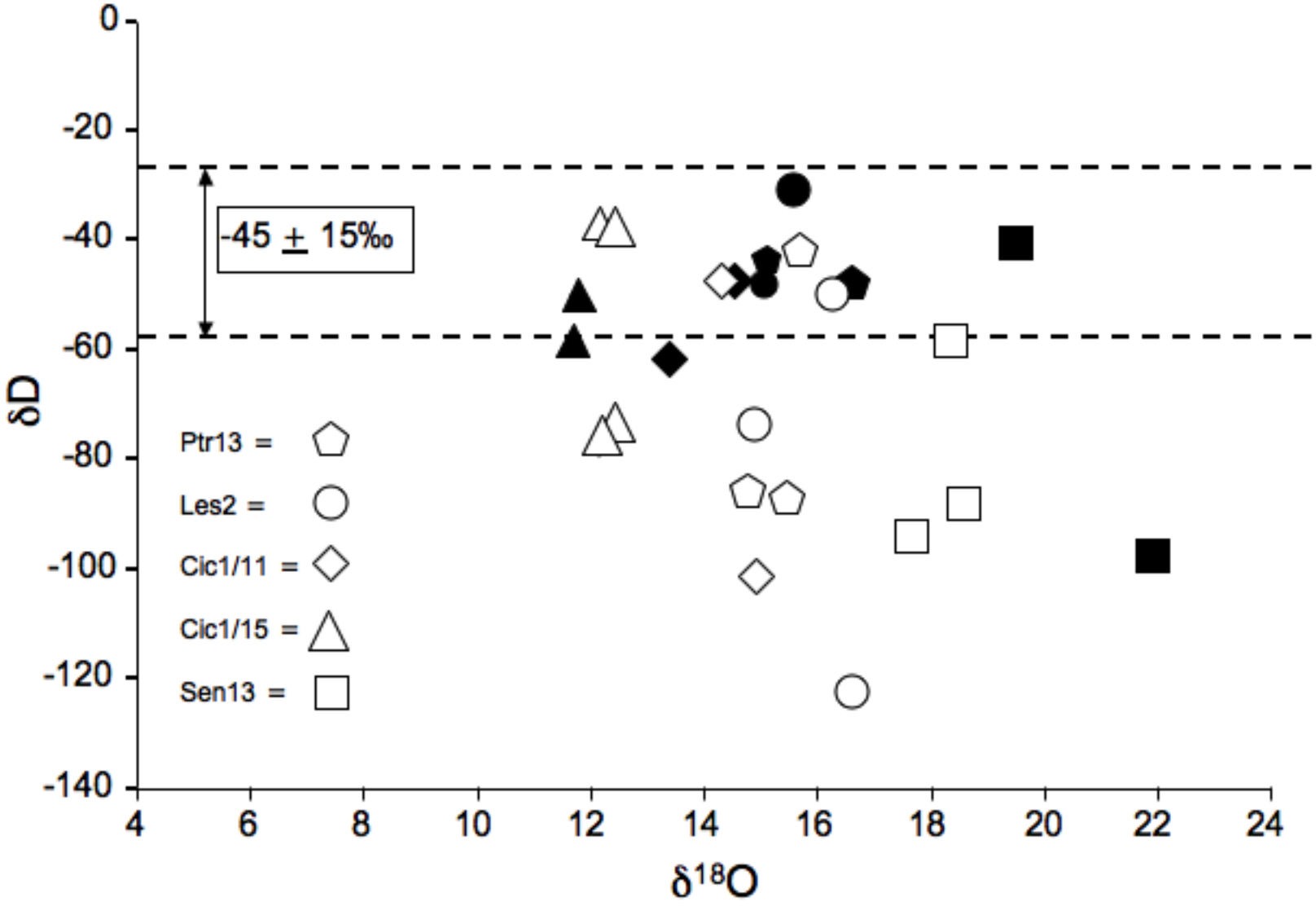

Figure
Click here to download high resolution image

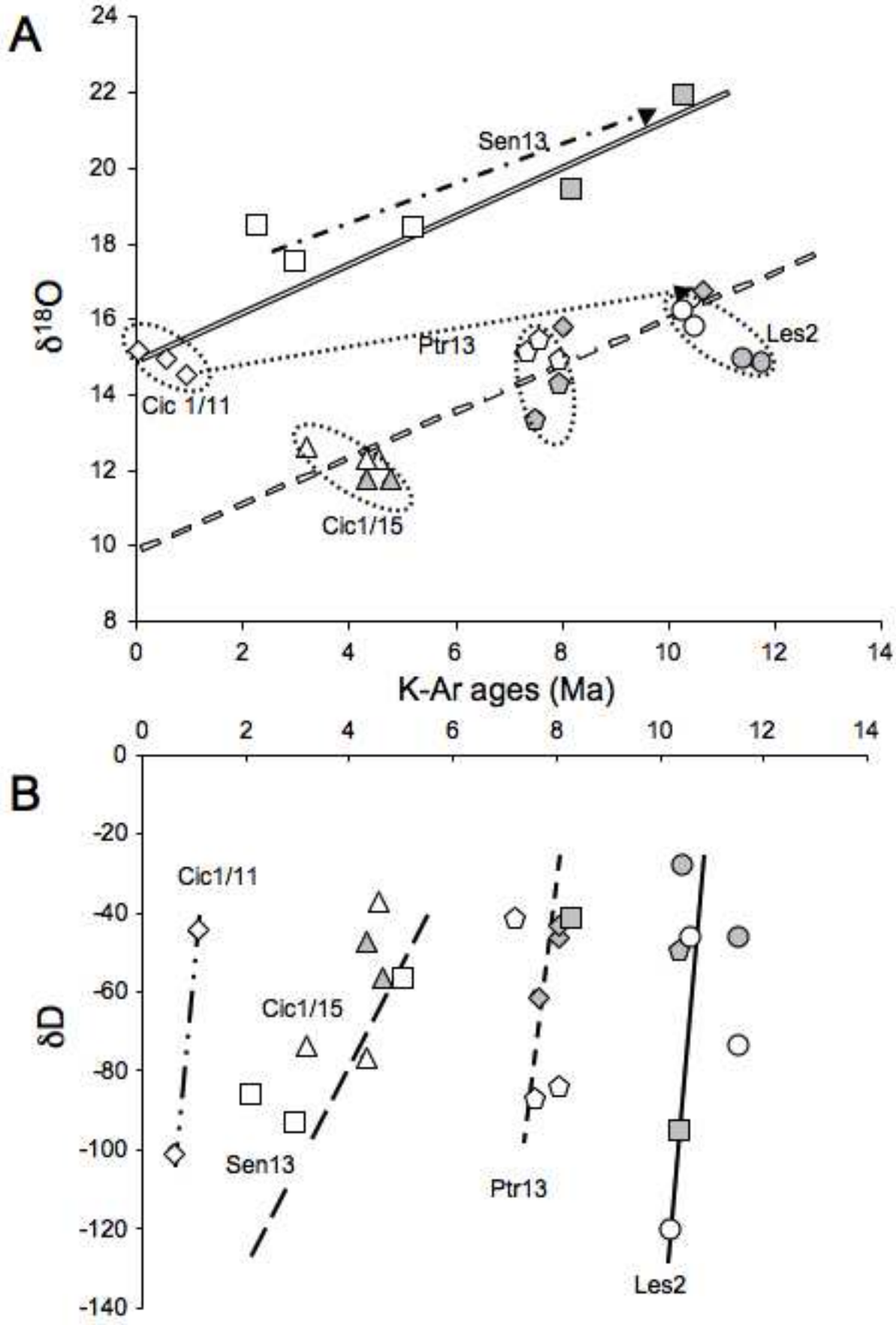

Figure
Click here to download high resolution image

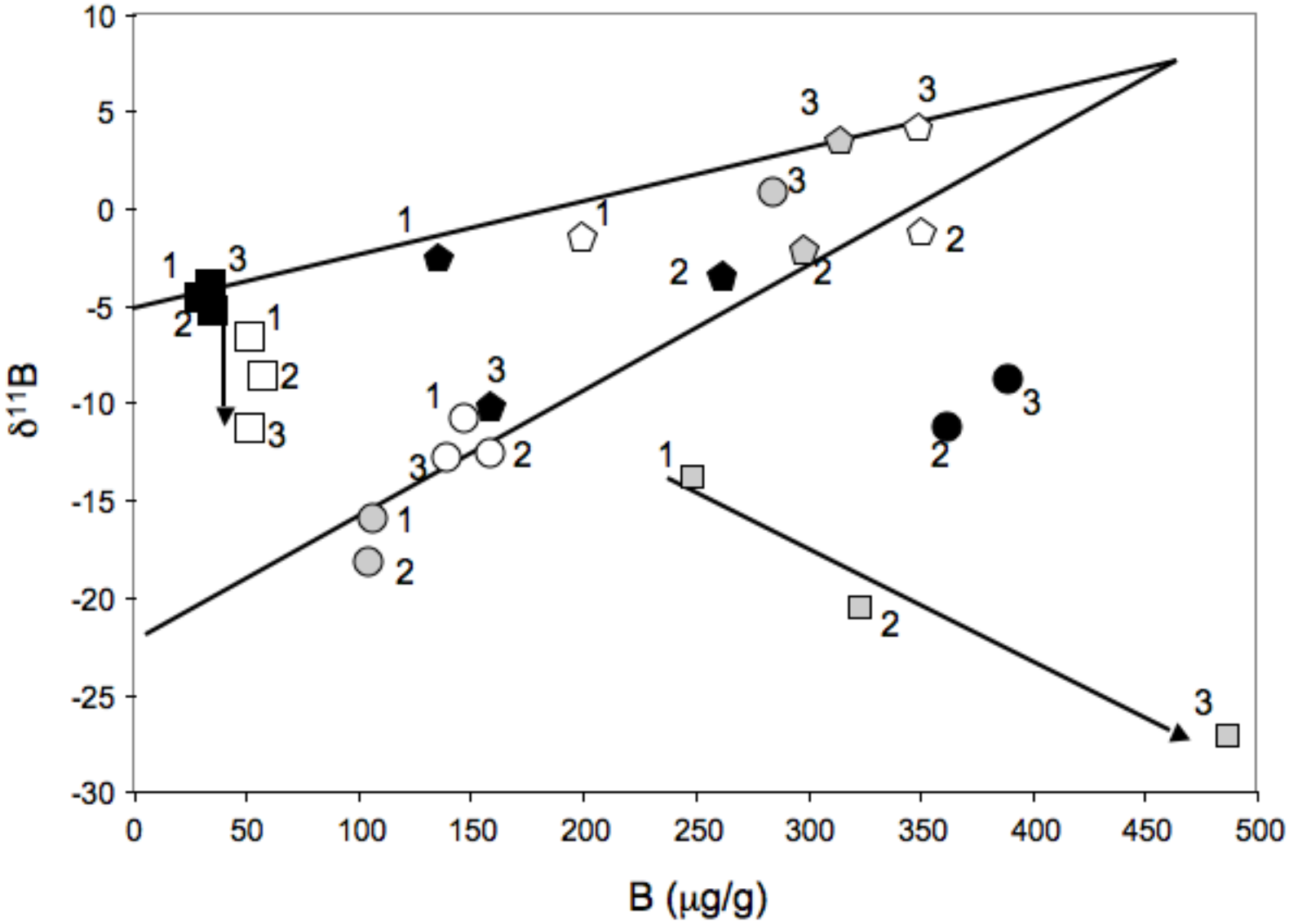

Figure
Click here to download high resolution image

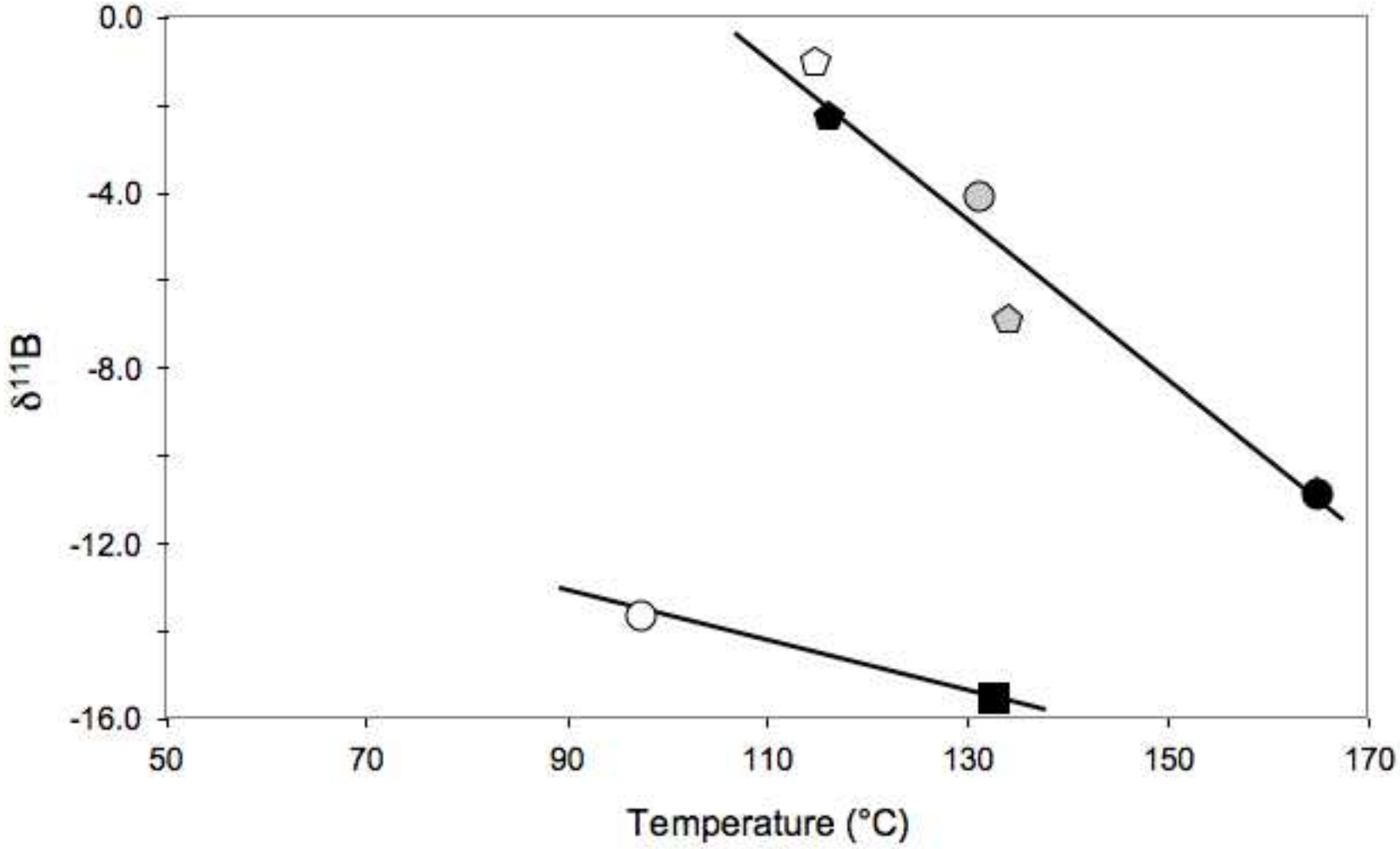

Figure
Click here to download high resolution image

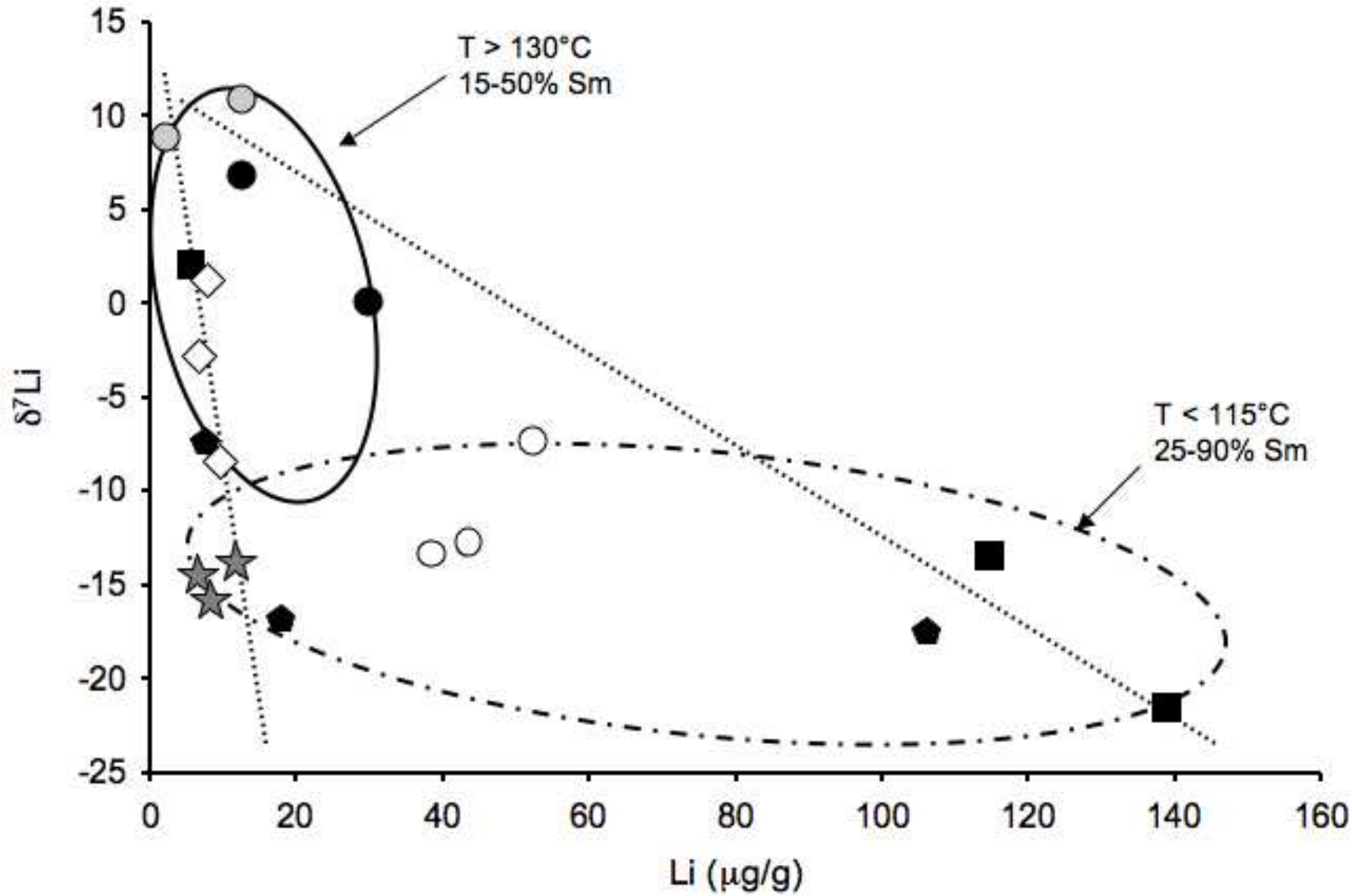

Figure
Click here to download high resolution image

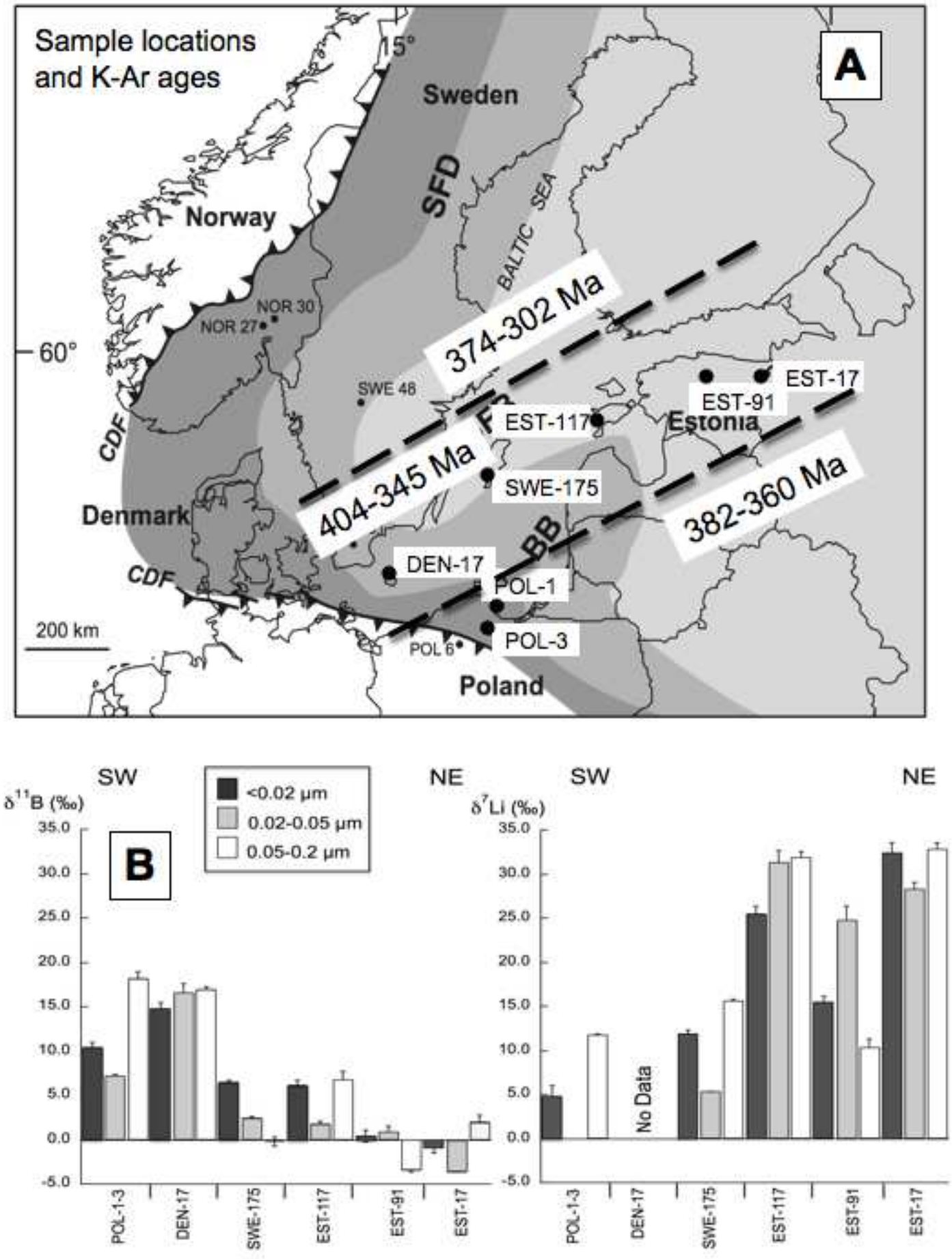

Figure
Click here to download high resolution image

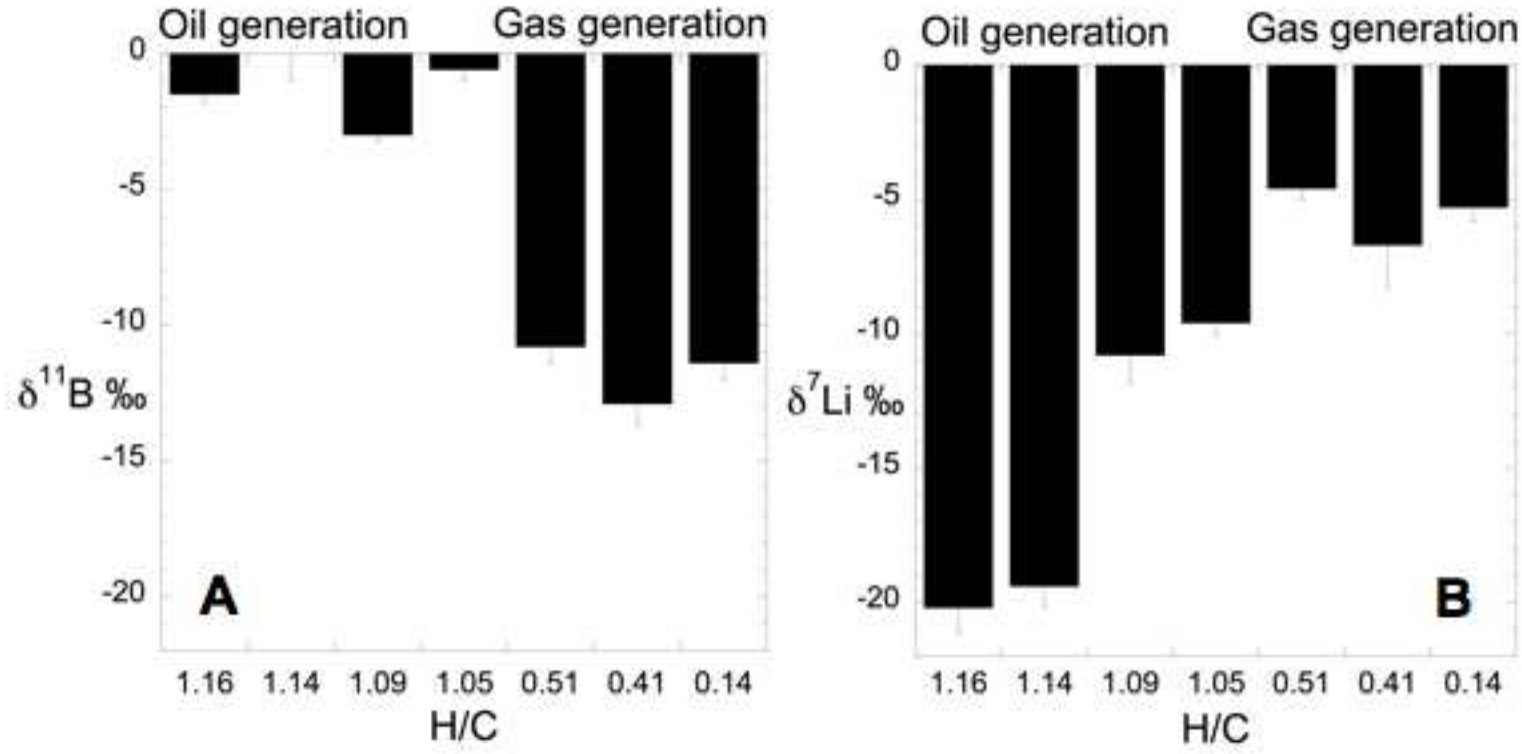

Figure
Click here to download high resolution image

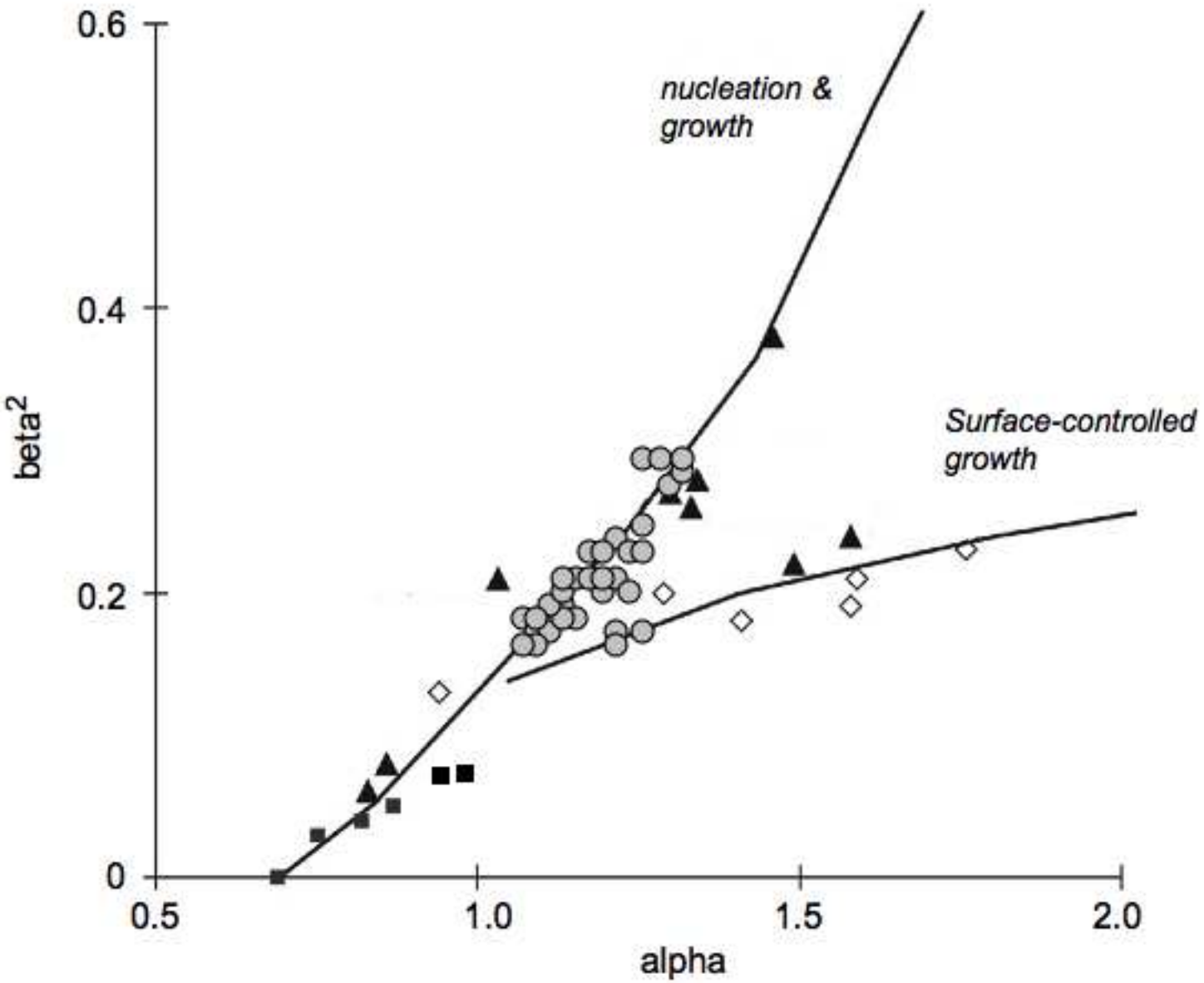

Figure
Click here to download high resolution image

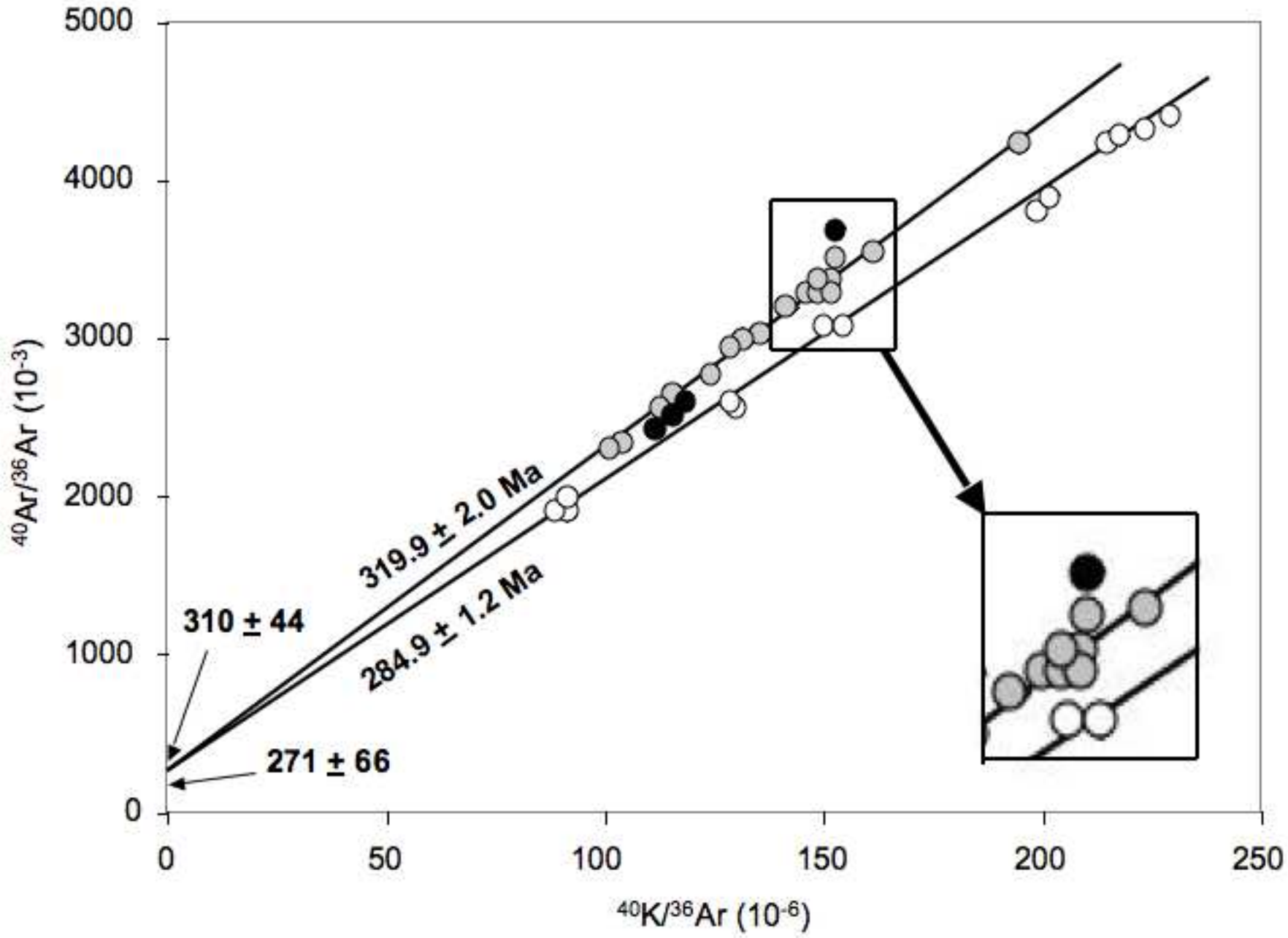

Figure
Click here to download high resolution image

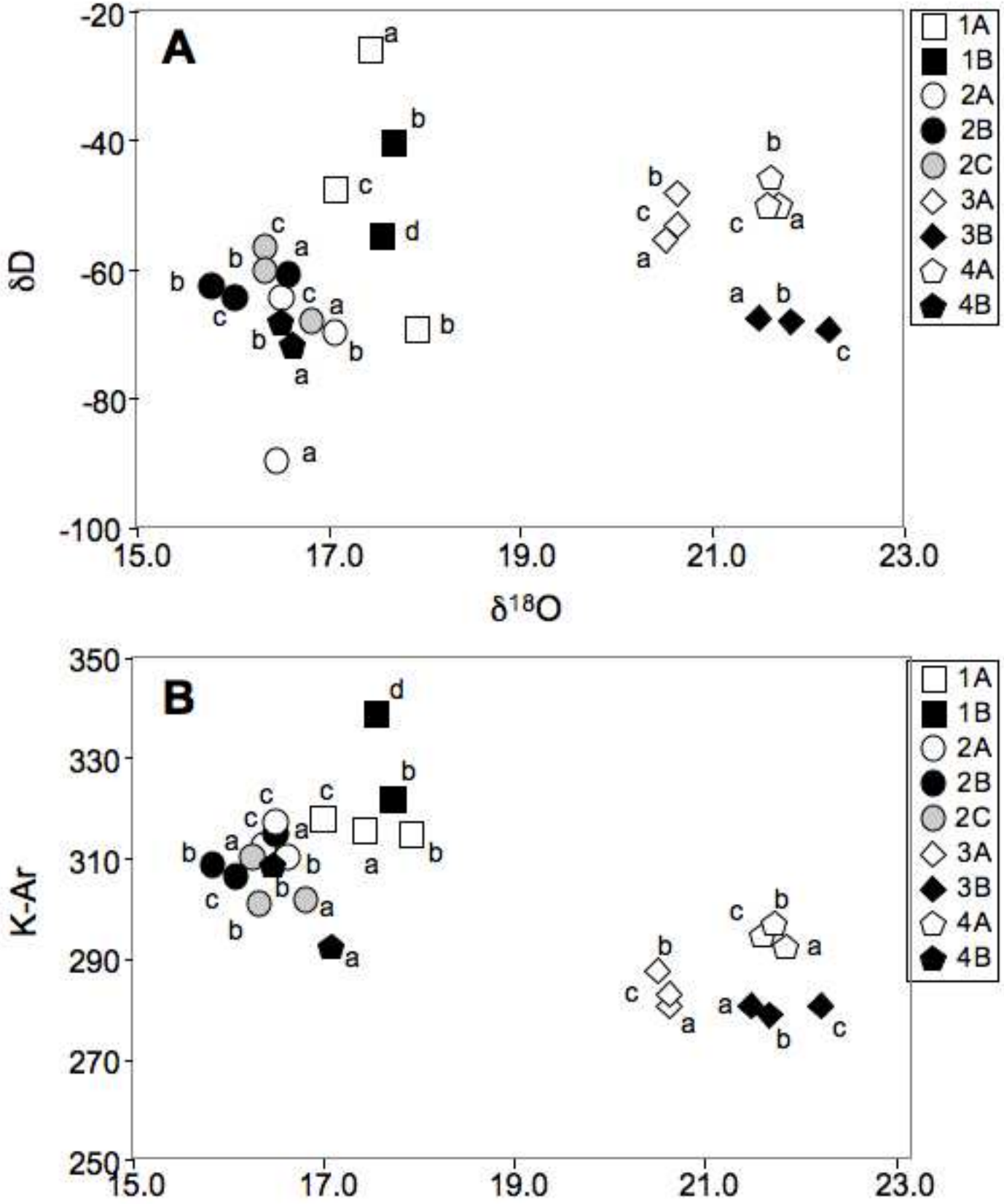

Figure
Click here to download high resolution image

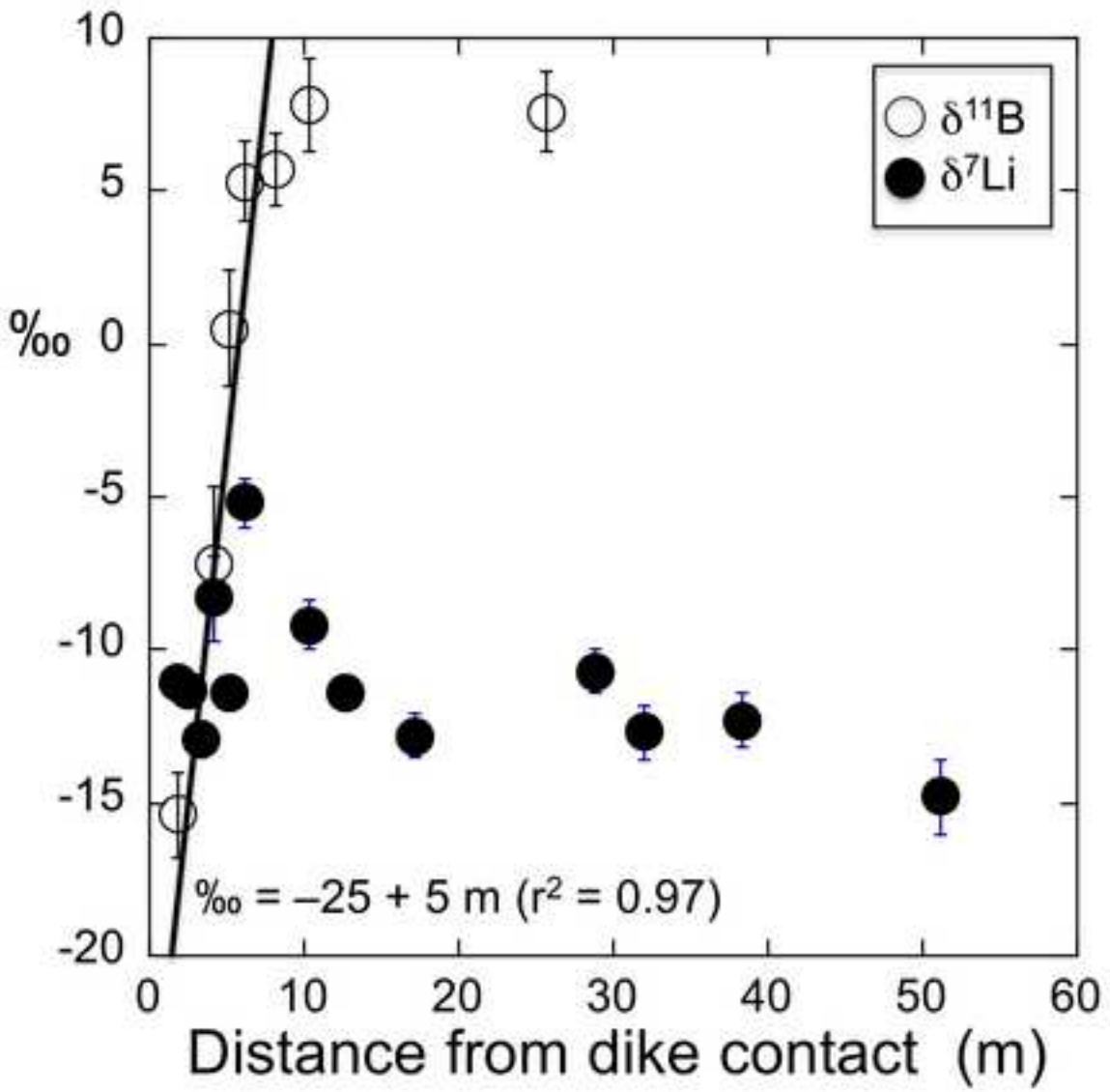

Figure

Click here to download high resolution image

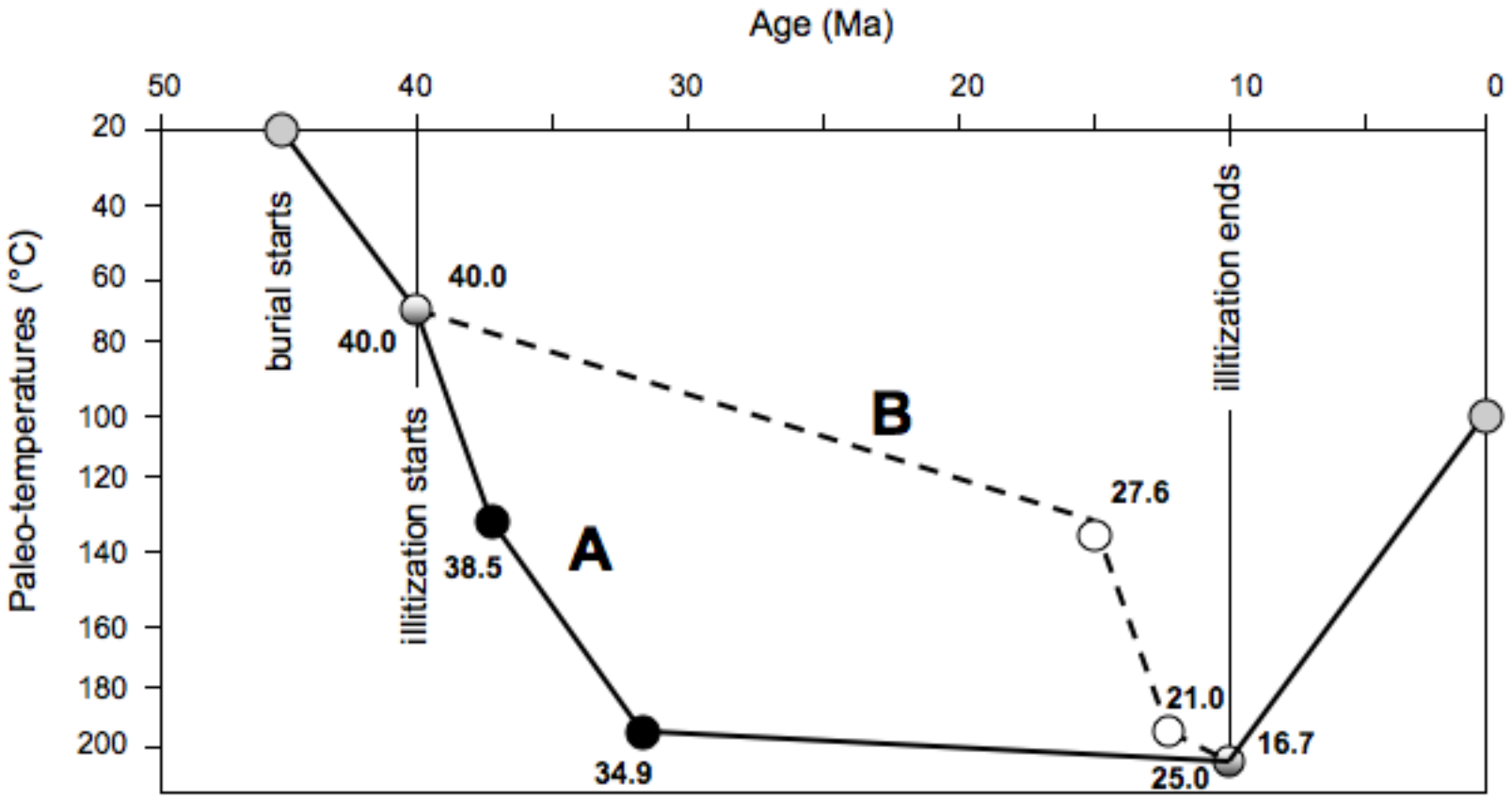

Figure

Click here to download high resolution image

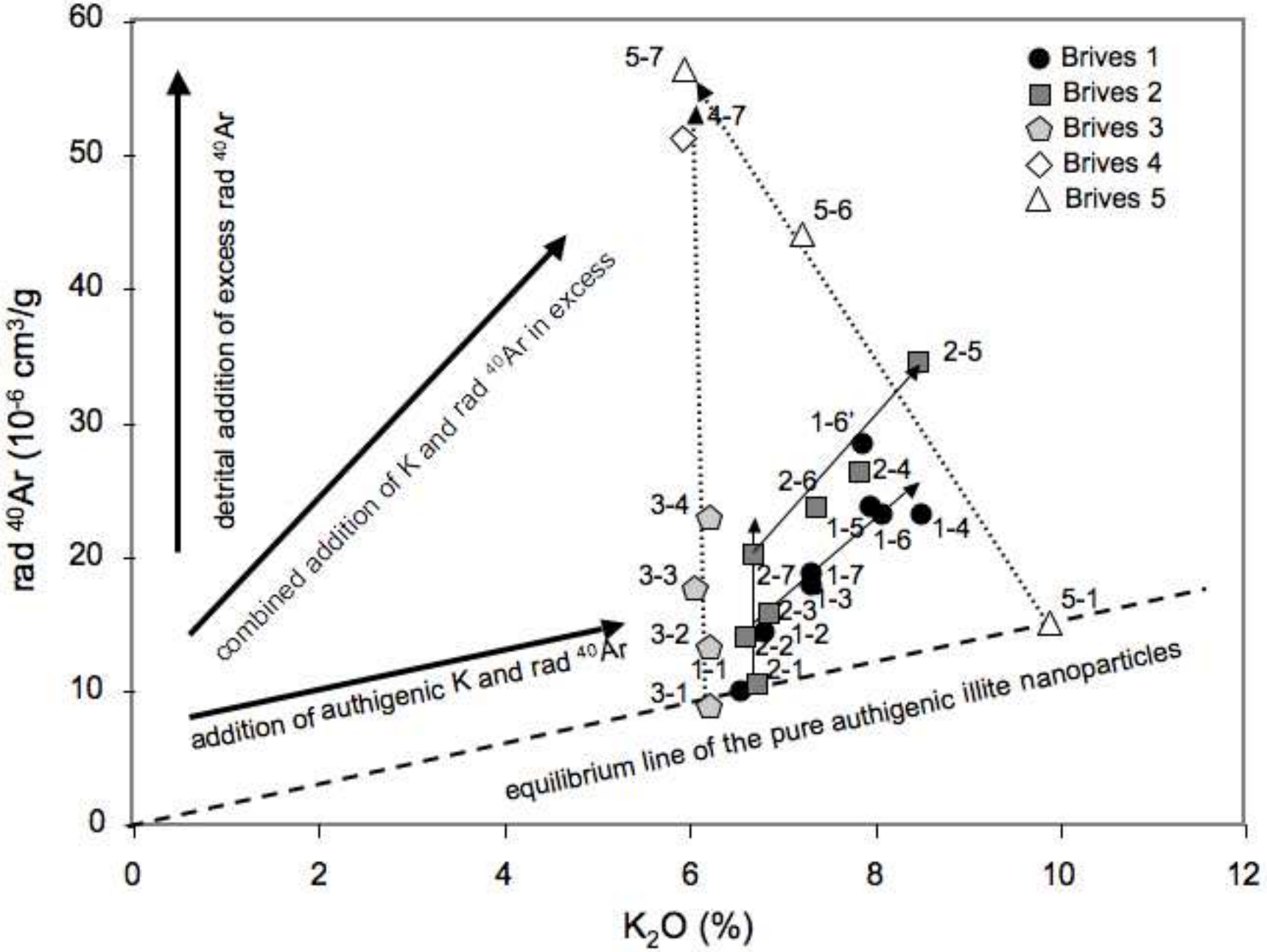

Figure
Click here to download high resolution image

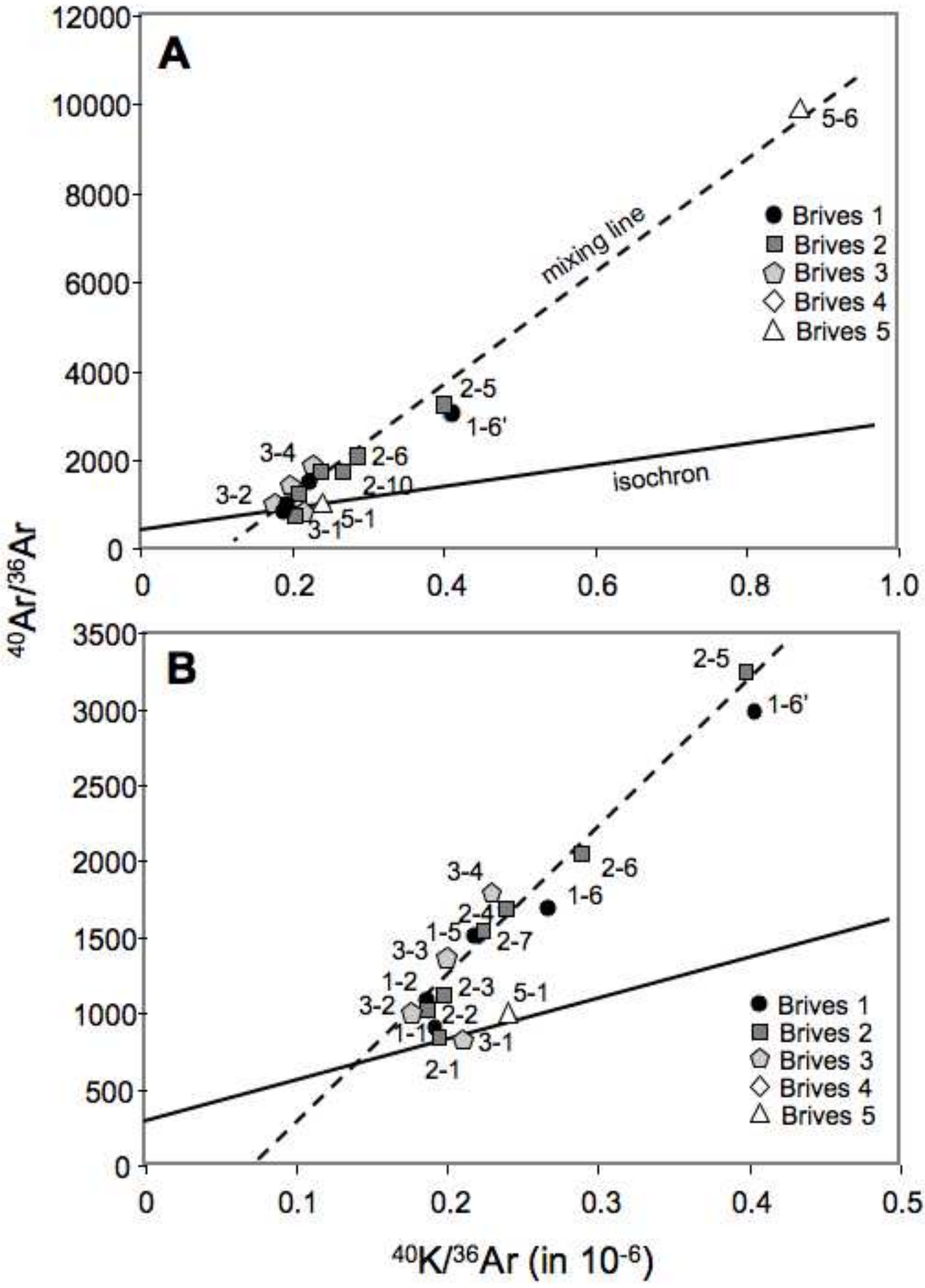

Figure
Click here to download high resolution image

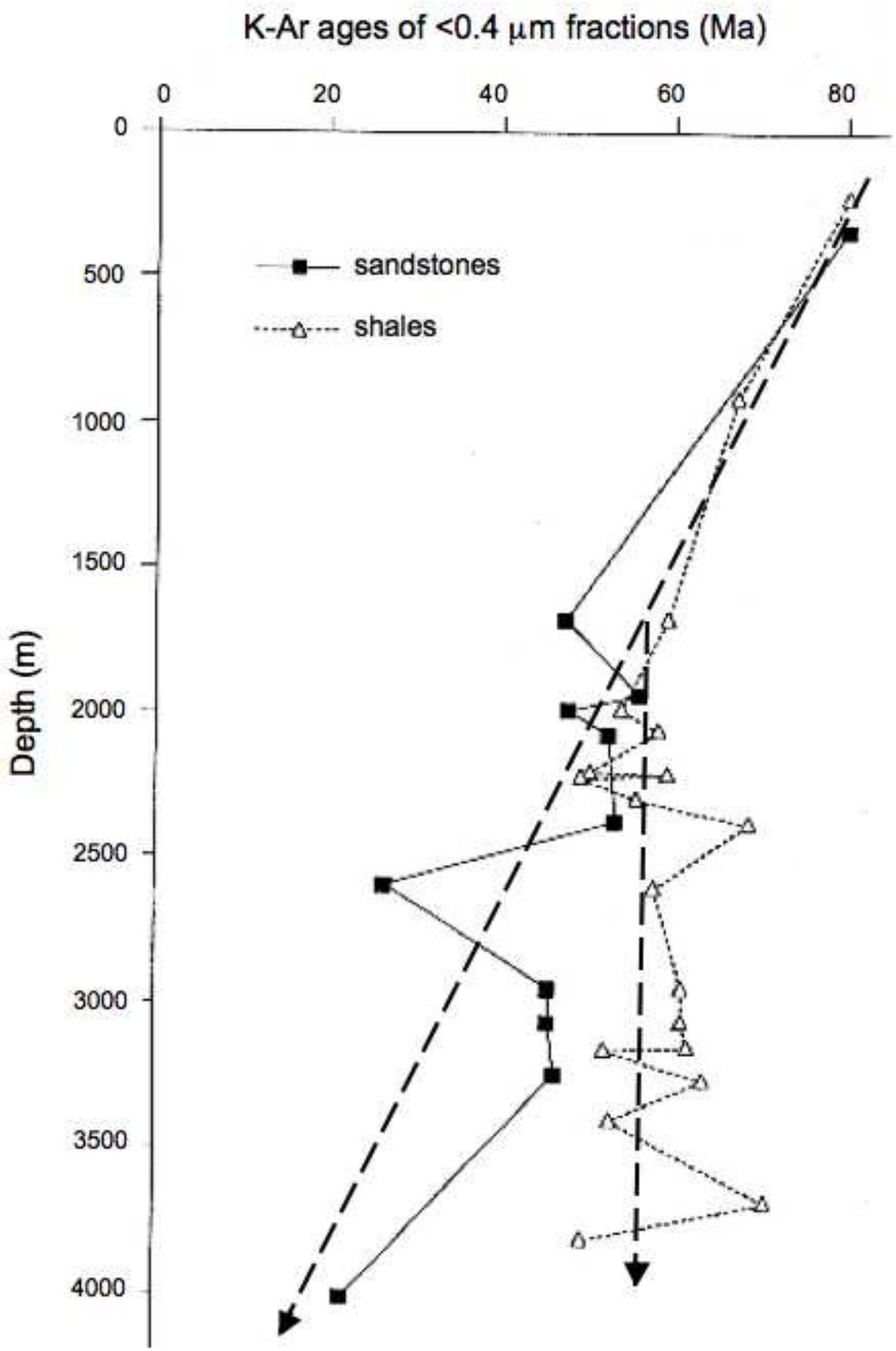

Figure

Click here to download high resolution image

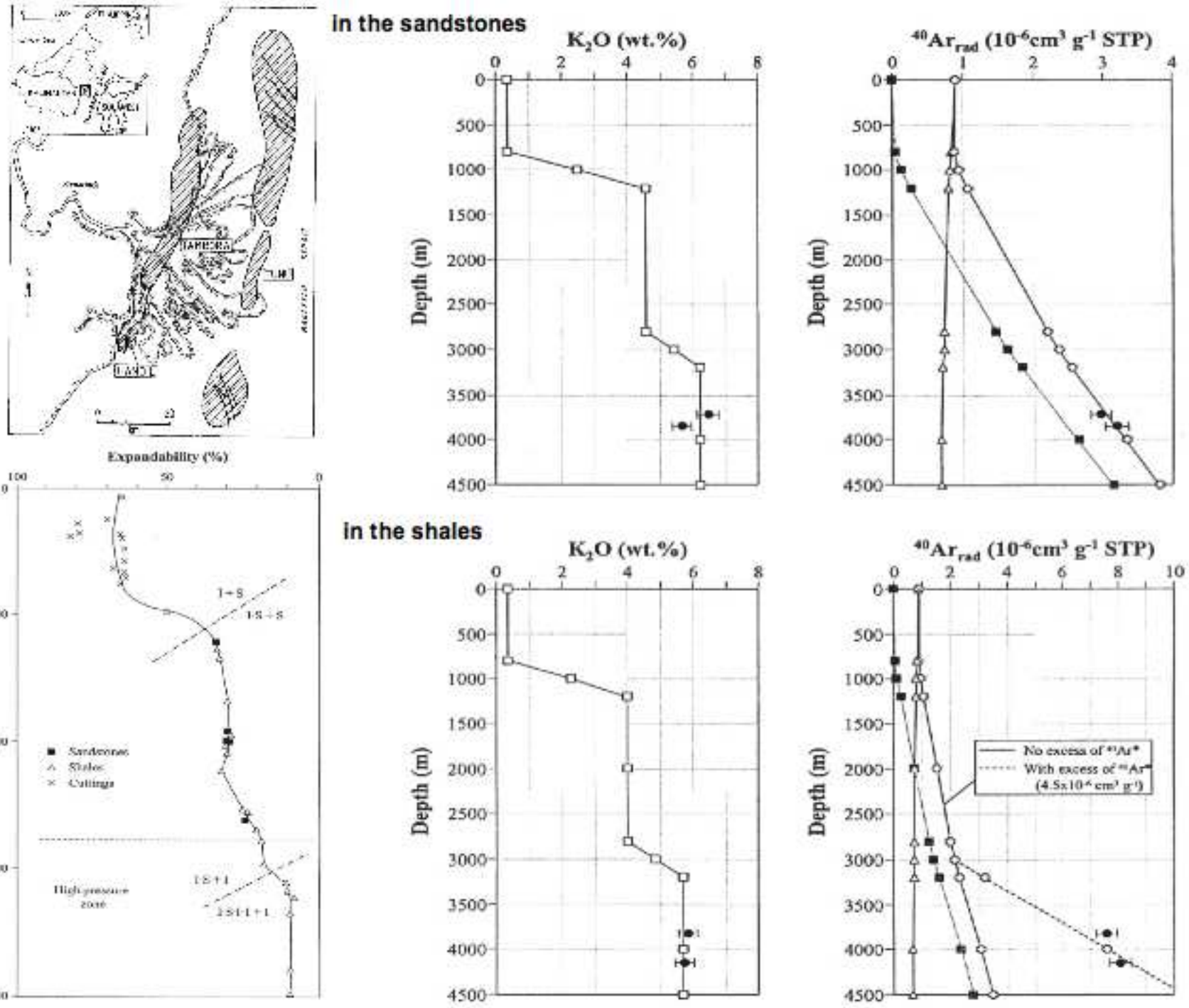

Figure
Click here to download high resolution image

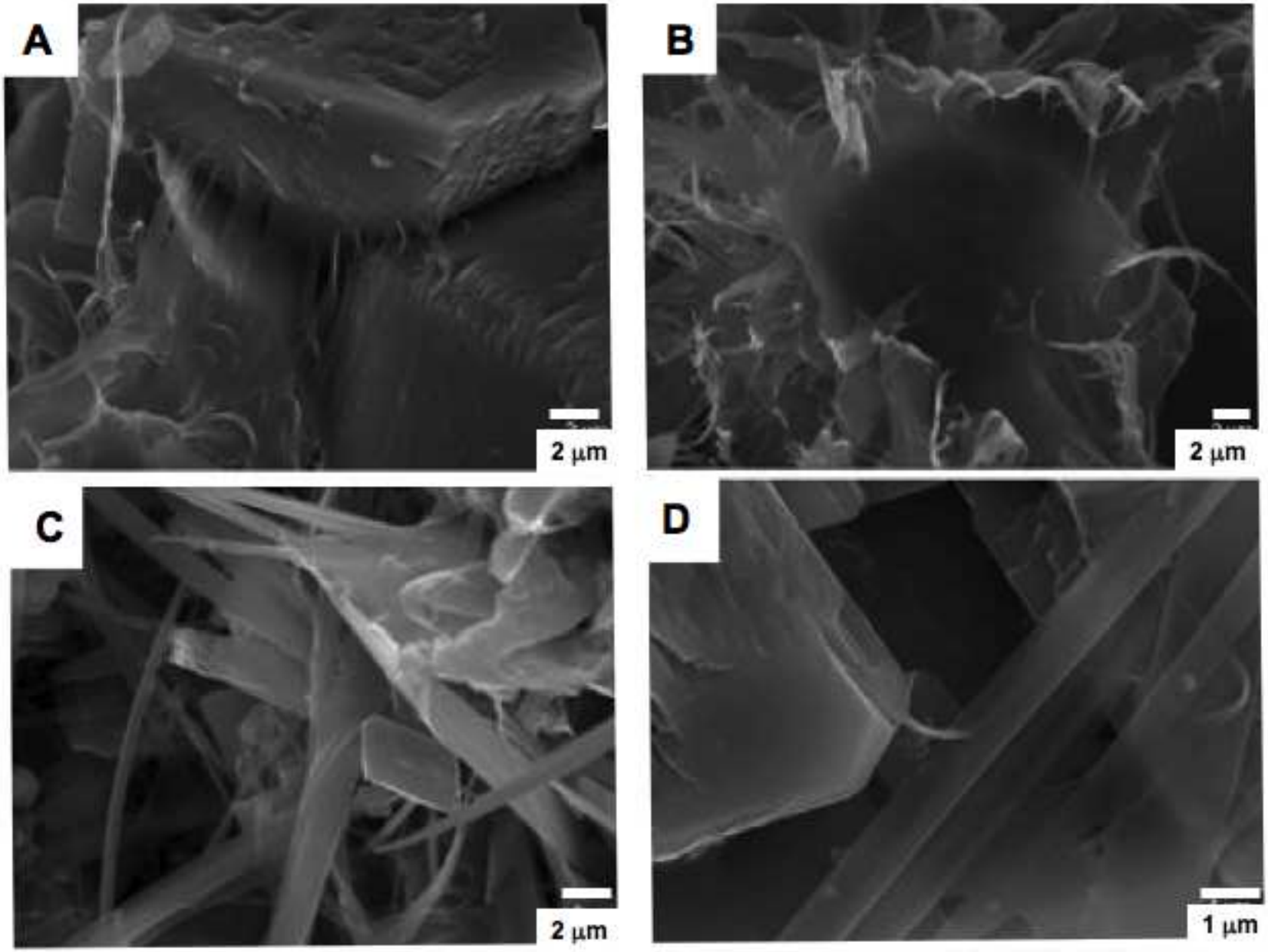

Figure

Click here to download high resolution image

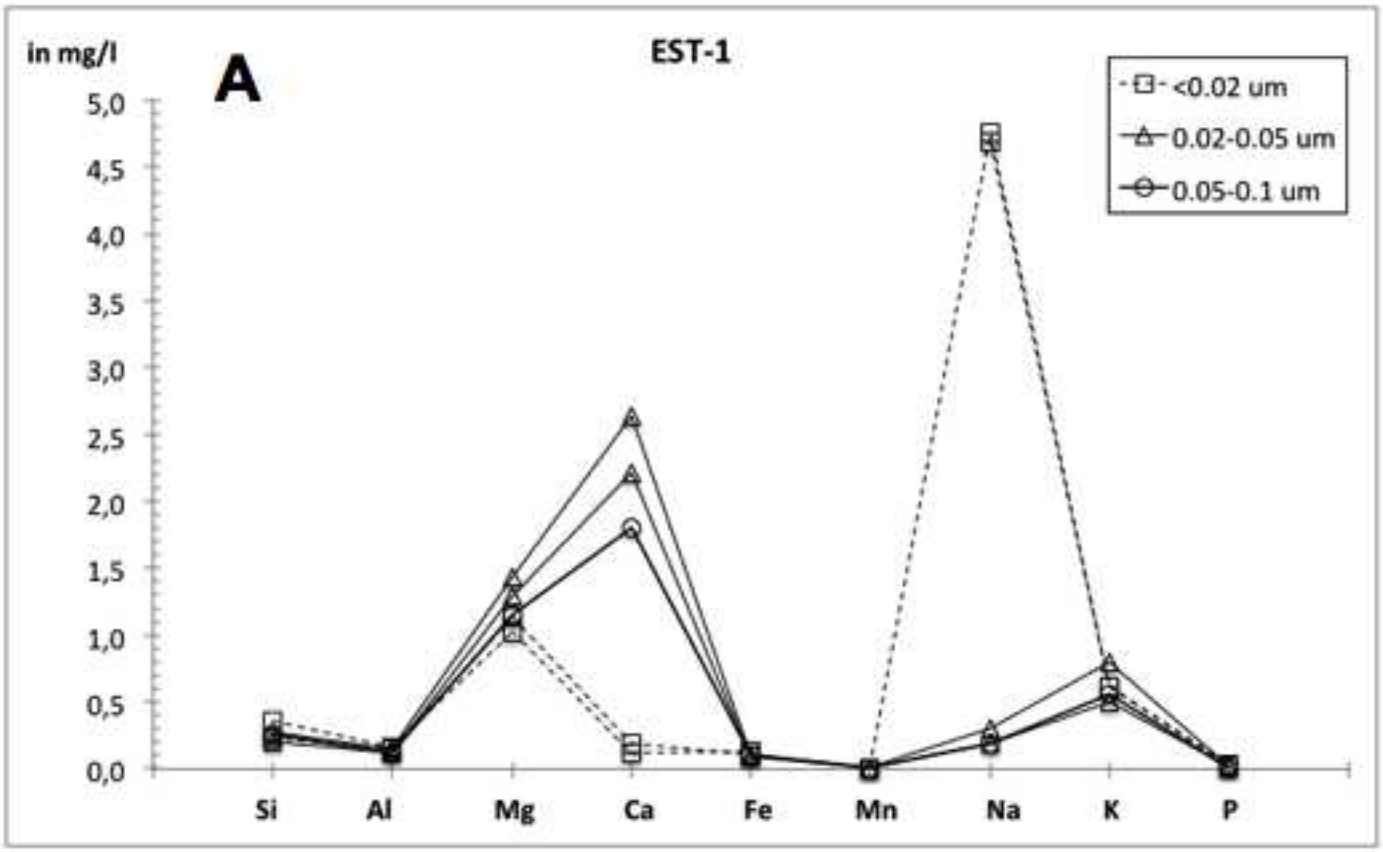

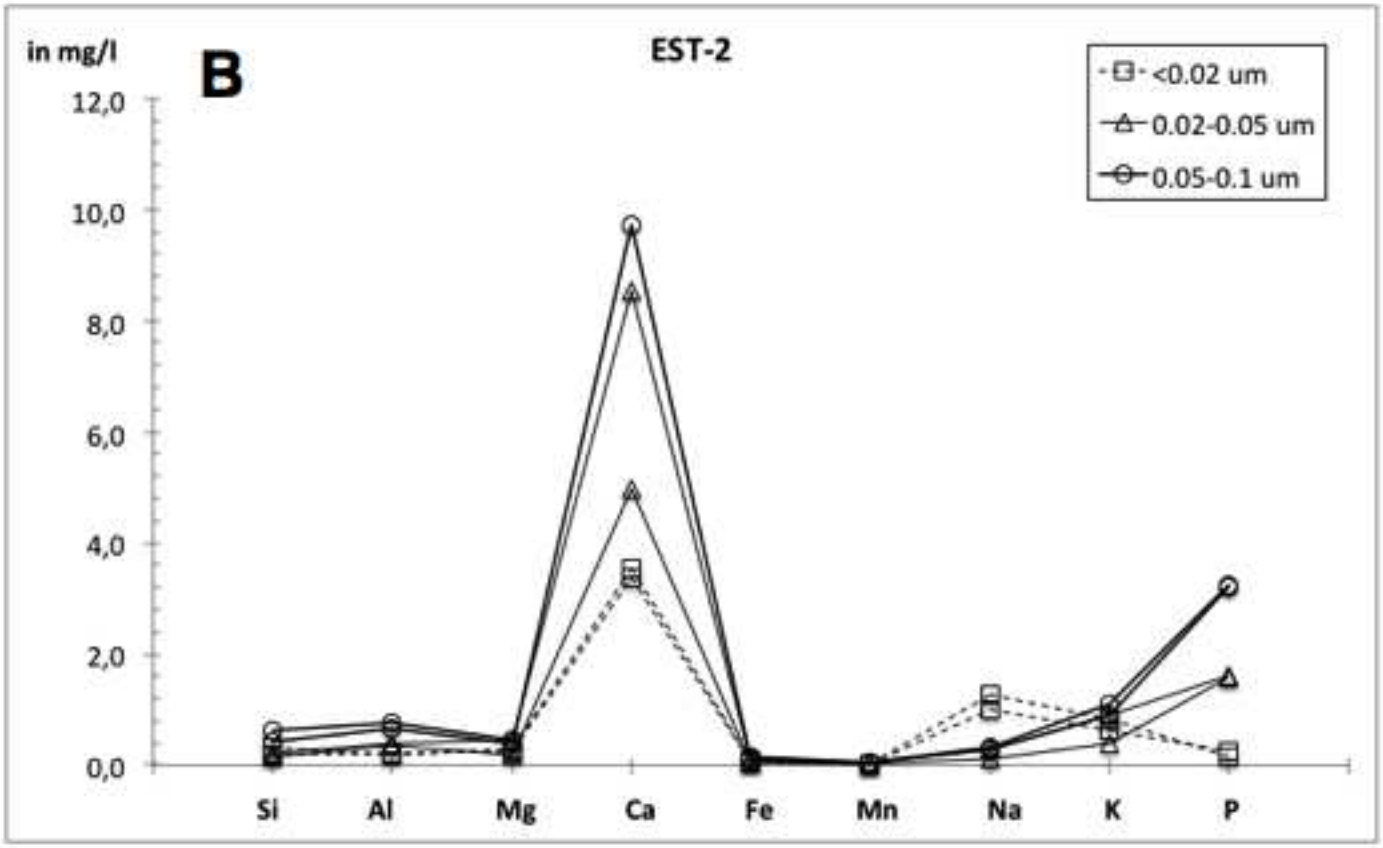

Figure
Click here to download high resolution image

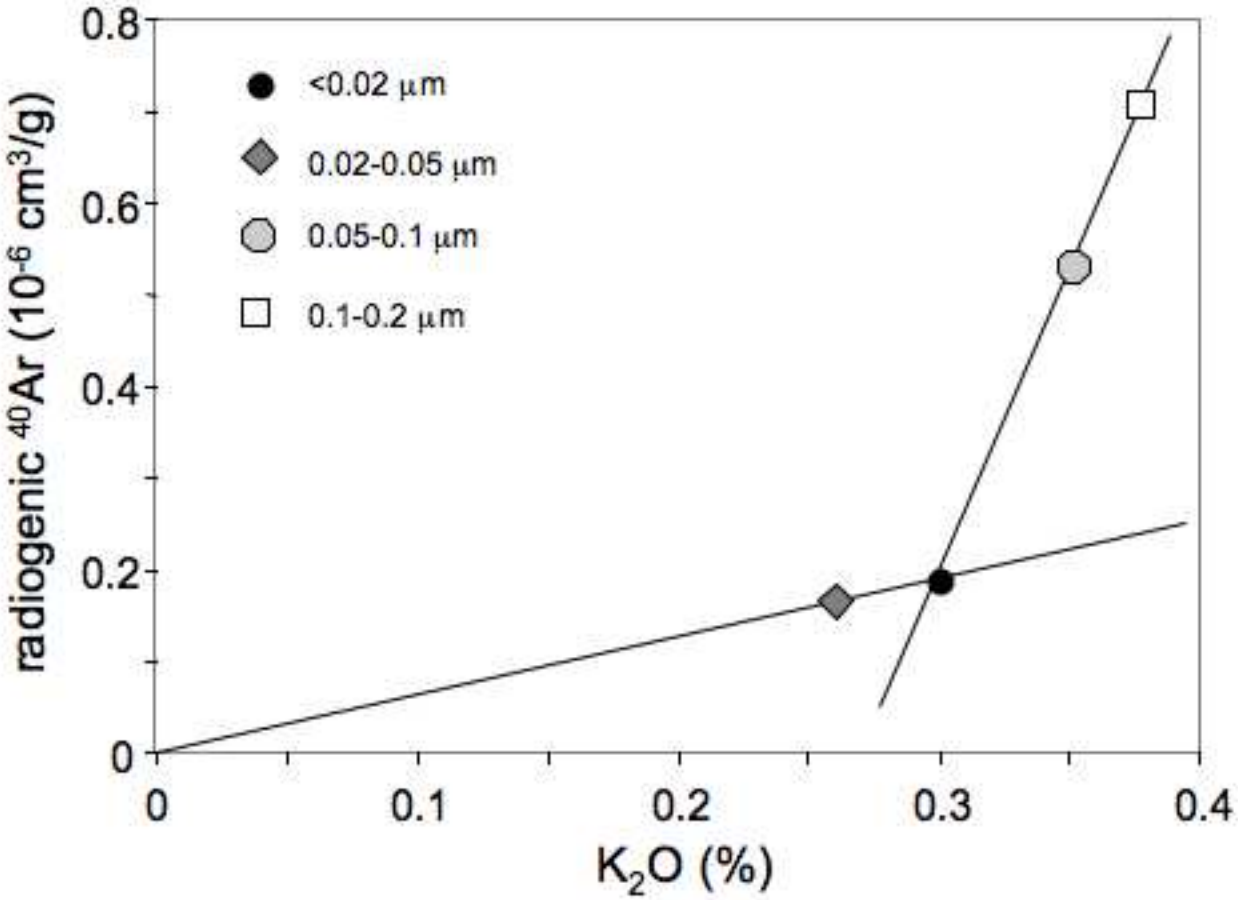

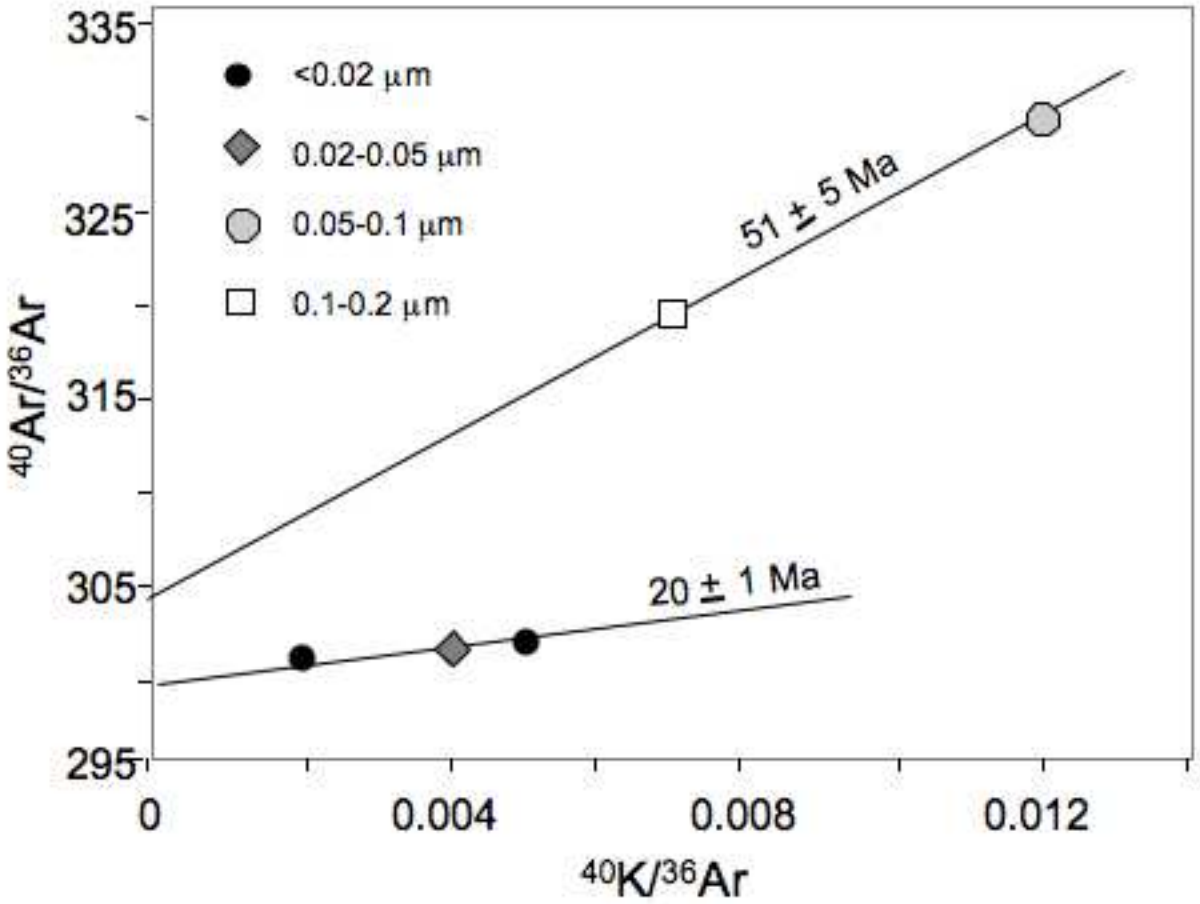

Figure

Click here to download high resolution image

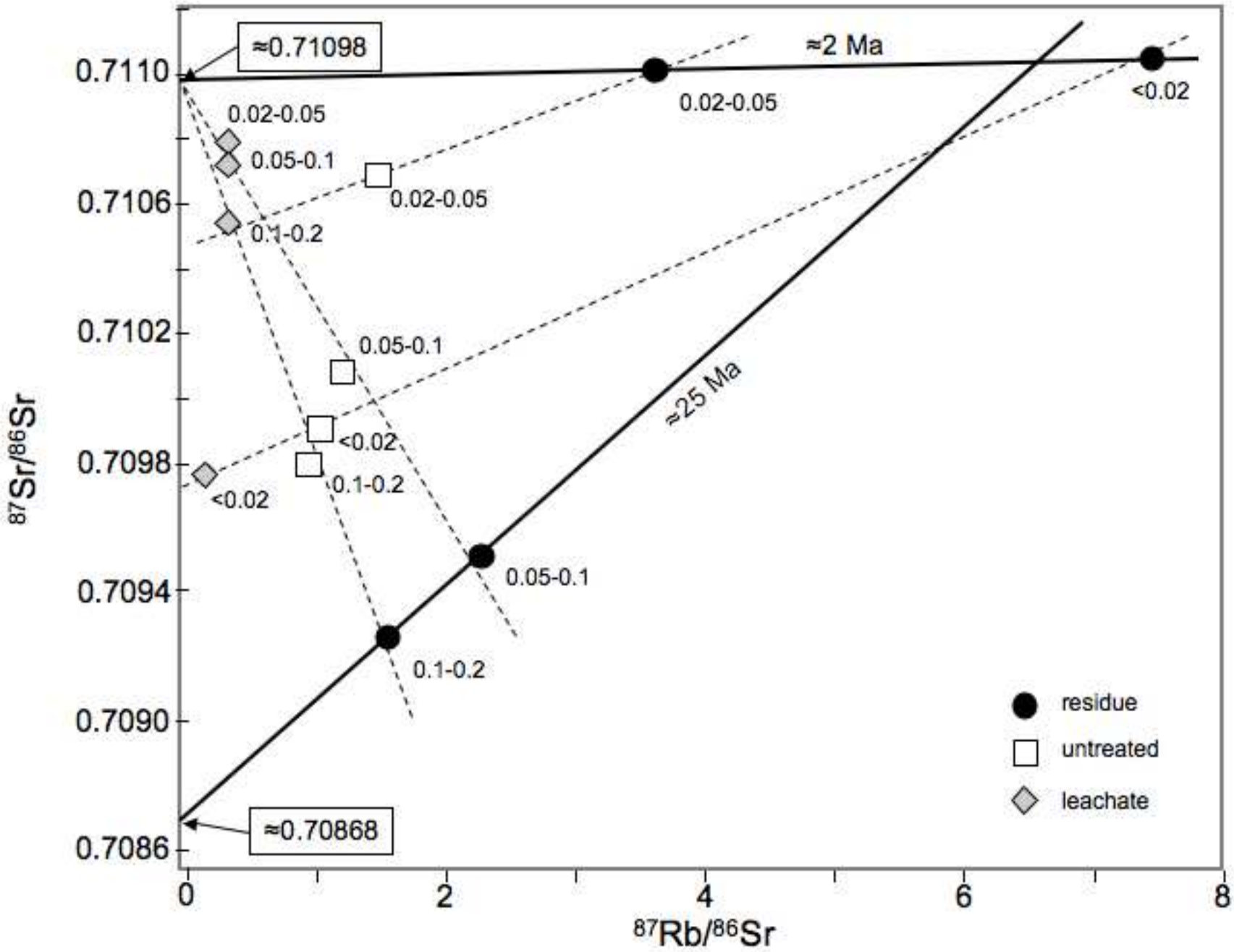

Figure
Click here to download high resolution image

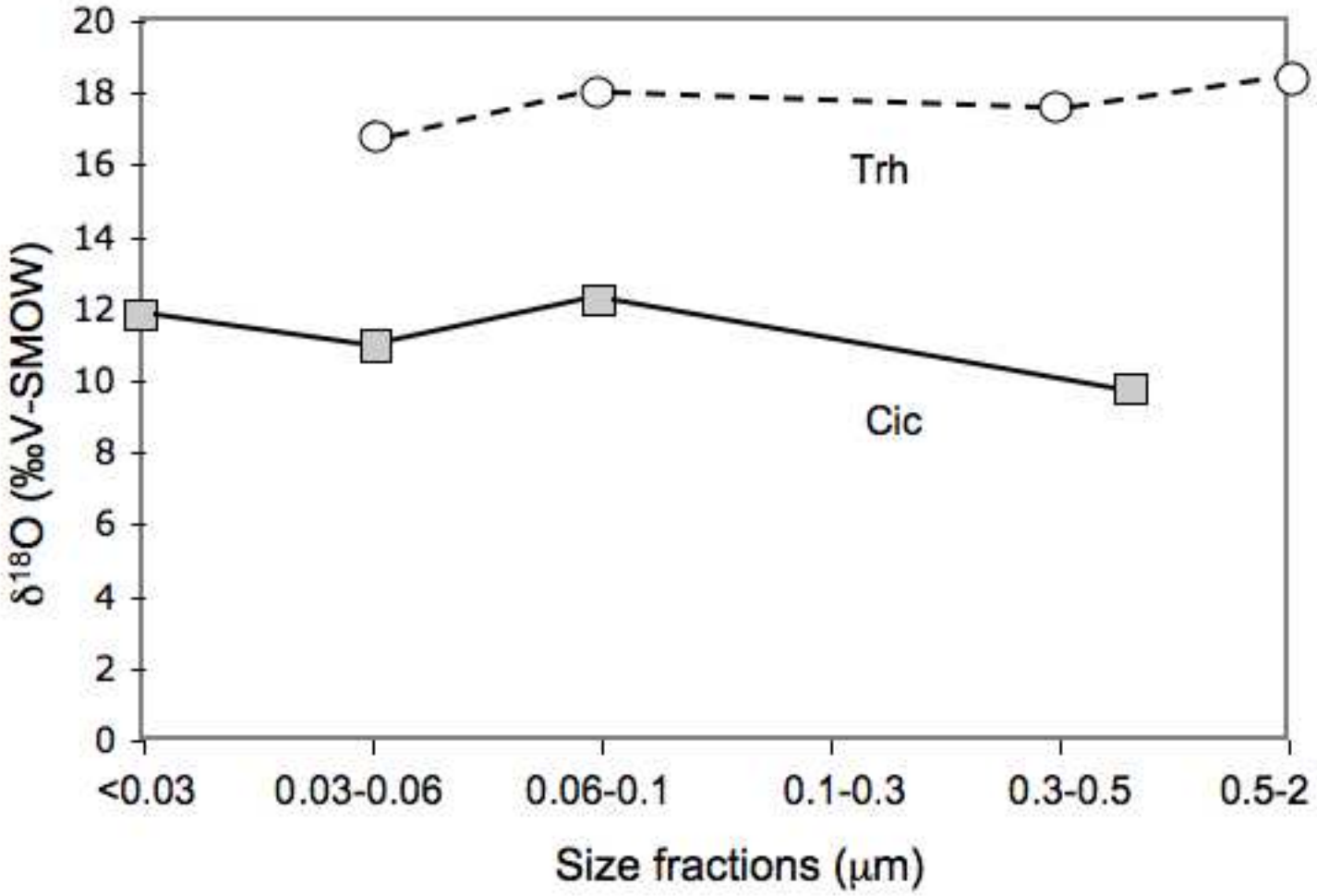

Figure
Click here to download high resolution image

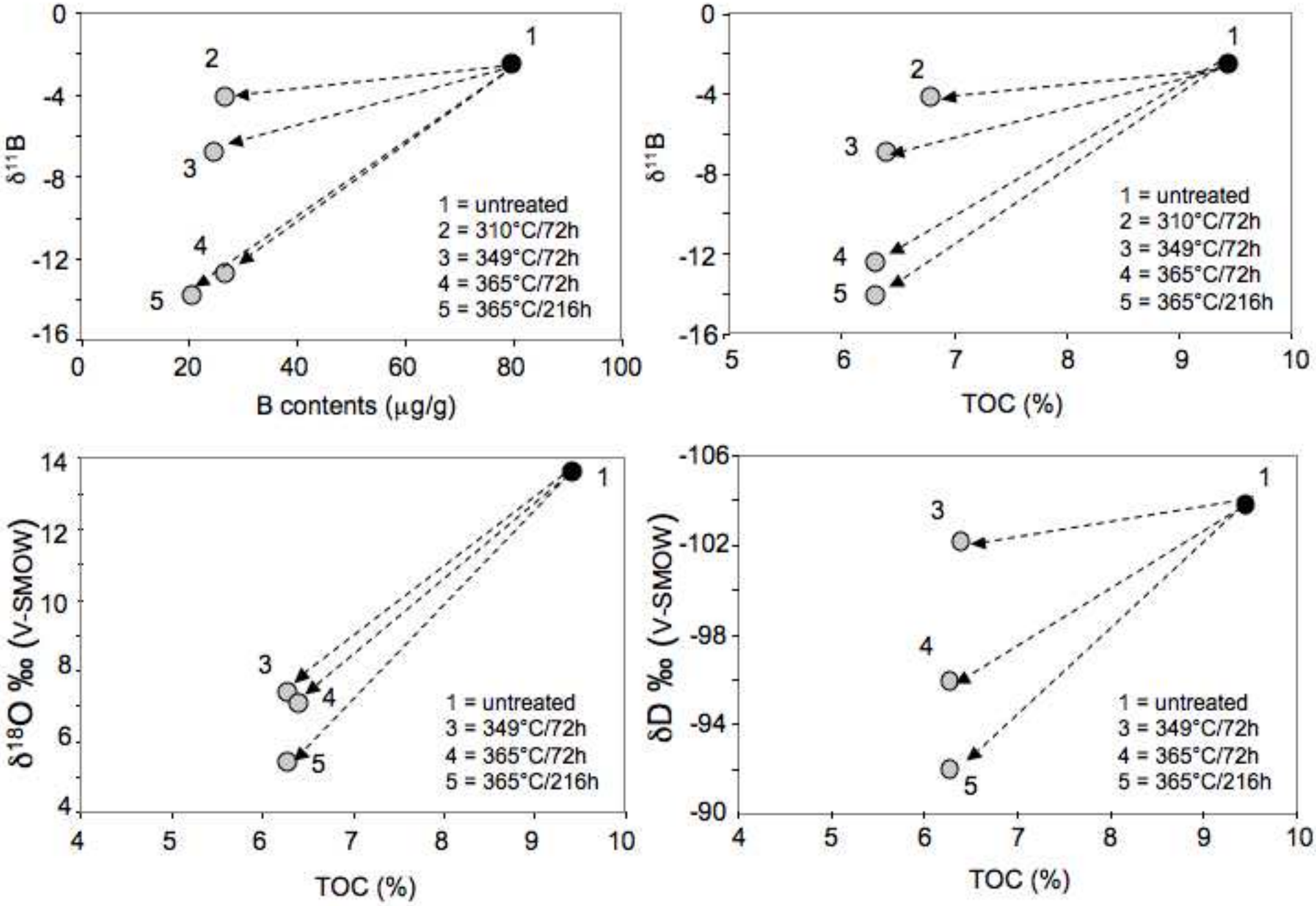

Figure
Click here to download high resolution image

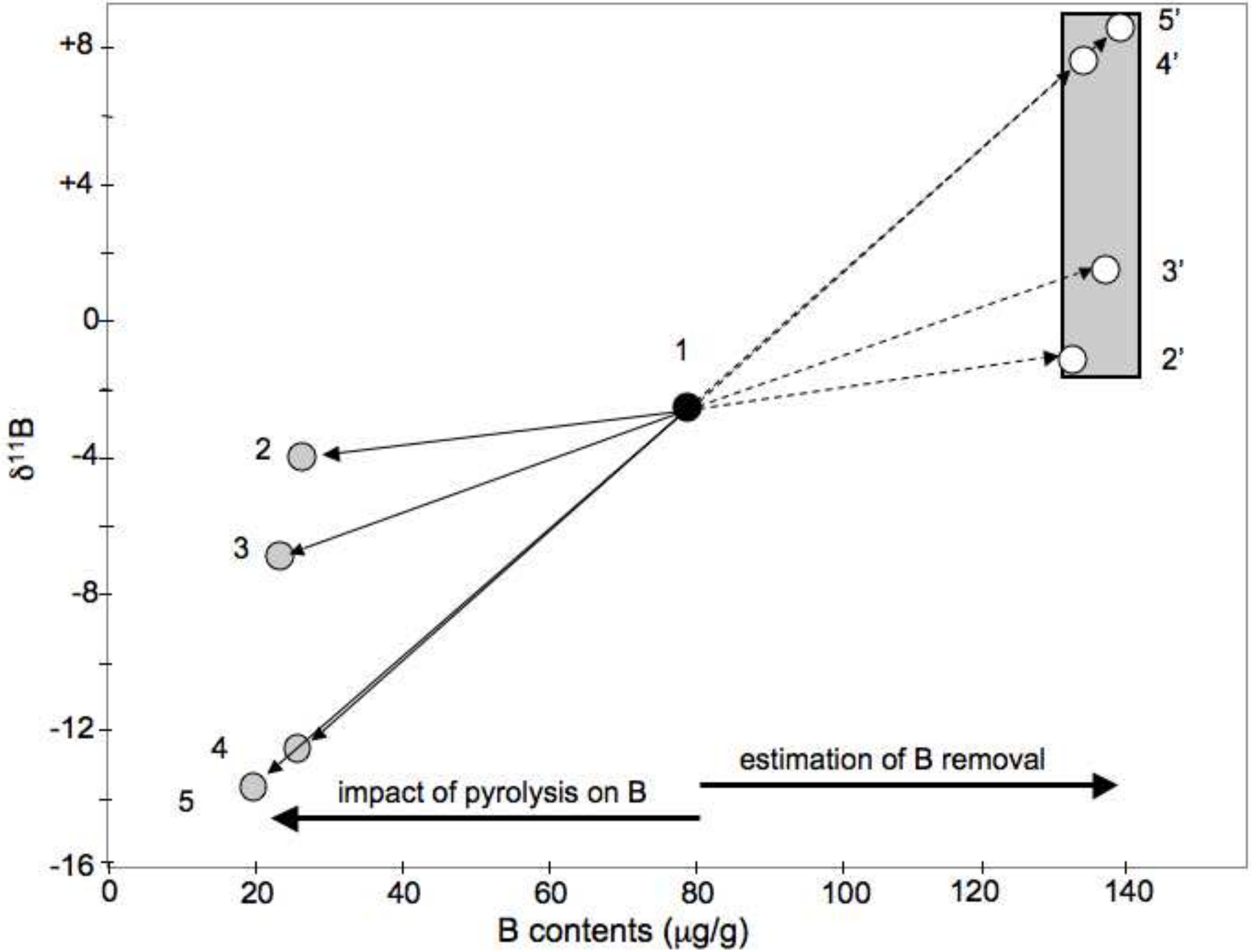

Table

Click here to download Table: ChemGeol_Table 1.xls

Sample ID	Size (m)	K_2O (%)	^{40}Ar (%)	rad ^{40}Ar ($10^{-6}cm^3/g$)	Age (Ma ±2)	$^{40}Ar/^{36}Ar$	$^{40}K/^{36}Ar$ (in 10^{-6})
Brives 1							
1-1	<0.03	6.51	64.06	9.94	46.8 (1.5)	882.2	0.191
1-2	0.03-0.05	6.82	71.02	14.58	65.2 (1.9)	1019.8	0.187
1-3	0.05-0.1	7.28	70.74	17.83	74.4 (2.4)	nd	nd
1-4	0.1-0.3	8.48	74.07	23.41	83.7 (2.6)	nd	nd
1-5	0.3-2	7.92	80.12	23.58	90.1 (2.3)	1486.8	0.220
1-6	2-10	8.03	82.71	23.39	88.2 (2.2)	1708.74	0.267
1-6'	2-10 US	7.84	90.08	28.45	109.2 (2.5)	2977.41	0.405
1-7	<10	7.29	73.79	18.67	77.8 (2.2)	nd	nd
Brives 2							
2-1	<0.03	6.68	65.32	10.52	48.2 (1.5)	852.1	0.195
2-2	0.03-0.05	6.62	70.50	13.71	63.1 (1.8)	1001.6	0.188
2-3	0.05-0.1	6.83	73.70	15.78	70.3 (2.0)	1123.7	0.198
2-4	0.1-0.3	7.35	82.47	23.71	97.4 (2.4)	1685.4	0.237
2-5	0.3-2	8.49	90.88	34.33	121.3 (2.7)	3239.2	0.398
2-6	2-10	7.80	85.61	26.16	101.2 (2.4)	2053.23	0.288
2-7	<10	6.70	80.33	19.98	90.2 (2.3)	1502.3	0.224
Brives 3							
3-1	<0.03	6.22	64.13	8.69	42.8 (1.4)	823.9	0.210
3-2	0.03-0.05	6.16	70.41	13.34	66.0 (1.9)	998.5	0.180
3-3	0.05-0.1	6.01	77.96	17.41	87.7 (2.3)	1340.6	0.200
3-4	0.1-0.3	6.23	83.55	22.48	108.6 (2.7)	1796.0	0.230
Brives 4							
4-7	<10	5.99	97.67	51.38	248.3 (5.4)	nd	nd
Brives 5							
5-1	<0.03	9.83	69.57	15.16	47.2 (1.4)	971.0	0.243
5-6	2-10	7.28	96.99	43.96	178.3 (3.8)	9823.04	0.873
5-7	<10	5.94	99.49	55.53	269.0 (6.0)	nd	nd

nd stands for not determined and US for ultrasonic treatment